Universidad de Alcalá

UNIVERSIDADE LUSÓFONA

Doctoral Program in Health Sciences D420

Lamiaceae extracts and compounds for topical application through nano delivery systems

Doctoral thesis presented by:

Filipe Jorge da Silva Pereira

Alcalá de Henares, 2017

DEPARTAMENTO DE CIENCIAS BIOMEDICAS

ESCOLA DE CIÊNCIAS E TECNOLOGIAS DA SAÚDE

En virtud del acuerdo de colaboración con la Universidade Lusófona de Humanidades e Tecnologías

Programa de doctorado D420 - ciencias de la salud

Extractos de *Lamiaceae* y compuestos para aplicación tópica através de un sistema nano de liberación

Tesis doctoral presentada por:

Filipe Jorge da Silva Pereira

Directores:

Prof. Dra. Patrícia Rijo
Prof. Dra. Catarina Reis
Prof. Dra. Ana M. Díaz Lanza

Alcalá de Henares, 2017

DPTO. CIENCIAS BIOMÉDICAS
Unidad Docente de Farmacología
Facultad de Medicina
Universidad de Alcalá
Ctra. Barcelona, Km. 33,600
28871 Alcalá de Henares (Madrid)
Telf.: 91 885 45 49 - Fax: 91 885 45 91
e-mail: dpto.biomedicas@uah.es

PROF. D. PEDRO DE LA VILLA POLO, COORDENADOR DEL PROGRAMA DE DOCTORADO EN CIENCIAS DE LA SALUD,

CERTIFICA:

Que el trabajo titulado: "***Lamiaceae extracts and compounds for topical application through nano delivery systems***" ha sido realizado por D. **Filipe Jorge da Silva Pereira**, bajo la dirección de las Dras. Ana María Díaz-Lanza, Profesora Titular de Farmacología del Dpto. de Ciencias Biomédicas, de la Universidad de Alcalá, Patrícia Dias de Mendonça Rijo Profesora Auxiliar y Profesora de Química Farmacéutica de la Escola de Ciências e Tecnologias da Saúde de la Universidade Lusófona de Humanidades e Tecnologias de Lisboa y Ana Catarina Beco Pinto Reis Profesora Asistente y Profesora de Tecnología Farmacéutica en la Faculdade de Farmácia de la Universidade de Lisboa, respectivamente y cumple todos los requisititos para su defensa pública como Tesis Doctoral.

Alcalá de Henares, 28 de julio de dos mil diecisiete.

DPTO. CIENCIAS BIOMÉDICAS
Unidad Docente de Farmacología
Facultad de Medicina
Universidad de Alcalá
Ctra. Barcelona, Km. 33,600
28871 Alcalá de Henares (Madrid)
Telf.: 91 885 45 49 - Fax: 91 885 45 91
e-mail: dpto.biomedicas@uah.es

PATRÍCIA DIAS DE MENDONÇA RIJO, PROFESORA AUXILIAR Y PROFESORA DE QUÍMICA FARMACÊUTICA DA UNIVERSIDADE LUSOFONA DE HUMANIDADES E TECNOLOGIAS, ANA MARÍA DÍAZ-LANZA, PROFESORA TITULAR DE UNIVERSIDAD DEL ÁREA DE FARMACOLOGÍA DEL DEPARTAMENTO DE CIENCIAS BIOMÉDICAS DE LA FACULTAD DE FARMACIA DE LA UNIVERSIDAD DE ALCALÁ Y ANA CATARINA BECO PINTO REIS, PROFESORA AUXILIAR Y PROFESORA DE TECNOLOGIA FARMACÉUTICA NA FACULDADE DE FARMÁCIA DE LA UNIVERSIDADE DE LISBOA.

CERTIFICAN:

Que la memoria para optar al Grado de Doctor, elaborada por Filipe Jorge da Silva Pereira, cuyo título es:

"Lamiaceae extracts and compounds for topical application through nano delivery systems"

ha sido realizada bajo su dirección y que reúne todos los requisitos necesarios para su juicio y calificación.

Y para que así conste, firman el presente certificado en Alcalá de Henares a 24 de julio de dos mil diecisiete.

Patrícia Rijo Catarina Pinto Reis Ana Mª Díaz-Lanza

Aos meus pais e avó

Acknowledgements

Those were excellent years of learning, with good and less good moments but that are part of my growth. I would like to leave a few words of appreciation to people who have been present on this journey.

Firstly, I would like to express my gratitude to my advisors Prof. Dr. Patrícia Rijo and Prof. Dr. Catarina Reis for all the support during PhD research. Without their support and efford, this work would never have been possible. I am also grateful to all CBios group, laboratory assistants and students of ULHT that I had pleasure to meet. I would also like to express my gratitude to Dr. Ana Mª Díaz-Lanza for its availability during all processes of the thesis. I would like to thank the support of my laboratory colleagues, Diogo Matias, Catarina Silva and Luis Roque. There were days of good humor and friendship that made this a much more pleasant journey. Also to Catarina Garcia and Ana Mota who I worked with, it was great to worked with you.

A very special gratitude goes out to research groups outside ULHT, with which I had the pleasure to work: Prof. Pedro Faísca and Prof. Carlos Afonso group from FFUL (specially to Carlos Monteiro and Monica Estevão), Prof. Lia Ascenção and Prof. Rodrigo Almeida group from FCUL (specially to Filipa, Catarina Antunes and Ana Carreira) and Prof. Rita Sobral from FCT-UNL.

A special mention to people of Gomensoro PZ, particularly to Luis Proença for availability of time and my colleague and friend Daniela Roque for your support.

I am grateful to my friends, that they are more than family, who have supported me along the way: João, Fernando, Carla, Telma and Janete. Also, I am grateful to my family members who supported me and encouraged all this time.

A special thanks to my companion Filipa Carneiro who attended me in this life course. Their understanding and support were essential during the last years.

To my pillars, my best friends, my parents, who always strove to give me the best education and the best of affections. I know the road to you has never been easy but it seems to have made up for it. I know that I can count on your support and you can always count on me. For my grandmother, thank you for your support and for being who you are. I really love you all.

Thanks for all your support!

Index

Figure index

Table index

Abstract

Antibiotic resistance is one of the major health problem affecting every continent, whether developed or developing countries. This problem is responsible of a high number of patients and a leading cause of deaths worldwide, without an effective form of therapy. The developments in the nanotechnology field has led to more efficient delivery systems, while new structures unveiled through natural resources showed high biological activity never studied before. The combination of a new drug delivery strategy with new bioactive molecules can lead to new therapeutic forms against this type of infections.

With this work, it is analysed the potencial and ability of 7α-acetoxy-6β-hydroxyroyleanone as a novel compound for the treatment of infections associated with resistant bacterias. In the same way, it is proposing that the combination of a therapeutic form of natural source (extract ou isolated compound) with an new technique of delivery using different types of nanoparticles for the treatment of topical infections.

7α-acetoxy-6β-hydroxyroyleanone extract from *Plectranthus grandidentatus* was optimized, through seven different methods of extraction. The highest quantity of the 7α-acetoxy-6β-hydroxyroyleanone was obtained through supercritical fluid extraction, delivering an amount of AHR about six times higher than that of the second-best method tested. 7α-acetoxy-6β-hydroxyroyleanone isolated was used for the characterization studies of their physicochemical properties. Important data, such as, molecular and crystal structure of 7α-acetoxy-6β-hydroxyroyleanone was obtained from single crystal X-ray diffraction and the thermal behavior of the compound was studied by differential scanning calorimetry.

The mechanism of action of high antibacterial activity and low cytotoxicity of 7α-acetoxy-6β-hydroxyroyleanone was studied on a type of Methicillin-resistant *Staphylococcus aureus* strain. In this approach, different studies were carried out. 7α-acetoxy-6β-hydroxyroyleanone had a non-significant effect in passive permeability, at same time, bacteria treated with this royleanone displayed cell wall disruption, without cell lysis.

The combination of nanoparticles with natural products was preliminary tested using two plants from *Lamiaceae* family. Different extracts from *Lavandula stoechas ssp. luisieri* and *Lavandula pedunculata* were prepared and established their antioxidant profile by lipid peroxidation inhibition and the antioxidant activity confirmed. Due to their high antioxidant activity, phenolic content and flavonoid amount, methanol extracts of *Lavandula stoechas ssp. luisieri* and *Lavandula pedunculata* were selected and encapsulated into Poly(lactic-co-glycolic acid) nanoparticles. The encapsulation of the extracts resulted in well-defined spherical shape PLGA nanoparticles and with a high encapsulation efficiency (>96%). Preliminar epidermal permeation of both extracts through ex-vivo human epidermis and their *in vitro* cytotoxicity in human keratinocytes studies were suggestive of their low risk of toxicity.

The combination of nanoparticles with 7α-acetoxy-6β-hydroxyroyleanone was also studied in this thesis. Through a different approach, distinct silver nanoparticles were successful synthesized using citrate and borohydride salts as reducing agents. Ampicillin, as model drug, and 7α-acetoxy-6β-hidroxyroyleanone as new therapeutic compound were associated with both type of silver nanoparticles. Particle characterization showed small, spherical and monodisperse nanoparticles. The antibacterial capacity of each compound was higher after conjugation with

silver nanoparticles. *In vivo* skin irritation test conducted in animal models showed absence of erythema or any skin color changes.

The study developed on this new molecule has resulted in promising results for future application as topical formulation. The knowledge of its chemical and mechanistic properties may result in structures with better therapeutic activity and minor adverse side effects. Ultimately, their combination with nanotechnology may lead to advantageous pharmacological properties for people infected with this type of bacteria.

Keywords: Antibiotic resistance; *Lamiaceae*; royleanone; silver nanoparticles; PLGA nanoparticles

Resumen

La resistencia a los antibióticos es uno de los principales problemas de salud que afectan a todos los continentes, ya sean países desarrollados o en desarrollo. Este tipo de infección es responsable de un elevado número de víctimas, siendo una de las más importantes causas de muerte en todo el mundo, sin una forma efectiva de terapia. Los desarrollos producidos en el campo de la nanotecnología han revelado formas más eficaces de terapéutica, mientras que se desvelan nuevas estructuras procedentes de nuevos recursos naturales nunca antes estudiados. Estas serán las nuevas terapias para este enorme problema.

Con este trabajo, se analiza el potencial y la capacidad de la 7α-acetoxi-6β-hidroxiarilanona como un nuevo compuesto para el tratamiento de infecciones asociadas con bacterias resistentes. Del mismo modo, se propone la combinación de una forma terapéutica de origen natural (extracto o compuesto aislado) con una nueva técnica de administración utilizando diferentes tipos de nanopartículas para el tratamiento de infecciones tópicas. La obtención de 7α-acetoxi-6β-hidroxiroiletanona a partir de *Plectranthus grandidentatus Gürke* se optimizaró, a través de siete métodos diferentes de extracción. La mayor cantidad de 7α-acetoxi-6β-hidroxiroiletanona se obtuvo mediante extracción con fluido supercrítico, suministrando una cantidad de AHR aproximadamente seis veces mayor que la del segundo método mejor evaluado. Se utilizó la 7α-acetoxi-6β-hidroxiarilanona aislada para los estudios de caracterización de sus propiedades fisicoquímicas. Se obtuvieron datos importantes, tales como la estructura molecular y cristalina de la 7α-acetoxi-6β-hidroxiarilanona a partir de la difracción de rayos X de cristal único y se estudió el comportamiento térmico del compuesto mediante calorimetría de barrido diferencial.

Se estudió el mecanismo de acción que justifica la alta actividad antibacteriana y la baja citotoxicidad de la 7α-acetoxi-6β-hidroxiroileanona sobre un tipo de cepa de *Staphylococcus aureus* resistente a la meticilina. Con este objetivo, se realizaron diferentes estudios sobre la interación de este posible nuevo antibiótico en la membrana y en la pared celular de la bacteria. La 7α-acetoxi-6β-hidroxiarilanona ha revelado un efecto no significativo en la permeabilidad pasiva, al mismo tiempo, las bacterias tratadas con esta royleanona muestran disrupción de la pared celular, sin revelar lisis celular.

La combinación de nanopartículas con productos naturales se ensayó utilizando dos plantas de la familia *Lamiaceae*. Para ello se prepararon diferentes extractos de *Lavandula stoechas ssp. Luisieri (Rozeira) Rozeira* y *Lavandula pedunculata (Mill.) Cav.* y se estableció su perfil antioxidante por inhibición de la peroxidación lipídica que confirmó dicha actividad. Debido a su alta actividad antioxidante, contenido fenólico y cantidad de flavonoides, los extractos metanólicos de *Lavandula stoechas ssp. Luisieri* y *Lavandula pedunculata* fueron seleccionados y encapsulados en nanopartículas de Poli (ácido láctico-co-glicólico). La encapsulación dio como resultado la formación de nanopartículas poligénicas de PLGA con una forma esférica bien definida y un alto rendimiento de encapsulación (>96%). La permeación epidérmica preliminar de ambos extractos a través de la epidermis humana y su citotoxicidad in vitro en estudios de queratinocitos humanos sugirieron riesgos bajos de toxicidad.

También se estudió la combinación de nanopartículas con 7α-acetoxi-6β-hidroxiroileanona. A través de un enfoque diferente, distintas nanopartículas de plata fueron sintetizadas con éxito usando sales de citrato y borohidruro como agentes reductores. La ampicilina, como modelo, y la 7α-acetoxi-6β-hidroxi-roiletanona como nueva forma terapéutica

se asociaron con ambos tipos de nanopartículas de plata sintetizadas. La caracterización mostró que se formaron nanopartículas pequeñas y monodispersas con forma esférica. La capacidad antibacteriana del antibiótico cuando se conjugó con nanopartículas de plata fue también elevada. La prueba de irritación cutánea in vivo realizada en modelos animales mostró ausencia de eritema o cambios de color de la piel.

En definitiva, el estudio desarrollado sobre esta nueva molécula muestra resultados prometedores para la futura aplicación como antibiótico. El conocimiento de sus propiedades químicas y mecánicas puede dar lugar a estructuras con mejor actividad terapéutica y menores efectos secundarios. Su combinación con la nanotecnología puede conducir a propiedades farmacológicas ventajosas para las personas infectadas con este tipo de bacterias.

Palabras llave: resistencia a los antibióticos; *Lamiaceae*; Roileanona; Nanopartículas de plata; Nanopartículas de PLGA

Abbreviations and acronyms list

AFM	Atomic force spectroscopy
AHR	7α-acetoxy-6β-hydroxyroyleanone
AgNP	Silver nanoparticles
AMP	Ampicillin
ATCC	American Type Culture Collection
$CDCl_3$	Deuterated chloroform
CF	5,6-carboxyfluorescein
CFU	colony-forming unit
CIP	Collection de l'Institut Pasteur
DAD	Diode array detector
DLS	Dynamic light scattering
DMSO	Dimethyl sulfoxide
DOPC	1,2-dioleoyl-*sn*-Glycero-3-phosphocholine
DPPH	2,2-diphenyl-1-picrylhydrazyl
DSC	Differential scanning calorimetry
HPLC	High pressure liquid chromatography
HPTS	8-hydroxypyrene-1,3,6-trisulfonic acid
LUVs	Large unilamellar vesicles
MDR	Multidrug resistant
MIC	Minimum inhibitory concentration
MRSA	Methicillin-resistant *Staphylococcus aureus*
MDR-TB	Multidrug-resistant *Mycobacterium tuberculosis*
NMR	Nuclear magnetic resonance
OD	Optical density
PBP2a	Penicillin-binding protein 2a
PBS	Phosphate-buffered saline
PI	Polydispersity index
PLGA	Poly (lactic-co-glycolic) acid
PSM	*N*-palmitoyl-sphingomyelin
POPC	1-palmitoyl-2-oleoyl-*sn*-glycero-3-phosphocholine
rpm	rotation per minute
SCF	Supercritical fluid

SCXRD	Single Crystal X-ray Diffraction
SD	Standard deviation
SEM	Scanning electron microscopy
SPR	Surface plasmon resonance
TFC	Total flavonoids content
VRE	vancomycin-resistant *Enterococcus faecalis*
VISA	Vancomycin-intermediate *Staphylococcus aureus*

Chapter 1

State of art, hypothesis and objectives

This chapter is based on the following article:

Ladeiras, D., Monteiro, C. M., **Pereira, F.**, Reis, C. P., Afonso, C. A. M., Rijo, P. Reactivity of Diterpenoid Quinones: Royleanones. *Current Pharmaceutical Design*. 2016. 22(12): 1682-1714

State of art, hypothesis and objectives

1.1 Introduction

The isolation of new natural products provides novel scaffolds with potential biological activities that may trigger the drug development [1]. Remarkably, around 60% of the isolated natural products are terpenoids [2]. The structural diversity of the terpenes are challenging to the synthetic chemists offering an open field for the design of new synthetic methodologies, mainly those directed towards the carbocyclic ring construction [3].

The diterpenoids are the second largest class of terpenes, with over 2200 compounds belonging to 130 distinct skeleton types. The interest in the isolation of these diterpenes is raising due to their noteworthy biological activities. Particularly, the diterpenoids with quinone cromophoric groups, which are predominant metabolites in the Lamiaceae plant family, have also been the subject of intensive research studies. Following these interests, several reviews have been published.

The natural diterpenes in their multiple aspects have been the subject of ongoing excellent periodic reviews authored by Hanson [4]–[6]. The biological activities of different abietanes diterpenes, or their synthetic derivatives, were as well reviewed up to 1992 [7] and more recently from the late 1980s up to 2014 by González [8], [9]. The majority of diterpenoid quinones, have an abietane or rearranged abietane skeletons and they include a considerable number of *o*-quinones, on which research studies have been extensively emphasizing the tanshinone diterpenoids [10]. Diterpenoid quinones have been extensively systematized up to 1994 considering their distribution, structure, chemistry and total synthesis [11], [12] as well the chemical and biological potentials of the diterpenoid quinone methides have been revised [13].

The Lamiaceae plants are rich in diterpene metabolites, namely in abietane quinones. *Salvia* is a genus known for the isolation of these compounds. Actually, Eugster and his co-workers have been pioneers in identifying an extensive number of abietane quinones from several *Plectranthus* species collected in Africa. A number of them were royleanones metabolites that are cyclic structures having the abietane carbon skeleton with a hydroxy-*para*-quinone structure. However, this class of royleanone compounds has not yet been subject of a review. Therefore, it will be highlighted the isolation, the synthesis and derivatization studies and, finally, an overview of the biological activities of royleanones and related rearranged compounds.

1.2 Royleanones, rearranged royleanones and royleanones-related diterpenes of natural origin

The name “royleanones” was first attributed to a yellow pigment derived from the plant *Inula royleana* by Edwards and co-workers in 1962. This yellow pigment was mainly a mixture of acetoxyroyleanone, royleanone and dehydroroyleanone. The common characteristic of these diterpenes is the chromophoric system on C-ring now known as royleanone system [14]. In fact, royleanone is the 12-hydroxy-11,14-*p*-benzoquinone chromophore on the ring C of an abietane skeleton. The simplest royleanone abietane **–** royleanone **1-** is an acidic compound (pKa 8.5 in 50% aqueous methanol) and a magenta color compound, in alkaline solutions [14].

Thenceforward, more royleanones have been discovered and studied, considering their biological activity or reactivity, using them in total synthesis or in derivatization studies. We now present, a literature review of 1962 subsequent studies and more recent descriptions of these interesting compounds.

1.3 Royleanone and royleanone-related abietanes

Tricyclic abietane quinones are mostly found in the Lamiaceae family predominating in the *Plectranthus* and *Salvia* genus. Typically, they have a quinonoid C ring and, in addition, they often have an oxidised B ring and may have an oxidised A ring and may show aromaticity. Hydroxyl and carbonyl functional groups occur frequently on C_{11}, C_7 and C_6 [11], [12].

Royleanones were first isolated from the roots of *Inula royleana* as a yellow pigment, by Handa's group in 1945 [15]. However, only in 1962 the chemical structures of royleanone **1**, 7α-acetoxyroyleanone **2** (initially named 9-acetoxyroyleanone), and 6,7-dehydroroyleanone **3** (primarily called 9-dehydroroyleanone) were assigned for the first time by Edwards and co-workers using degradation and synthesis studies [14]. They synthetized the royleanone **1** from ferruginol with 98% hydrogen peroxide in acetic acid, with sulphuric acid as catalyst, in a yield of 7% [14]. Later on 1974, from the same plant species, a novel royleanone derivative, 7-ketoroyleanone **4**, was identified [16]. Mostly of the royleanone derivatives isolated from natural sources were found in the 70's and 80's.

In 1988, 16-acetoxy-7-*O*-acetylhorminone **5** and 16-acetoxy-12-*O*-acetylhorminone **6**, two new horminone (7α-hydroxyroyleanone **7**) derivatives, were isolated from the Chinese medicinal plant *Rabdosia lophanthoides* (current accepted name *Isodon lophanthoides*) [17]. Lophanthoidins A-F (**8**-**13)**, the royleanone derivatives discovered in the following year from the same plant, having hydroxyl or acetoxyl groups on C-16 and oxygen functions at both C-6 and C-7, with lophanthoidin D **11** and F **13** being 6α-ethoxyl derivatives [18]. Besides 6,7-dehydroroyleanone **3** and horminone **7**, it was also found a new cytotoxic compound, 7-*O*-methylhorminone **14**, from *Lepechinia bullata.*[19]

Taxoquinone (7β-hydroxyroyleanone) **15**, primarily isolated from *Taxodium distichum*, differs from horminone **7** structure, only in the configuration at the C-7 hydroxyl group (β-equatorial and α-axial configuration, respectively) [20].

6β-acetoxy-7α-hydroxyroyleanone **16**, present in *Taiwania cryptomerioides*, has the simplest structure of royleanone with an additional acetoxyl and hydroxyl functional groups [21].

Investigations on *Coleus zeylanicus* (*Plectranthus hadiensis*) gave rise to 6β,7β-dihydroxyroyleanone **17** and 7β-acetoxy-6β-hydroxyroyleanone **18**, being the known stereoisomer 7α-acetoxy-6β-hydroxyroyleanone **19** also isolated from this plant [22].

In 1971 and 1974, it was described two new royleanone type compounds, isolated from the roots of *Salvia nemorosa*, nemorone **20** and it alkaline hydrolysis product, deacetylnemorone **21** , both with a formyl group at C-10 [23], [24]. In addition, an abietane type diterpene quinone isolated from *Salvia ballotaeflorae* (*Salvia ballotiflora*), conacytone **22**, is related to nemorone **20**. Through the hydrolysis and loss of the ester group at C-7, the oxidation of the β-methyl group at C-4 of nemorone **20** and the subsequent formation of the hemiacetal group [25]. These compounds were later isolated from *Salvia pubescens* [26]. Also, the 7α-*O*-methyl-conacytone **23** was found in *Salvia candicans*, which is an artifact when methanol was used on the separation methodology [27].

In 1983, a new quinone was elucidated as the 20-hydroxy-7α-acetoxyroyleanone **24**, which differs from the 7α-acetoxyroyleanone **2** by replacement of the methyl group at C-10 with a hydroxymethyl group [28]. Two years later, two new ethoxyl derivatives were found in *Salvia lavandulaefolia* (*Salvia officinalis* subsp. *Lavandulifolia*), 7α-ethoxyroyleanone **25** and 7α-ethoxy-12-*O*-methylroyleanone **26**, which may be artifacts arising from the ethanol extraction [29].

From the roots of *Salvia apiana*, 16-hydroxyroyleanone **27** was reported for the first time with a proposed biogenetic pathway, a route to highly oxidized abietatrienes [30].

A new royleanone with a lactone δ from *Salvia sessei* was named as sessein (7α-acetyl-12-hydroxyabieta-8,12-diene-11,14-dione-19,20-δ-lactone) **28** [31]. From the aerial parts of *Salvia regla*, besides sessein **28**, the deacetylsessein **29** and 19-hydroxy-7α-acetoxyroyleanone **30** (an isomer of the 20-hydroxy-7α-acetoxyroyleanone **24** isolated from *Salvia lanata*) were also isolated [32]. In 1995, 19-dihydro-deacetylsessein **31**, was identified from *Salvia candicans*, as an isomer of conacytone **22** [27].

8,9-Epoxy-7-oxoroyleanone methyl ether **32**, a compound obtained from *Taiwania cryptomerioides*, was able to be semi-synthetized using 7-hydroxyroyleanone as starting material [33].

In 1999, *Salvia nutans* afforded three novel 12-deoxyroyleanones (see structure **33**), 12-deoxy-6,7-dehydroroyleanone **34**, 12-deoxy-6-hydroxy-6,7-dehydroroyleanone **35** and 12-deoxy-7,7-dimethoxy-6-ketoroyleanone **36** [34]. 12-Deoxy-royleanone **33** was isolated from a natural source for the first time in 2002 from *Salvia cilicica* [35]. Moreover, hypargenin F (5-

hydroxy-6,7-dehydroroyleanone) **37**, a compound isolated from *Salvia hypargeia*, has an additional tertiary hydroxyl located at C-5 [36].

The synthesis of the derivative, royleanone 12-methyl ether **38** was previously reported, but it was isolated for the first time from Nature, later in 2009 from *Salvia barrelieri* [37].

Furthermore, agastaquinone **39**, a cytotoxic diterpenoid quinone, was isolated in 1995 for the first time, from *Agastache rugosa* [38].

In 1988, the new diterpene canariquinone **40** was isolated from the flowers of *Salvia canariensis* [39]. The formation of canariquinone **40** was suggested throught oxidations and nucleophilic additions indicating as intermediate an methylene quinone [39]. A new abietane quinone, atuntzensin A **41**, was isolated for the first time from *Isodon grandifolia* [40]. This compound structure is similar to canariquinone **40**, but atuntzensin A **41** has a hydroxyl group at 7α position instead of an ethoxyl group in **40** [40].

Columbaridione **42**, a novel quinone compound with a (20→7)lactone group on an unrearranged abietane diterpene, was discovered from the aerial parts of *Salvia columbariae* [41].

More recently in 2012, a new abietane quinone, named xantoquinone **43**, was reported from *Salvia xanthocheila* [42].

Miltionone I **44**, is a 20-*nor*-abietane diterpenoid having a 2-hydroxy-1,4-naphthaquinone moiety substitution pattern, found in *Salvia miltiorrhiza* [43].

A compound found in *Salvia regla*, reglin (deacetyloxysessein-7α-(3β-hydroxy-olean-12-en-28-oate)) **45**, is an abietane quinone diterpene with similar signals spectrum to sessein **28**, although the 7'-OH group was not esterified by the acetic acid, but by the triterpenoid 3β-hydroxyolean-12-en-28-oate (see reglin **45** structure) [44]. This compound **45** could be an artifact, however, when a solution of ethyl acetate of a mixture of ursolic and oleanolic acids and deacetylsessein **29** was stirred in acidic medium, no reglin was found [44].

12-Deoxy derivative of danshenxinkun B **46** was isolated from *Salvia glutinosa*, 20 years later from the discovery of danshenxinkun A **47** and B **48** in 1976 [45]. The oleoyl danshenxinkun A **47** was also isolated, as a minor compound, in *Salvia miltiorrhiza* [46].

From two unclassified *Plectranthus* species from Abyssinia, Eugster and co-workers isolated several known royleanone type compounds, and the 6β,7α-dihydroxyroyleanone **49** [47]. These plants were later re-examined which allowed the discovery of the novel 8α,9α-epoxy-7-oxoroyleanone **50**, being the first diterpenoid epoxyquinone ever isolated [48].

From leaf-glands of the South-African *Plectranthus myrianthus* (*Plectranthus hereroensis*), the novel 7α-formyloxy-6β-hydroxyroyleanone **51** was found [49] and that was the first record of a co-occurrence of coleons and royleanones in the same plant.

In 1979, the 6β-hydroxyroyleanone **52**, isolated for the first time from a natural source, and the novel 7α-acetyloxy-6β,20-dihydroxyroyleanone **53**, were isolated from *Coleus carnosus* (*Plectranthus amboinicus*), along with other royleanone and coleon compounds [50].

Additionally, more novel dimeric compounds named grandidones were isolated from *Plectranthus grandidentatus*, *Plectranthus myrianthus* and *Coleus carnosus* (*Plectranthus amboinicus*) [51]. Both grandidone A **54** and 7-epigrandidone A **55,** as well as, grandidone B **56** and 7-epigrandidone B **57** are C-7 acetals of 6,7-dioxoroyleanone with catecholes of coleons [51]. The unstable grandidone C **58** is a C_7-$C_{7'}$ linked *bis*-6-oxoroyleanone with C_2-symmetry. Grandidone D **59** and 7-epigrandidone D **60** are described [51] as spiro-dihydrofurans formed from grandidone C **58** and the absolute configuration of all dimers was established by partial syntheses [51].

The red leaf-glands of *Plectranthus argentatus* allowed the isolation of coleon U quinone **61**, previously semi-synthetized, besides the 8α,9α-epoxycoleon-U-quinone **62** and 6β-formyloxy-7α-hydroxyroyleanone **63** [52].

Recently, two new diterpene quinones with typical abietane structure, namely 7α,19-diacetoxy-royleanone **64** and 7α-methoxy-19-acetoxy-royleanone **65** were isolated from *Salvia corrugata*, together with the new 7-dehydroxy-conacytone **66** [53].

The antioxidant 7-oxoroyleanone-12-methyl ether **67**, which was previously synthesized [54], was elucidated as a new natural abietane quinone from *Salvia barrelieri* [55]. Moreover, the roots of *Salvia napifolia* yielded the designated 7,20-epoxyroyleanone **68** [56].

Cryptoquinone **69**, a new cytotoxic and antifungal compound was isolated from *Cryptomeria japonica* [57]. Additionally, the cytotoxic 7*β*-hydroxy-11,14-dioxoabieta-8,12-diene **70** was isolated from *Hyptis martiusii* [58].

Two compounds that resembles horminone **7**, 12-methyl-5-dehydrohorminone **71** and 12-methyl-5-dehydroacetylhorminone **72** were isolated *Salvia multicaulis* [59].

In 1992, both triptoquinone A **73** and B **74** were elucidated by spectroscopic methods from *Tripterygium wilfordii* [60]. In addition, *Dracocephalum komarovi* allowed the isolation of dracocequinone A **75** and its 19-keto derivative, dracocequinone B **76** with an ester carbonyl at C-19 [61].

Other royleanones have been isolated namely, royleanonic acid **77**, isolated from *Salvia plebeia* [62] and *Rosmarinic officinalis* [63], 7α-acetoxyroyleanone-12-methyl ether **78** isolated

from *Hyptis verticillata* [64] and *Salvia barrelieri* [55], 16-acetoxy-7α-hydroxyroyleanone **79** from *Isodon lophanthoids* [65] and *Plectranthus hereroensis* [66], [67] and 16-acetoxy-7α-methoxyroyleanone **80** isolated from *Isodon lophanthoides* [18] and *Isodon lophanthoids* [65].

The subsequent Table 1 comprises royleanones and related-royleanone compounds described in literature covering 1962 to 2014.

Table 1.1 Royleanone natural occurring compounds.

Compound	Plant species [Ref.]	Compound	Plant species [Ref.]
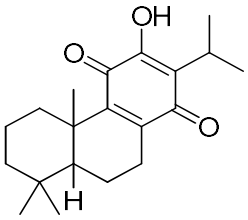 ***Royleanone** 1*	*Inula royleana* DC. [14], [16] *Isodon lophanthoides* (Buch.-Ham. ex D.Don) H.Hara [18] *Taxodium distichum* (L.) Rich. [20] *Salvia aethiopis* L. [28] *Salvia officinalis* subsp. *lavandulifolia* (Vahl) Gams [29] *Salvia nutans* L. [34] *Salvia aethiopis* L. [68] *Salvia barrelieri* Etl.[55] *Salvia phlomoides* Asso [69] *Salvia moorcroftiana* Wall. ex Benth. [70] *Salvia officinalis* L. [71] *Lepechinia chamaedryoides* (Balb.) Epling [72] *Plectranthus grandidentatus* Gürke [67], [73] *Plectranthus amboinicus* (Lour.) Spreng. [50] *Peltodon longipes* A.St.-Hil. ex Benth.[74], [75] Unclassified *Plectranthus* species from Abyssinia [47], [48]	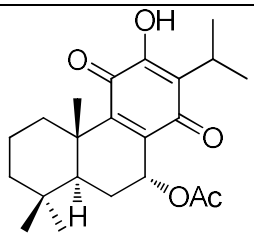 7α-Acetoxyroyleanone ***(or 7-O-acetylhorminone)** 2*	*Inula royleana* DC. [14], [16] *Salvia nemorosa* L. [24] *Salvia pubescens* Benth. [26] *Salvia officinalis* subsp. *lavandulifolia* (Vahl) Gams [29] *Salvia nutans* L. [34] *Salvia barrelieri* Etl.[55] *Salvia phlomoides* Asso [69] *Salvia moorcroftiana* [70], [76] *Salvia officinalis* L. [71] *Salvia chionantha* Boiss. [77] *Salvia kronenburgii* Rech.f. [77] *Salvia xanthocheila* Boiss. ex Benth. [78] *Salvia hypoleuca* Benth. [79] *Salvia blepharochlaena* Hedge & Hub.-Mor. [80] *Plectranthus amboinicus* (Lour.) Spreng. [50] *Hyptis martiusii* Benth. [58] *Peltodon longipes* A.St.-Hil. ex Benth. [74], [75]

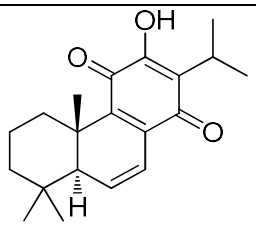 ***6,7-Dehydroroyleanone** 3*	*Inula royleana* DC. [14] *Isodon lophanthoides* (Buch.-Ham. ex D.Don) H.Hara [18] *Lepechinia bullata* (Kunth) Epling [19] *Taiwania cryptomerioides* Hayata [21] *Salvia officinalis* subsp. *lavandulifolia* (Vahl) Gams [29] *Salvia reptans* Jacq. [81] *Plectranthus lanuginosus* (Hochst. ex Benth.) Agnew [82] *Plectranthus grandidentatus* Gürke [73], [83] *Plectranthus forsteri Benth.* 'Marginatus' [84] *Taxodium distichum* (L.) Rich. [85], [86] *Tetradenia riparia* (Hochst.) Codd [87] *Isodon lophanthoides* var. gerardianus [88] *Lepechinia chamaedryoides* (Balb.) Epling [72] *Plectranthus amboinicus* (Lour.) Spreng. [50] Unclassified *Plectranthus* species from Abyssinia [47], [48]
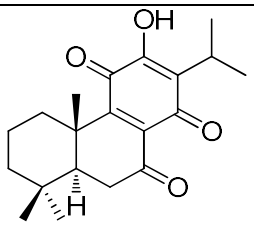 7-Oxoroyleanone ***(or 7-ketoroyleanone)** 4*	*Inula royleana* DC. [16] *Salvia moorcroftiana* Wall. ex Benth. [70] *Peltodon longipes* A.St.-Hil. ex Benth. [74], [75] Unclassified *Plectranthus* species from Abyssinia [47], [48]

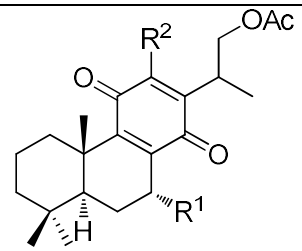 *R^1* *R^2* *5* ***OAc*** ***OH*** *6* ***OH*** ***OAc*** 16-Acetoxy-7-*O*-acetylhorminone **5** 16-Acetoxy-12-*O*-acetylhorminone **6**	*Isodon lophanthoides* (Buch.-Ham. ex D.Don) H.Hara [18]
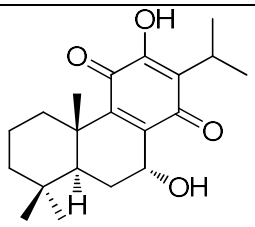 Horminone ***(or 7α-hydroxyroyleanone)*** *7*	*Isodon lophanthoides* (Buch.-Ham. ex D.Don) H.Hara [18] *Lepechinia bullata* (Kunth) Epling [19] *Salvia nemorosa* L. [24] *Salvia moorcroftiana Wall. ex Benth.* [70] *Salvia hypargeia* Fisch. & C.A.Mey. [36] *Salvia nutans L.* [34] *Salvia barrelieri* Etl. [55] *Salvia sahendica* Boiss. & Buhse [89] *Salvia chionantha* Boiss. [77] *Salvia kronenburgii* Rech.f. [77] *Salvia blepharochlaena* Hedge & Hub.-Mor. [80] *Salvia reptans* Jacq. [81] *Salvia officinalis* L. [71] *Salvia viridis* L. [90] *Taiwania cryptomerioides* Hayata [91] *Lepechinia chamaedryoides* (Balb.) Epling [72] *Plectranthus amboinicus* (Lour.) Spreng. [50] *Plectranthus hereroensis* Engl. [66], [67], [92] *Plectranthus grandidentatus* Gürke [67], [73], [83] *Plectranthus sanguineus* Britten [93] *Peltodon longipes* A.St.-Hil. ex Benth. [74], [75] Unclassified *Plectranthus* species from Abyssinia [47], [48]

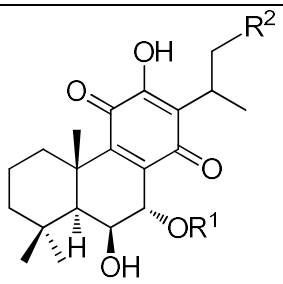

R¹ *R²*

8 ***Me*** ***OAc***

9 ***Ac*** ***OAc***

10 ***Ac*** ***OH***

11 ***Et*** ***OH***

12 ***H*** ***OAc***

13 ***Et*** ***OAc***

Lophanthoidin A **8**
Lophanthoidin B **9**
Lophanthoidin C **10**
Lophanthoidin D **11**
Lophanthoidin E **12**
Lophanthoidin F **13**

Isodon lophanthoides (Buch.-Ham. ex D.Don) H.Hara [17]

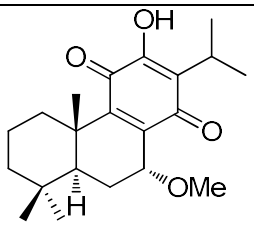

7-O-Methylhorminone *14*

Lepechinia bullata (Kunth) Epling [19]

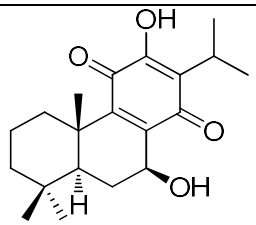

Taxoquinone
(7β-hydroxyroyleanone) *15*

Taxodium distichum (L.) Rich. [20]
Taiwania cryptomerioides Hayata [91]
Salvia moorcroftiana Wall. ex Benth. [70]
Lepechinia chamaedryoides (Balb.) Epling [72]
Metasequoia glyptostroboides Hu & W.C.Cheng [94]–[96]
Unclassified *Plectranthus* species from Abyssinia [47], [48]

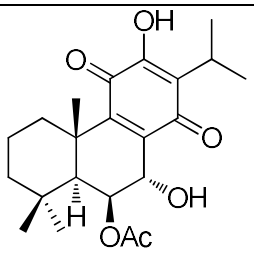

6β-Acetoxy-7α-hydroxyroyleanone *16*

Taiwania cryptomerioides Hayata [21], [97], [98]

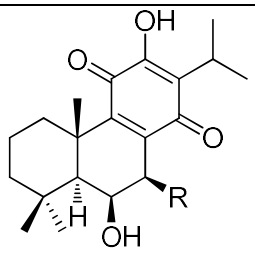 *17* ***R = OH*** *18* ***R = OAc*** 6β,7β-Dihydroxyroyleanone **17** 7β-Acetoxy-6β-hydroxyroyleanone **18**	*Plectranthus hadiensis* (Forssk.) Schweinf. ex Sprenger [22] *Plectranthus forsteri* Benth. 'Marginatus' [84] *Plectranthus madagascariensis* (Pers.) Benth. [99]
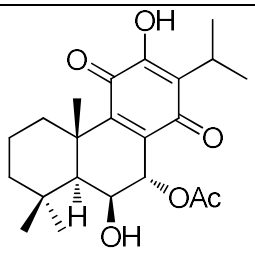 ***7α-Acetoxy-6β-hydroxyroyleanone*** *19*	*Plectranthus hadiensis* (Forssk.) Schweinf. ex Sprenger [22] *Plectranthus amboinicus* (Lour.) Spreng. [50] *Plectranthus argentatus* S.T.Blake [52] *Plectranthus sanguineus* Britten [93] *Plectranthus grandidentatus* Gürke [67], [73], [83], [100], [101] Unclassified *Plectranthus* species from Abyssinia [47], [48]
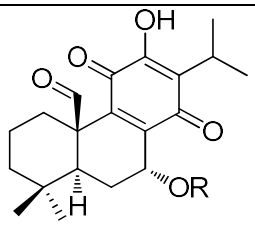 *20* ***R = Ac*** *21* ***R = H*** Nemorone **20** Desacetylnemorone **21**	**20 -** *Salvia nemorosa* L. [24] *Salvia pubescens* Benth. [26] **21** - *Salvia nemorosa* L. [23] *Salvia pubescens* Benth. [26]
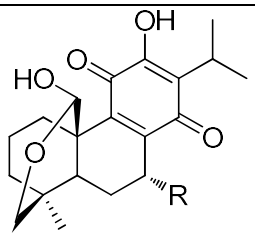 *22* ***R = OH*** *23* ***R = OMe*** Conacytone **22** 7α-*O*-Methylconacytone **23**	**22 -** *Salvia ballotiflora* Benth. [25] *Salvia pubescens* Benth. [26] *Salvia candicans* M.Martens & Galeotti [27] **23** - *Salvia candicans* M.Martens & Galeotti [27] *Salvia corrugata* Vahl [53] *Salvia pubescens* Benth. [102]
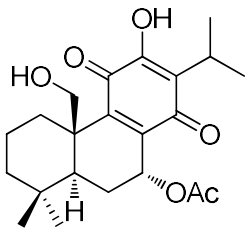 ***20-Hydroxy-7α-acetoxyroyleanone*** *24*	*Salvia aethiopis* L. [28]
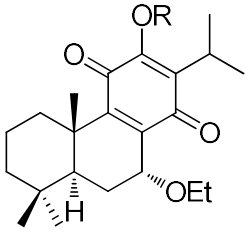 *25* ***R = H*** *26* ***R = Me*** 7α-Ethoxyroyleanone **25** 7α-Ethoxy-12-*O*-methylroyleanone **26**	**25** - *Salvia officinalis* subsp. *lavandulifolia* (Vahl) Gams [29] *Peltodon longipes* A.St.-Hil. ex Benth. [75] **26** - *Salvia officinalis* subsp. *lavandulifolia* (Vahl) Gams [29]

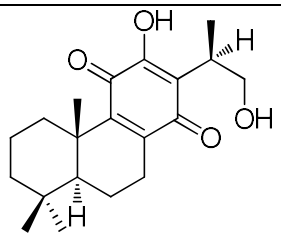

Salvia apiana Jeps. [30]

16-Hydroxyroyleanone *27*

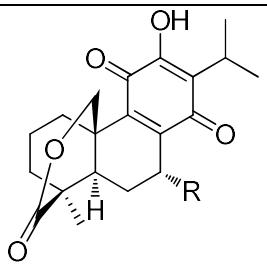

28 - *Salvia sessei* Benth. [31]
Salvia regla Cav. [32], [44]

29 - *Salvia regla* Cav. [32], [44]

28 ***R = OAc***

29 ***R = OH***

Sessein **28**
Deacetylsessein **29**

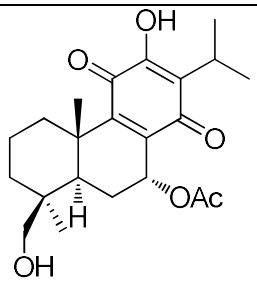

Salvia regla Cav. [32]

19-Hydroxy-7α-acetoxyroyleanone *30*

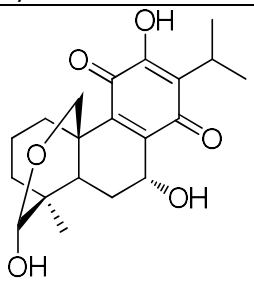

Salvia candicans M.Martens & Galeotti [27]

19-Dihydro-deacetylsessein *31*

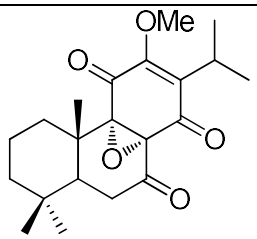

Taiwania cryptomerioides Hayata [33]

8,9-Epoxy-7-oxoroyleanone methyl ether *32*

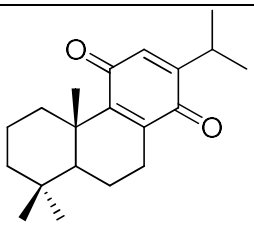

Salvia cilicica Boiss*.* [35]

12-Deoxyroyleanone *33*

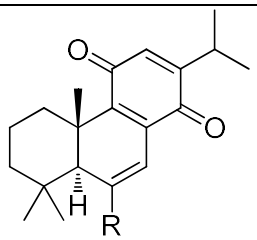

Salvia nutans L. [34]

34 ***R = H***

35 ***R = OH***

12-Deoxy-6,7-dehydroroyleanone **34**
12-Deoxy-6-hydroxy-6,7-dehydroroyleanone **35**

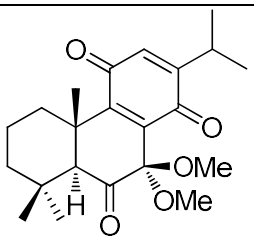

Salvia nutans L. [34]

12-Deoxy-7,7-dimethoxy-6-ketoroyleanone *36*

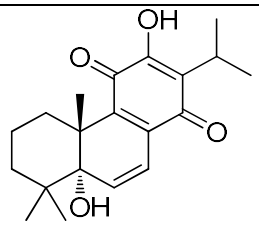 Hypargenin F ***(or 5-hydroxy-6,7-dehydroroyleanone)*** *37*	*Salvia hypargeia* Fisch. & C.A.Mey. [36]
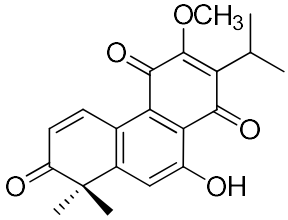 ***Agastaquinone,*** *39*	*Agastache rugosa* (Fisch. & C.A.Mey.) Kuntze [38], [103]
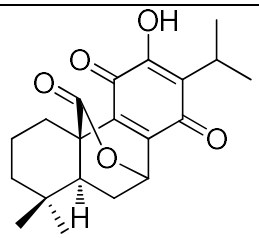 ***Columbaridione,*** *44*	*Salvia columbariae* Benth. [41] *Salvia officinalis* L. [104], [105]
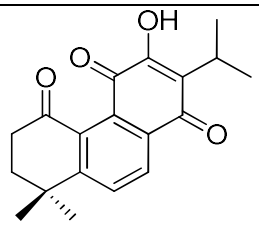 ***Miltionone I*** *46*	*Salvia miltiorrhiza* Bunge [43]
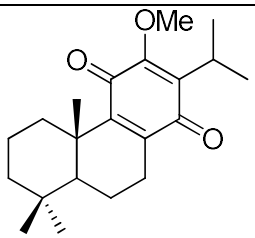 ***Royleanone 12-methyl ether*** *38*	*Salvia barrelieri* Etl. [37]
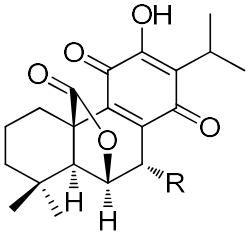 **40** R = OEt **41** R = OH Canariquinone **42** Atuntzensin A **43**	**40** – *Salvia canariensis* L. [39] **41** – *Isodon grandifolia* var. atuntzensis [40] *Salvia officinalis* L. [104], [105]
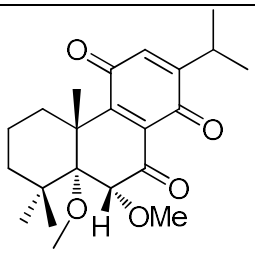 ***Xantoquinone,*** *45*	*Salvia xanthocheila* Boiss. ex Benth. [78]
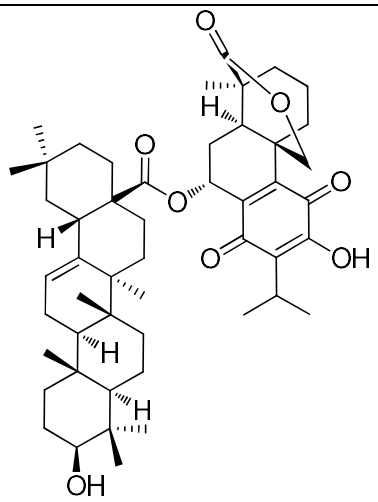 ***Reglin*** *47*	*Salvia regla* Cav. [44]

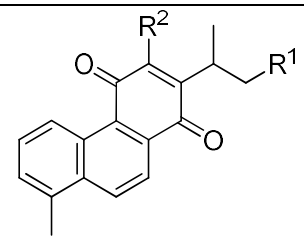

R¹ *R²*

48 ***H*** ***H***

49 ***OH*** ***OH***

50 ***H*** ***OH***

12-Deoxydanshenxinkun B, **46**
Danshexinkun A (and Oleoyl), **47**
Danshenxinkun B, **48**

46 – *Salvia glutinosa* L. [45]

47 – *Salvia miltiorrhiza* Bunge [46], [106]

48 – *Salvia miltiorrhiza* Bunge [43], [107]
Salvia glutinosa L. [45]

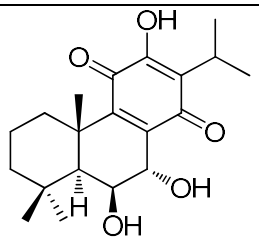

6β,7α-Dihydroxyroyleanone, *51*

Plectranthus amboinicus (Lour.) Spreng. [50]
Unclassified *Plectranthus* species from Abyssinia [47], [48]
Plectranthus hereroensis Engl. [49]
Plectranthus argentatus S.T.Blake [52]
Plectranthus edulis Agnew [108]
Plectranthus sanguineus Britten [93]
Plectranthus sp. from Rwanda [109]
Plectranthus grandidentatus Gürke [67], [83], [101], [110]

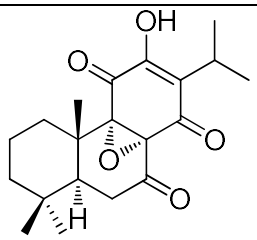

8α,9α-Epoxy-7-oxoroyleanone, *52*

Unclassified *Plectranthus* species from Abyssinia [48]

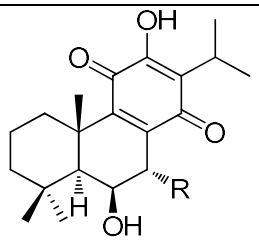

R¹ *R²*

53 ***Me*** ***OCHO***

54 ***Me*** ***H***

55 ***CH_2OH*** ***OAc***

7α-Formyloxy-6β-hydroxyroyleanone
(or 7-O-formylhorminone), *56*

6β-Hydroxyroyleanone, *57*

7α-Acetyloxy-6β,20-dihydroxyroyleanone, *58*

51 – *Plectranthus hereroensis* Engl. [49]
Plectranthus argentatus S.T.Blake [52]
Plectranthus sanguineus Britten [93]

52 – *Plectranthus amboinicus* (Lour.) Spreng. [50]
Plectranthus sanguineus Britten [93]
Plectranthus grandidentatus Gürke [67], [73]

53 – *Plectranthus amboinicus* (Lour.) Spreng. [50]

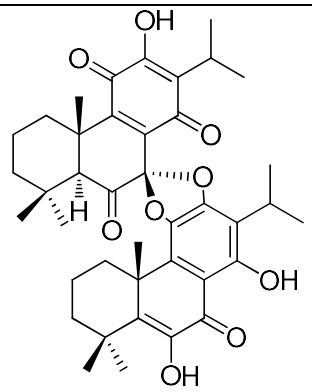

Grandidone A, *59*

Plectranthus hereroensis Engl. [51]
Plectranthus sanguineus Britten [93]
Plectranthus grandidentatus Gürke [51], [101], [110]

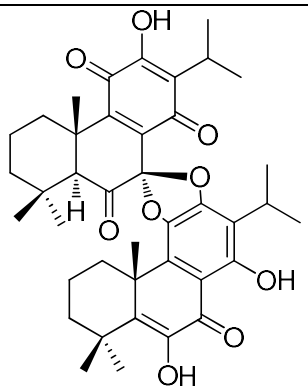

7-Epigrandidone A, *60*

Plectranthus grandidentatus Gürke [51]
Plectranthus hereroensis Engl. [51]
Plectranthus sanguineus Britten [93]

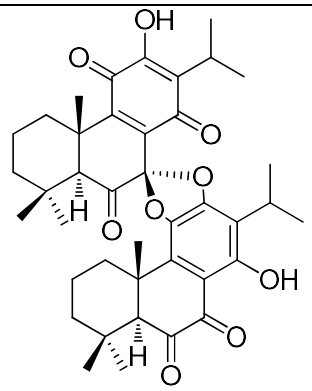 ***Grandidone B,*** *61*	*Plectranthus grandidentatus* Gürke [51] *Plectranthus amboinicus* (Lour.) Spreng. [51] *Plectranthus sanguineus* Britten [93]
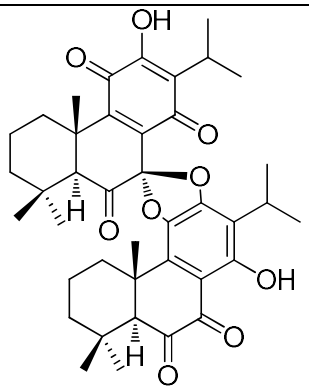 ***7-Epigrandidone B,*** *62*	*Plectranthus grandidentatus* Gürke [51] *Plectranthus amboinicus* (Lour.) Spreng. [51] *Plectranthus sanguineus* Britten [93]
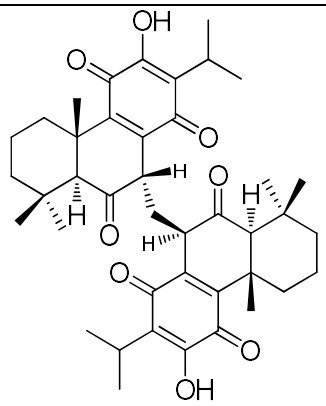 ***Grandidone C,*** *63*	*Plectranthus grandidentatus* Gürke [51], [73]
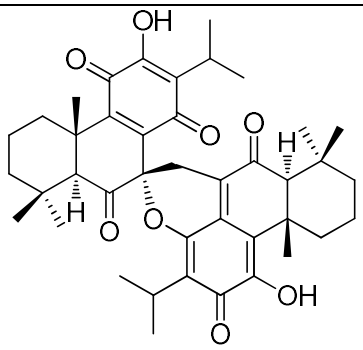 ***Grandidone D,*** *64*	*Plectranthus grandidentatus* Gürke [51], [73]
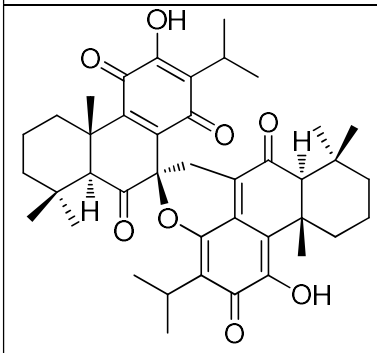 ***7-Epigrandidone D,*** *65*	*Plectranthus grandidentatus* Gürke [51], [73]
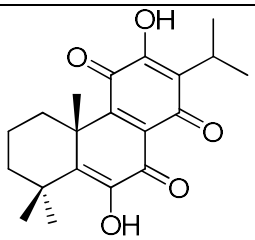 ***Coleon U quinone,*** *66*	*Plectranthus argentatus* S.T.Blake [52] *Plectranthus sanguineus* Britten [93] *Plectranthus madagascariensis* (Pers.) Benth. [99] *Plectranthus forsteri* Benth. 'Marginatus' [111]
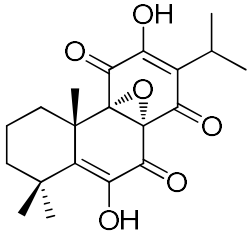 ***8α,9α-Epoxycoleon-U-quinone,*** *67*	*Plectranthus argentatus* S.T.Blake [52] *Plectranthus sanguineus* Britten [93]
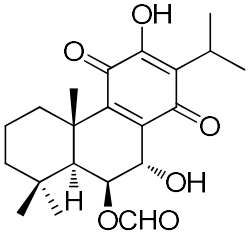 ***6β-Formyloxy-7α-hydroxyroyleanone,*** *68*	*Plectranthus argentatus* S.T.Blake [52] *Plectranthus sanguineus* Britten [93]

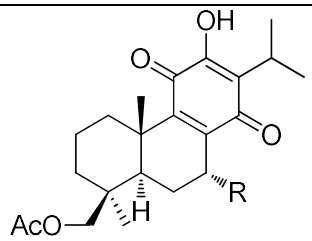 *69* ***R = OMe*** *70* ***R = OAc*** 7α,19-Diacetoxy-royleanone, **64** 7α-Methoxy-19-acetoxy-royleanone, **65**	*Salvia corrugata* Vahl [53]
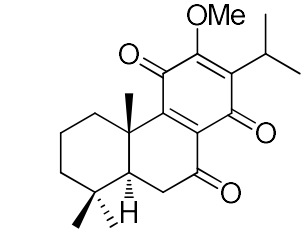 ***7-Oxoroyleanone-12-methyl ether,*** *72*	*Salvia barrelieri* Etl. [55]
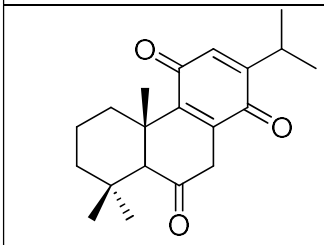 ***Cryptoquinone,*** *74*	*Cryptomeria japonica* (Thunb. ex L.f.) D.Don [57]
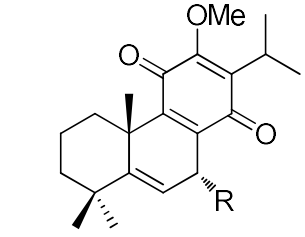 *76* ***R = OH*** *77* ***R = OAc*** 12-Methyl-5-dehydrohorminone, **71** 12-Methyl-5-dehydroacetylhorminone, **72**	*Salvia multicaulis* Vahl [59]
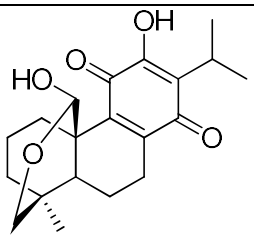 ***7-Dehydroxy-conacytone,*** *71*	*Salvia corrugata* Vahl [53]
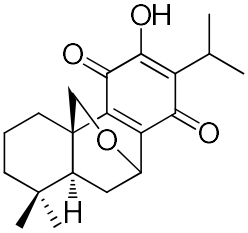 ***7,20-Epoxyroyleanone,*** *73*	*Salvia napifolia* Jacq. [56] *Lepechinia chamaedryoides* (Balb.) Epling [72]
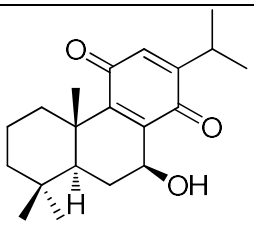 ***7β-Hydroxy-11,14-dioxoabieta-8,12-diene,*** *75*	*Hyptis martiusii* Benth.[58]
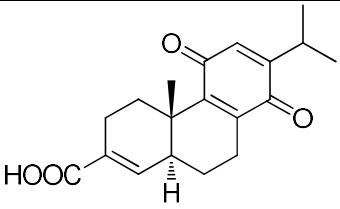 ***Triptoquinone A,*** *78*	*Tripterygium wilfordii* var regelil [60], [112]

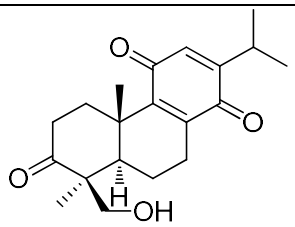 ***Triptoquinone B,*** *79*	*Tripterygium wilfordii* var regelil [60]	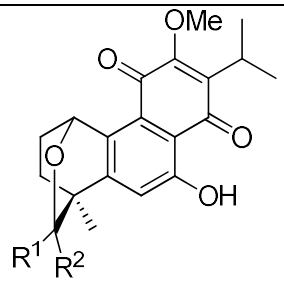 *80* ***R¹=R² = H*** *81* ***R¹,R² = =O*** Dracocequinone A, **75** Dracocequinone B, **76**	*Dracocephalum komarovii* Lipsky [61]
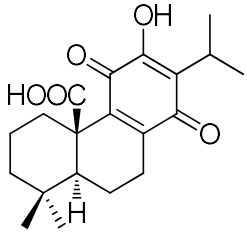 ***Royleanonic acid,*** *82*	*Salvia plebeia* R.Br. [62] *Rosmarinus officinalis* L. [63]	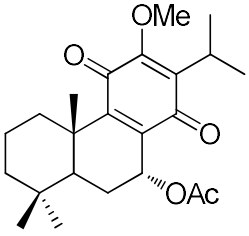 7α-Acetoxyroyleanone-12-methyl ether ***(or 7-acetylhorminone-12-methyl ether),*** *83*	*Salvia barrelieri* Etl. [55] *Hyptis verticillata* Jacq. [64]
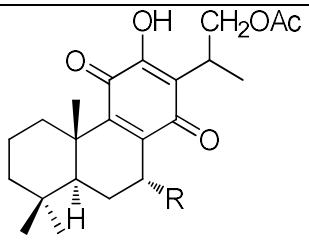 *84* ***R = OH*** *85* ***R = OMe*** 16-Acetoxy-7α-hydroxyroyleanone, **79** 16-Acetoxy-7α-methoxyroyleanone, **80**	**79** – *Plectranthus hereroensis* Engl. [66], [67] *Isodon lophanthoids* var. micranthus [65] **80** – *Isodon lophanthoides* (Buch.-Ham. ex D.Don) H.Hara [18] *Isodon lophanthoids* var. micranthus [65]		

1.4 Rearranged royleanones

A large group of diterpenoid quinones have been isolated with rearranged skeletons. Further abietanes, including some with a seco ring A structures, *abeo*-abietanes and also other related diterpenoid quinones, will be described and their structures are presented in Table 2 and Table 3.

1.4.1 *Seco*-abietanes

Seco ring A structures of abietane diterpenes have been isolated and described in literature (Table 2). The biosynthesis of *seco*-compounds **81**-**85** through an acid catalyzed migration of the 10-methyl group proposed [113] explains the presence of the methyl group at

C-5 and not at C-10, as it is in the abietane skeleton. In 1984, salvipisone **81** was isolated from *Salvia aethiopis*, and its structure was confirmed by an oxidation with hydrogen peroxide in acetic acid [68]. This compound **81** was later found in *Salvia argentea* and *Salvia sclarea* [114]–[117]. 12-Deoxy-salvipisone **82**, is lacking an hydroxy group at C-12 in comparison with salvipisone **81**, and was established from *Zhumeria majdae* [118], and 2,3-dehydrosalvipisone **83** was found in *Salvia sclarea* [119]. In 2006, the 12-deoxy-salvipisone **82** and its isomer sahandinone **84** was reported for the first time as a natural product, from *Salvia sahendica* [75], [89].

Salvia prionitis allowed the discovery of a new *seco*-abietane compound. 4-Hydroxy-sapriparaquinone **85** is resultant from the corresponding quinone methide abietane diterpenoid through an acid-catalyzed migration of the l0-methyl group to C-5 complemented by a fission of ring A [113].

The analysis of *Plectranthus edulis* led to the identification of the coleon A **86**, coleon A lactone **87** and a naphthoquinone **88** [108].

Table 1.2 *Seco*-abietane quinones natural occurring compounds

Compound	**Plant species [Ref.]**	**Compound**	**Plant species [Ref.]**
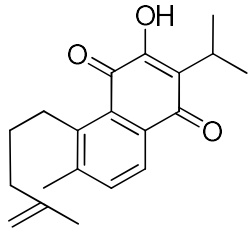 Salvipisone, **81**	*Salvia aethiopis*[68] *S. argentea* [114]–[117] *S. sclarea* L. [114]–[117]	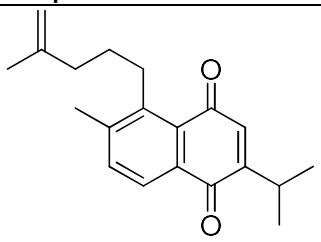 12-Deoxy-salvipisone, **82**	*Zhuraeria majdae* Rech[118] *Salvia sahendica* Boiss. & Buhse[75], [89]
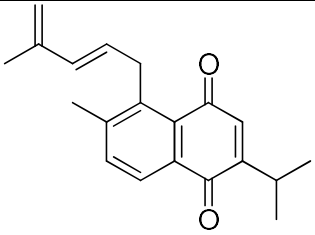 2,3-Dehydrosalvipisone U, **83**	*S. sclarea*[119]	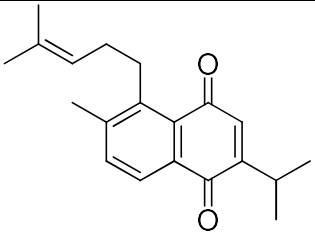 Sahandinone, **84**	*Salvia sahendica* Boiss. & Buhse[75], [89]

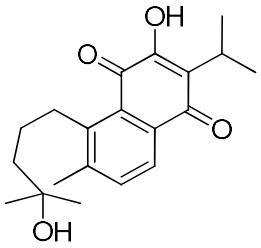 4-Hydroxy-sapriparaquinone, **85**	*Salvia prionitis*[113]
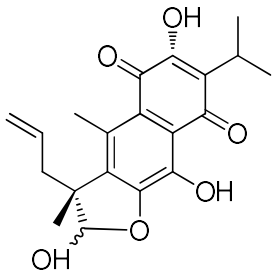 Coleon A, **86**	*Plectranthus edulis* (Vatke) T.T. AYE[108]
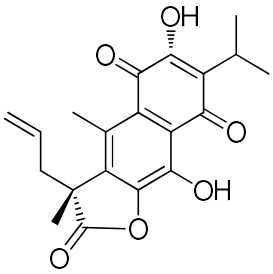 Coleon A Lactone, **87**	*Plectranthus edulis* (Vatke) T.T. AYE[108]
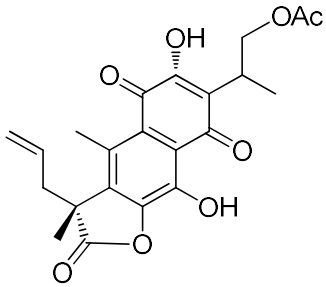 Naphthoquinone, **88**	*Plectranthus edulis* (Vatke) T.T. AYE[108]

1.4.2 *Abeo*-abietanes

Abeo-abietanes is another type of rearranged abietane skeleton found in literature. The isolated structures have 6-5-6 rings skeletons but also 6-7-6 fused-rings skeletons are described and found in Nature (Table 3). Rearranged abietane compounds with an uncommon skeleton of fused 6-5-6 rings were primarily found in *Taiwania cryptomerioides* by Cheng's group [91]. The fused-rings skeleton of taiwaniaquinone A **89** and its 7-hydroxylated derivatives taiwaniaquinone B **90** and C **91**, were apparently biogenetically formed from the pinacol rearrangement of abietane-6,7-diol [91]. Taiwaniaquinone D **92** and taiwaniaquinone E **93** were later isolated by Cheng *et al.* from the same plant [120]. In 2003, a novel 5(6→7)*abeo*abietane type compound, taiwaniaquinone F **94**, was elucidated from the bark of *Taiwania cryptomerioides*, being a taiwaniaquinone A **89** methyl ether derivative [121].

From the root of *Salvia dichroantha* it was reported the isolation and structure elucidation of a novel diterpene designated as dichroanone **95** with a rearranged abietane skeleton with 6-5-6 fused tricyclic skeletons [122].

The 6-5-6-membered ring system is a unique skeleton and only a few compounds with this tricyclic ring systems structure have been reported.

Icetexone **96** and anastomosine **97**, two icetexane diterpenes with a *trans*-19,6-olide function, were isolated from *Salvia candicans* [27]. Later, from *Salvia pubescens*, the 19(*R*)-acetoxy-19-deoxoicetexone **98**, other icetexane with a cyclic ketalic moiety and a quinone

system, was established [102]. Also, other new icetexane diterpene, komaroviquinone **99**, was found in *Dracocephalum komarovii* [123].

Two highly oxidized diterpene quinones, fruticulin A **100** and demethyl-fruticulin A **101** were found in *Salvia fruticulosa* [124], [125]. These compounds may be biogenetically related to icetexone **96** [124], [125]. Recently, fruticulin C **102** was isolated from *Salvia corrugata* [53].

From *Plectranthus sanguineus*, a novel tricyclic, seven-membered anhydride compound, sanguinone A **103**, was isolated [93].

1.4.3 Other abietane quinones

Other naturally occurring royleanone related skeletons have been described along the literature.

Recently, a new rearranged abietane quinone has been reported from *Salvia przewalskii* [126]. Salviskinone A **104** has the methyl group at C-10 in abietane skeleton, shifted to the C-5 position and a plausible biogenetic pathway was proposed where the probable precursor may be hypargenin F **37** or its isomer. The absolute stereochemistry of **104** was not determined, but the proposed biosynthetic path allows to suggest that the only asymmetric center configuration of C-5 is *R* [126].

A novel diterpene quinone with rearranged abietane skeleton, aegyptinones B **105**, was isolated from *Salvia aegyptiaca* roots [127]. Biosynthetically, the novel aegyptinone B **105** may arise from 6,7-dehydroroyleanone **3**, frequently found in *Salvia* species [127]. Few years later, the 12,16-dideoxy-aegyptinone B **106**, with a less hydroxy groups at C-12 and C-16 comparing to aegyptinone B **105**, was isolated from *Zhumeria majdae*, and a biosynthetic pathway, with methyl and/or alkyl shifts from an abietane derivative, was proposed for the formation of 12,16-dideoxy-aegyptinone B **106** and 12-deoxy-salvipisone **82** [118].

Isodon coetsa, a plant used in traditional Chinese folk medicine led to the isolation of two rearranged abietane derivatives, with a 2-hydroxyl propyl group linked to the C-13 position. These two abietanes containing a different side chain at the C-13 position, sincoetsin A **107** and sincoetsin B **108**, differs from each other in a methyl group at the C-7-*O* position [128].

Rüedi and Eugster group have identified a large number of diterpenoids from *Plectranthus* and *Coleus* species, many of which quinonoid compounds, that will be here described [129]–[133]. Coleon G **109** and Coleon J **110**, possessing an enedione chromophore, were isolated from *Coleus somaliensis* (*Plectranthus lanuginosus*) [130], [131]. *Plectranthus caninus* allowed the isolation of the new *spiro*-cyclopropyl-cyclohexendion-diterpenes, the

coleons M **111**, N **112**, P **113**, Q **114**, R **115** and barbatusin **116**, and from the *Coleus somaliensis* (*Plectranthus lanuginosus*) the novel coleon O **117** [134].

Nine new royleanones and coleons compounds were established for the first time from *Coleus coerulescens* (*Plectranthus barbatus*), that is 7,12-bis(*O*-desacetyl)-coleon N **118**; 12-*O*-desacetyl-coleon N **119** (major compound); 6,12-bis (*O*-desacetyl)-coleon R **120**; 12-*O*-desacetyl-coleon R **121**; coleon Y **122** (major compound); 3-*O*-desacetyl-3-*O*-formyl-coleon Y **123** (major compound); bis(*abeo*)-royleanone **124**; di-*abeo*-7α-methoxy-royleanone **125**; and di-*abeo*-3α,18-diacetoxy-royleanone **126**. This work suggests that the opening of the cyclopropane-ring by the solvent followed by tautomerisation, oxidation to hydroxy-*p*-benzoquinones or elimination to quinomethanes and subsequent nucleophilic attack of the solvent leads to compounds with a 2'-substituted propyl group at C (13) [135].

Novel Coleon Z **127** and derivatives: 12β-*O*-acetyl-coleon Z **128**, 12β-*O*-acetyl-7-*O*-formyl-7-*O*-desacetyl-coleon Z **129**, 12β-*O*-Acetyl-17-acetoxy-coleon Z **130** and 12β-*O*-acety1-17-formyloxy-coleon Z **131;** coleon Q **114**, N **112**, O **117** and P **113** derivatives: 6-*O*-acetyl-19-acetyloxy-coleon Q **132**, 12-*O*-desacetyl-7-*O*-acetyl-19-acetyloxy-coleon Q **133**, 12-*O*-desacetyl-7-*O*-acetyl-3β, 19-diacetyloxy-coleon Q **134,** 7-desoxy-12-*O*-desacetyl-3-acetyloxy-coleon N **135**, 19-acetyloxy-coleon O **136**, 7-*O*-acetyl-19-acetyloxy-12-*O*-desacetyl-coleon P **137**, 6-*O*-acetyl-17-acetyloxy-12-*O*-desacetyl-coleon P **138** were isolated from *Solenostemon sylvaticus*, *S. monostachys* (*Plectranthus monostachyus*) and *Coleus garckeanus* (*Plectranthus garckeanus*) [136], [137]. Few years later, the structures of coleon Q **114** and coleon P **113** and Z derivatives **127-131** were revised [138].

In 1982, Rüedi and Eugster established from *Plectranthus lanuginosus* novel compounds named lanugones, which structurally belong to the subgroups of royleanones and coleons [82]. Lanugones A **139**, B **140**, C **141**, D **142**, E **143**, F **144**, G **145**, H **146**, I **147**, J **148**, K **149** and K' **150** constitute a wide diverse chromophoric systems and oxydation levels among diterpenoids in a single plant species. The isopropyl group followed the subsequent metabolic stages: isopropyl → hydroxyisopropyl → dihydrofuran and spirocyclopropane → allyl- and 2-hydroxypropyl groups [82].

A novel *abeo*-royleanone (6β,7α-dihydroxy(allyl)royleanone **151**) and four new spirocoleons 12-*O*-desacetyl- coleon Q **152**, 7-*O*-acetyl-12-*O*-desacetil-19-hydroxy-coleon Q **153**, 18-acetoxy-12-*O*-desacetyl-coleon Q **154** and 3,18-Di-*O*-desacetyl-3,18-di-O-formyl-coleon Y **155,** were found in the re-examined *Plectranthus lanuginosus* [139].

The structures of new 1,4-phenanthranquinones named as plectranthons A **156**, B **157**, C **158**, and D **159**, biogenetically derived from abietanoic precursors, were isolated from

Plectranthus sp. from Rwanda. Compounds **156, 157** and **159** were the first natural C_{20}-phenanthrenes of diterpenoid origin [140]. Later, from a *Plectranthus* sp. from the borders of Lake Kiwu (Rwanda), plectranthons E **160**, F **161**, G **162**, H **163**, I **164**, J **165**, K **166** and L **167** were isolated. These highly modified abietanoid compounds have notable features of the hydroxylation pattern and these extensive dehydrogenation and oxygenation reactions probably precede the degradation of the ring system [109].

Fruticulin B **168** was isolated from *Salvia fruticulosa* [124], [125] and the designated 7α,12-dihydroxy-17(15→16)-*abeo*-abieta-8,12,16-triene-11,14-dione **169** was isolated from *Plectranthus hereroensis* [67], [92]. In addition, from the leaf glands of *Plectranthus barbatus* was isolated the spirocoleon plectrin **170** [141].

The analysis of *Plectranthus edulis* led to the identification of numerous new diterpenoids, including novel royleanones **171-174** and spirocoleons **175-186** [108].

The following Table 3 contains the natural occurring rearranged abietane quinones (*abeo*-abietanes and other diterpenoid quinones) described in literature.

Table 1.3 Natural occurring rearranged abietane quinones (*abeo*-abietanes and other diterpenoid quinones) described in literature.

Compound	Plant species [Ref.]	Compound	Plant species [Ref.]
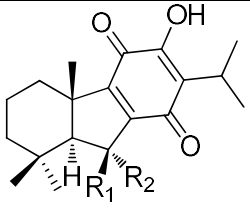 *R¹* *R²* *89* ***H*** ***CHO*** *90* ***OH*** ***CHO*** *91* ***CHO*** ***OH*** Taiwaniaquinone A **89** Taiwaniaquinone B **90** Taiwaniaquinone C **91**	**89** – *Taiwania cryptomerioides Hayata* [91], [121] **90**, **91** – *Taiwania cryptomerioides Hayata* [91]	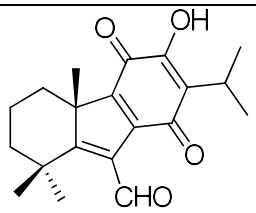 ***Taiwaniaquinone D*** *92*	*Taiwania cryptomerioides* Hayata [120], [121]
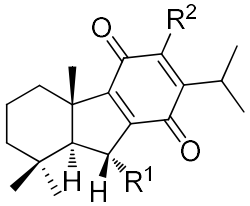 *R¹* *R²* *93* ***COOMe*** ***OH*** *94* ***CHO*** ***OMe*** Taiwaniaquinone E **93** Taiwaniaquinone F **94**	**93** – *Taiwania cryptomerioides Hayata* [120] **94** – *Taiwania cryptomerioides Hayata* [121]	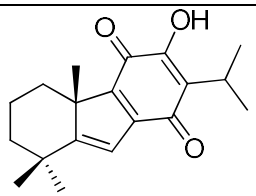 ***Dichroanone*** *95*	*Salvia dichroantha* Stapf [122]
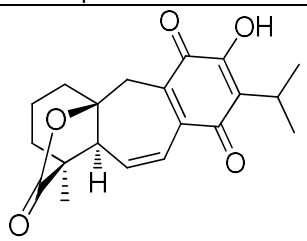 ***Icetexone*** *96*	*Salvia candicans M.Martens & Galeotti* [27] *Salvia pubescens Benth.* [102]	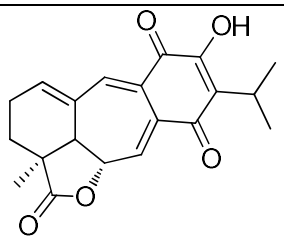 ***Anastomosine*** *97*	*Salvia candicans* M.Martens & Galeotti [27]
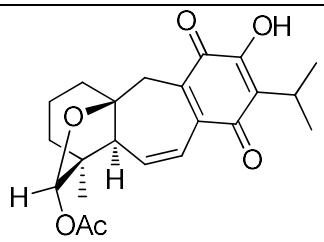 ***19(R)-Acetoxy-19-deoxoicetexone*** *98*	*Salvia pubescens Benth.* [102]	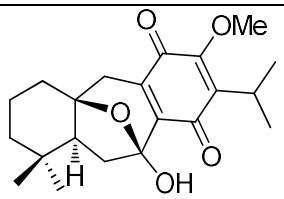 ***Komaroviquinone*** *99*	*Dracocephalum komarovi* Lipsky [61], [123], [142]

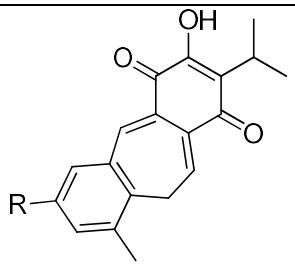

Salvia fruticulosa Benth. [124], [125]
Salvia corrugata Vahl [53]

100 ***R = OCH₃***

101 ***R = OH***

Fruticulin A **100**
Demethyl-fruticulin A **101**

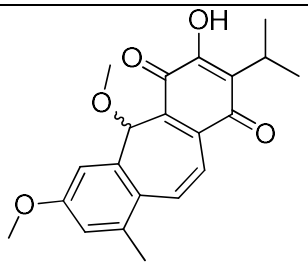

Salvia corrugata Vahl [53]

Fruticulin C *102*

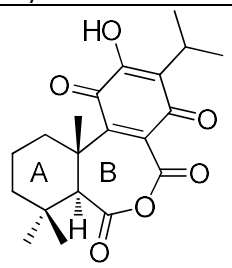

Plectranthus sanguineus Britten [93]

Sanguinone A (A/B *trans*) **103**

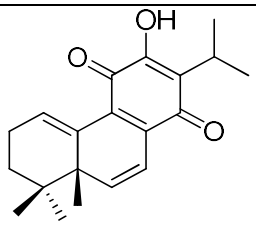

Salvia przewalskii Maxim.[126]

Salviskinone A *104*

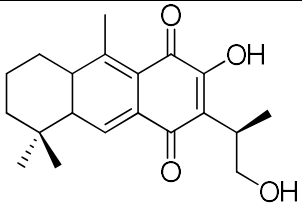

Salvia aegyptiaca L.[127]

Aegyptinone B *105*

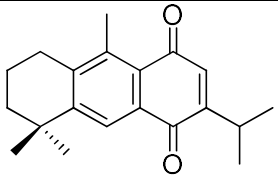

Zhuraeria majdae Rech.f. & Wendelbo [118]

12,16-Dideoxy-aegyptinone B *106*

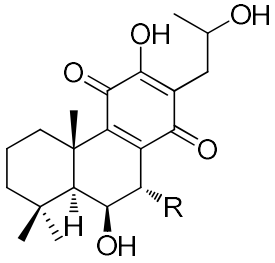

Isodon coetsa (Buch.-Ham. ex D.Don) Kudô [128]

107 ***R = OH***

108 ***R = OMe***

Sincoetsin A **107**
Sincoetsin B **108**

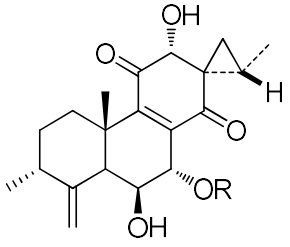

Plectranthus lanuginosus (Hochst. ex Benth.) Agnew [130], [139]

109 ***R = Ac***

110 ***R = H***

Coleon G **109**
Coleon J **110**

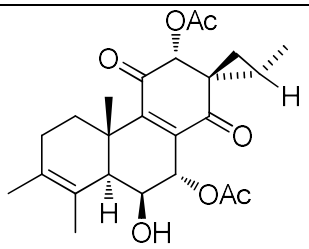 ***Coleon M*** *111*	*Plectranthus caninus Roth* [134]
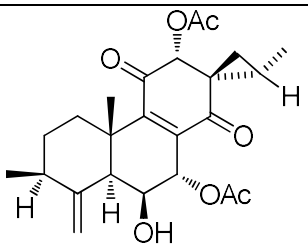 ***Coleon N*** *112*	*Plectranthus caninus Roth* [134]
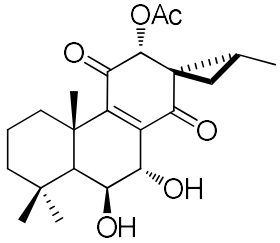 ***Coleon P*** *113*	*Plectranthus caninus Roth* [134]
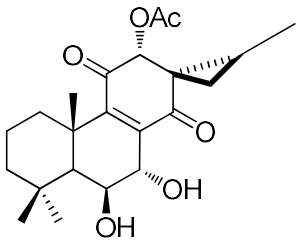 ***Coleon Q*** *114*	*Plectranthus caninus Roth* [134]
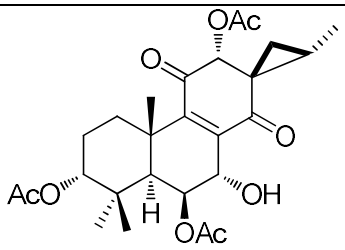 ***Coleon R*** *115*	*Plectranthus caninus Roth* [134]
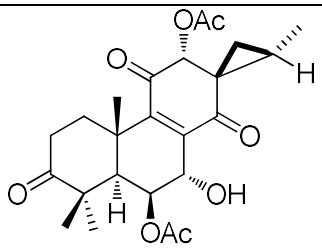 ***Barbatusin*** *116*	*Plectranthus caninus Roth* [134]
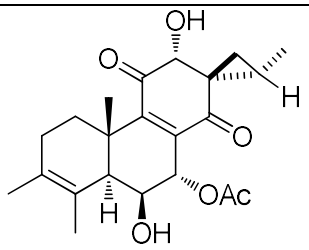 ***Coleon O*** *117*	*Plectranthus lanuginosus (Hochst. ex Benth.) Agnew*[134], [139] *Plectranthus barbatus Andrews* [135] *Solenostemon sylvaticus (Gürke ex Engl.) Agnew* [136] *Plectranthus garckeanus (Vatke) J.K.Morton* [136]
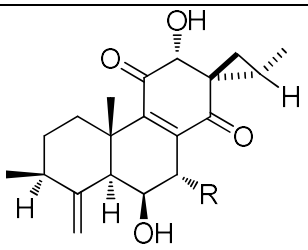 *118* ***R = OH*** *119* ***R = OAc*** 7,12-Bis(*O*-desacetyl)-coleon N **118** 12-*O*-Desacetyl-coleon N **119**	*Plectranthus barbatus Andrews* [135]

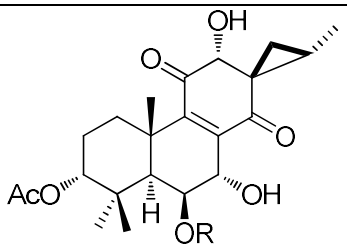 *120* ***R = H*** *121* ***R = CHCH₃*** 6,12-Bis (*O*-desacetyl)-coleon R **120** 12-*O*-Desacetyl-coleon R **121**	*Plectranthus barbatus Andrews* [135]
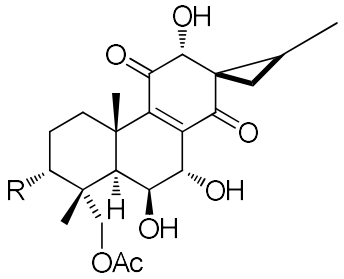 *122* ***R = OAc*** *123* ***R = OCHO*** Coleon Y **122** 3-*O*-Desacetyl-3-*O*-formyl-coleon Y **123**	*Plectranthus barbatus Andrews* [135] *Plectranthus lanuginosus (Hochst. ex Benth.) Agnew* [139]
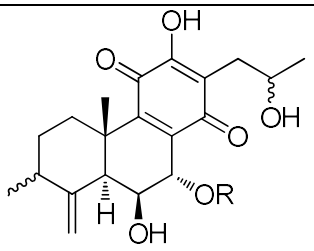 *124* ***R = H*** *125* ***R = Me*** Bis(*abeo*)-royleanone **124** Di-*abeo*-7α-methoxy-royleanone **125**	**124** – *Plectranthus barbatus Andrews* [135], [139] *Plectranthus lanuginosus (Hochst. ex Benth.) Agnew*[139] **125** – *Plectranthus barbatus Andrews* [135]
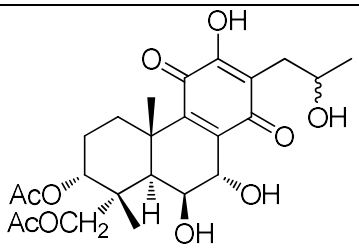 ***Di*-abeo-*3α,18*-diacetoxy-royleanone** *126*	*Plectranthus barbatus Andrews* [135]

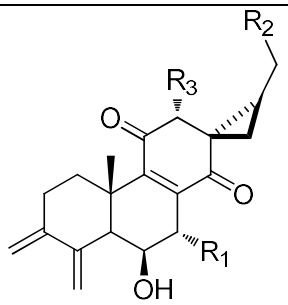

R¹ *R²* *R³*

127 ***OAc*** ***H*** ***OH***

128 ***OAc*** ***H*** ***OAc***

129 ***OCHO*** ***H*** ***OAc***

130 ***OAc*** ***OAc*** ***OAc***

131 ***OAc*** ***OCHO*** ***OAc***

Coleon Z **127**
12β-*O*-Acetyl-coleon Z **128**
12β -*O*-Acetyl-7-*O*-formyl-7-*O*-desacetyl-coleon Z **129**
12β -*O*-Acetyl-17-acetoxy-coleon Z **130**
12β -*O*-Acety1-17-formyloxy-coleon Z **131**

127 – *Solenostemon sylvaticus (Gürke ex Engl.) Agnew* [136]
Plectranthus garckeanus (Vatke) J.K.Morton [136]
Plectranthus edulis Agnew [108]

128-131 – *Plectranthus monostachyus (P.Beauv.) B.J.Pollard* [137], [138]

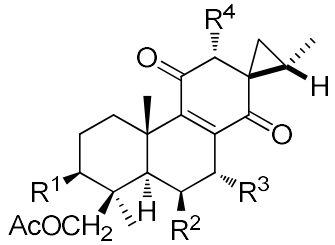

R¹ *R²* *R³* *R⁴*

132 ***H*** ***OAc*** ***OH*** ***Ac***

133 ***H*** ***OH*** ***OAc*** ***OH***

134 ***OAc*** ***OH*** ***OAc*** ***OH***

6-*O*-Acetyl-19-acetyloxy-coleon Q **132**
12-*O*-Desacetyl-7-*O*-acetyl-19-acetyloxy-coleon Q **133**
12-*O*-Desacetyl-7-*O*-acetyl-3β 19-diacetyloxy-coleon Q **134**

Solenostemon sylvaticus (Gürke ex Engl.) Agnew [136]
Plectranthus garckeanus (Vatke) J.K.Morton [136]

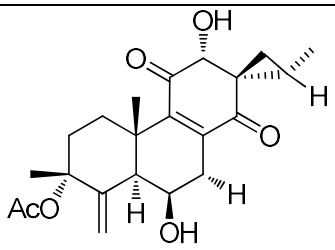

7-Desoxy-12-O-desacetyl-3-acetyloxy-coleon N *135*

Solenostemon sylvaticus (Gürke ex Engl.) Agnew [136]

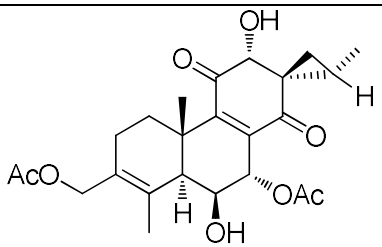

19-Acetyloxy-coleon O *136*

Solenostemon sylvaticus (Gürke ex Engl.) Agnew [136]

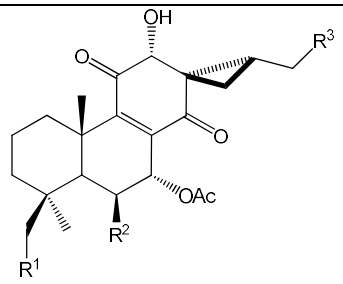

R¹ *R²* *R³*

137 ***OAc OH H***

138 ***H OAc OAc***

7-*O*-Acetyl-19-acetyloxy-12-*O*-desacetyl-coleon P **137**
6-*O*-Acetyl-17-acetyloxy-12-*O*-desacetyl-coleon P **138**

137 – *Solenostemon sylvaticus (Gürke ex Engl.) Agnew* [136]

138 – *Solenostemon sylvaticus (Gürke ex Engl.) Agnew* [136]
Plectranthus garckeanus (Vatke) J.K.Morton [136]

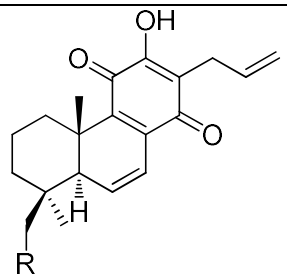

139 ***R = H***

140 ***R = OH***

141 ***R = OCHO***

Lanugone A **139**
Lanugone B **140**
Lanugone C **141**

139 – *Plectranthus edulis Agnew* [108]
Plectranthus lanuginosus (Hochst. ex Benth.) Agnew [82]

140 and **141** – *Plectranthus lanuginosus (Hochst. ex Benth.) Agnew* [82]

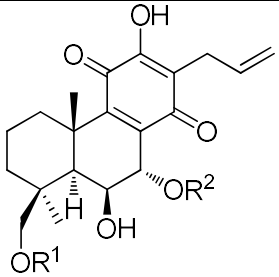

R¹ *R²*

142 ***CHO H***

143 ***H CHO***

Lanugone D **142**
Lanugone E **143**

Plectranthus lanuginosus (Hochst. ex Benth.) Agnew [82]

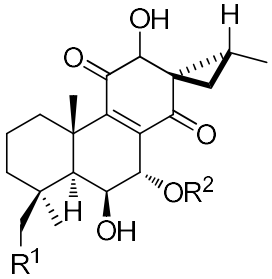

R¹ *R²*

144 ***H H***

145 ***H CHO***

146 ***OH CHO***

147 ***OCHO H***

148 ***OCHO CHO***

Lanugone F **144**
Lanugone G **145**
Lanugone H **146**
Lanugone I **147**
Lanugone J **148**

144 and **145** – *Plectranthus edulis Agnew* [108]

Plectranthus lanuginosus (Hochst. ex Benth.) Agnew [82]
146-**148** – *Plectranthus lanuginosus (Hochst. ex Benth.) Agnew* [82]

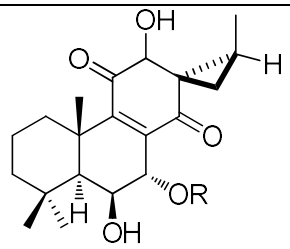 *149* ***R =Ac*** *150* ***R = CHO*** Lanugone K **149** Lanugone K' **150**	*Plectranthus lanuginosus (Hochst. ex Benth.) Agnew* [82]
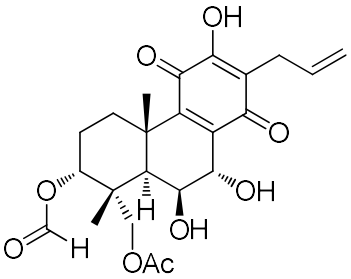 ***6β,7α-Dihydroxy(allyl)royleanone*** *151*	*Plectranthus lanuginosus (Hochst. ex Benth.) Agnew* [139]
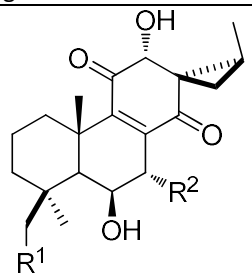 *R¹ R²* *152* ***H OH*** *153* ***OH OAc*** 12-*O*-Desacetyl- coleon Q (or 15-epilanugon F) **152** 7-*O*-Acetyl-12-*O*-desacetil-19-hydroxy-coleon Q **153**	*Plectranthus lanuginosus (Hochst. ex Benth.) Agnew*[139]
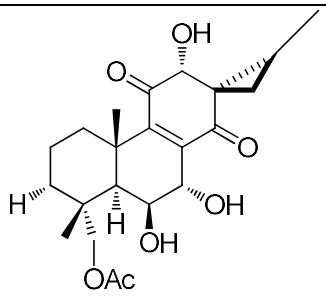 *R¹ R²* *154* ***H OAc*** *155* ***OCHO OCHO*** ***18-Acetoxy-12-O-desacetyl-coleon Q*** *156* ***3,18-Di-O-desacetyl-3,18-di-O-formyl-coleon Y*** *157*	*Plectranthus lanuginosus (Hochst. ex Benth.) Agnew* [139]
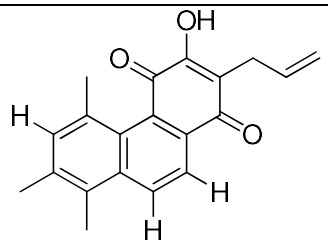 ***Plectranthon A*** *158*	*Plectranthus sp*. from Rwanda [109], [140]
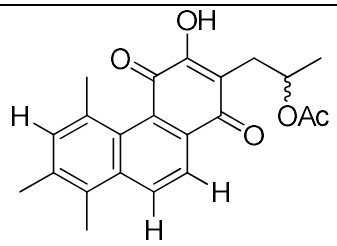 ***Plectranthon B*** *159*	*Plectranthus sp*. from Rwanda [109], [140]

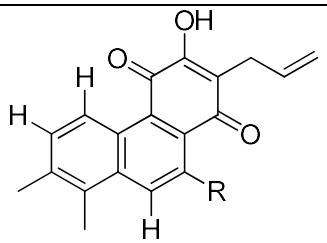

160 ***R = H***

161 ***R = Me***

Plectranthon C **158**
Plectranthon D **159**

Plectranthus sp. from Rwanda [109], [140]

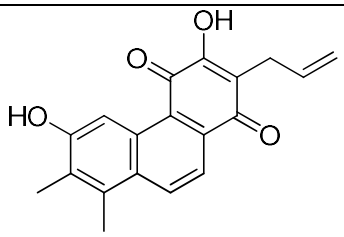

Plectranthon E *162*

Plectranthus sp. from Rwanda [109]

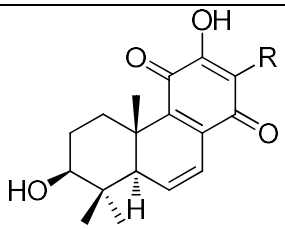

163 ***R = $CH_2CH=CH_2$***

164 ***R = $CH_2CH(OAc)CH_3$***

Plectranthon F **161**
Plectranthon G **162**

Plectranthus sp. from Rwanda [109]

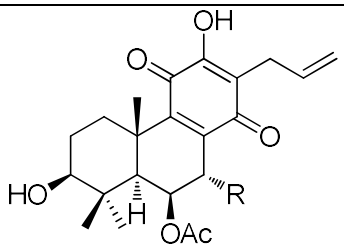

165 ***R = H***

166 ***R = OH***

Plectranthon H **163**
Plectranthon I **164**

Plectranthus sp. from Rwanda [109]

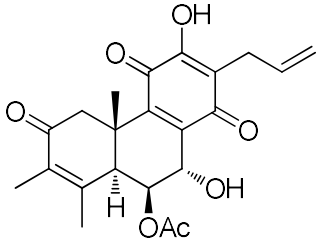

Plectranthon J *167*

Plectranthus sp. from Rwanda [109]
Plectranthus barbatus Andrews [141]

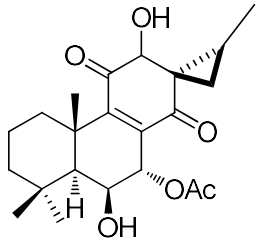

Plectranthon K *168*

Plectranthus sp. from Rwanda [109]

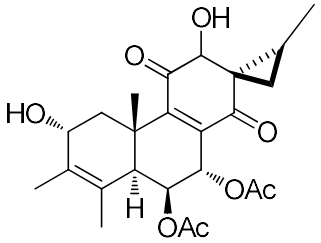

Plectranthon L *169*

Plectranthus sp. from Rwanda [109]

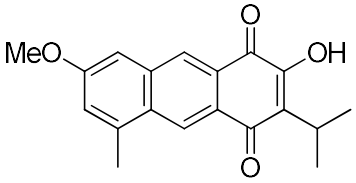

Fruticulin B *170*

Salvia fruticulosa Benth.[124], [125]

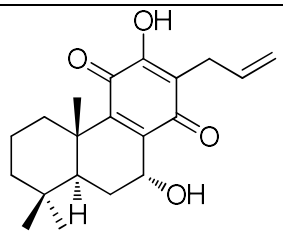 ***7α,12-Dihydroxy-17(15→16)*-abeo-*abieta-8,12,16-triene-11,14-Dione (horminone derivative)*** *171*	*Plectranthus hereroensis Engl.*[67], [92]
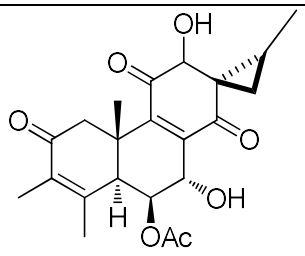 ***Plectrin*** *172*	*Plectranthus barbatus Andrews* [141]
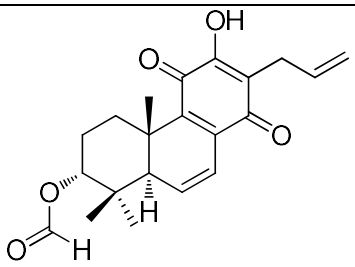 ***Royleanone*** *173*	*Plectranthus edulis Agnew* [108]
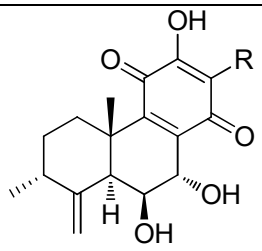 *174* ***R = Allyl*** *175* ***R = $CH_2CH(OH)CH_3$*** Royleanone **172** and **173**	*Plectranthus edulis Agnew* [108]
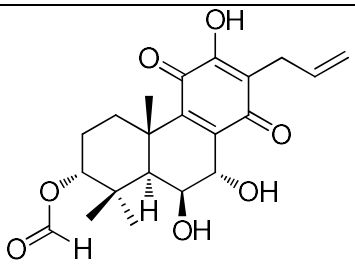 ***Royleanone*** *176*	*Plectranthus edulis Agnew* [108]
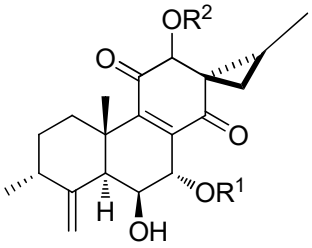 *R^1* *R^2* *177* ***Ac*** ***Ac*** *178* ***CHO*** ***Ac*** *179* ***Ac*** ***H*** *180* ***H*** ***Ac*** *181* ***CHO*** ***H*** *182* ***H*** ***H*** Spirocoleon **175-180**	*Plectranthus edulis Agnew* [108]

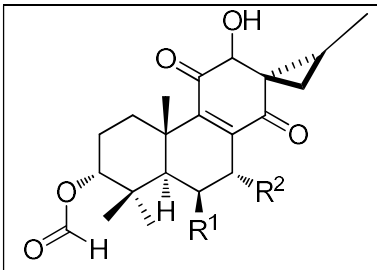 *Plectranthus edulis Agnew* [108] *R¹ R²* *183* ***OAc OH*** *184* ***OH H*** *185* ***OH OCHO*** Spirocoleon **181-183**	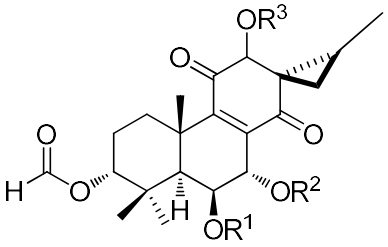 *Plectranthus edulis Agnew* [108] *R¹ R² R³* *186* ***Ac H Ac*** *187* ***H CHO H*** Spirocoleon **184** and **185**
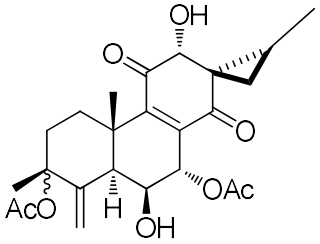 *Plectranthus edulis Agnew* [108] ***Spirocoleon*** *188*	

1.5 Total synthesis

An overview of royleanone synthetic studies will be described. Initially, it will be described the schemes of the first synthesis used to obtained royleanones. Subsequently, it will be referred the main reactions used to synthesize each roylenones described in later literature (Table 4).

1.5.1 Royleanones and derivatives

One of the first reports on total synthesis of royleanone's precursor abietic acid **187** remounts 1967, when Fugita and co-workers described the transformation of Enmein into (+)-abietane and, abietic acid into (-)-abietane. Later on 1977, Fukui and co-workers [143] reported the conversion of (-)-abietic acid **187** into several 11-oxygenated tricyclic diterpenes including (+/-) royleanone **1** (**Erro! A origem da referência não foi encontrada.**1).

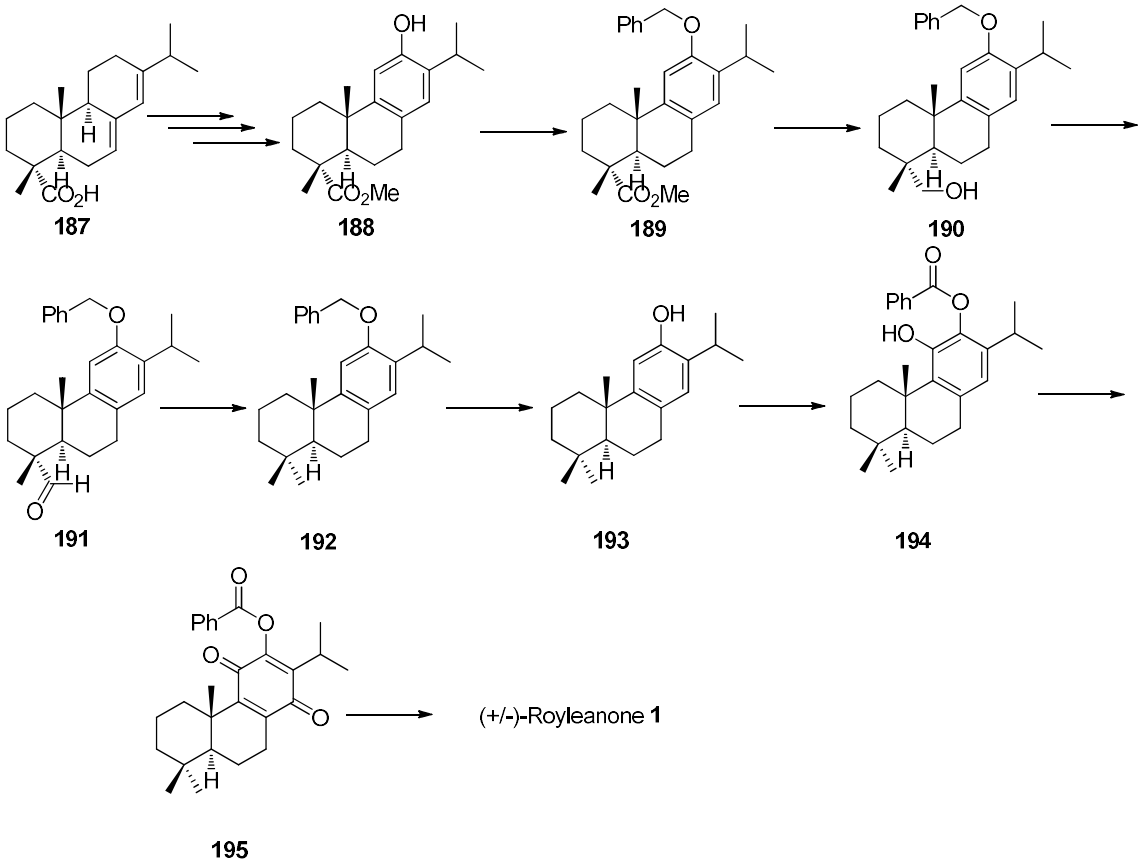

Scheme 1 Total synthesis of royleanone 1 [143]

In order to isolate royleanone **1**, first the authors performed the etherification of **188** with benzyl chloride to obtain the benzyl ether **189**, which, on reduction with lithium aluminium hydride followed by oxidation of the resulting alcohol **190**, yielded a formyl derivative **191**. Huang Minlon reduction of **191** gave ferruginol benzyl ether **192**, which, by Pd-C hydrogenation, afforded ferruginol **193**. The oxidation of **193** with benzoyl peroxide in chloroform at room temperature gave a phenol **194**. The phenol **194** was easily converted into (+/-)-royleanone **1** by oxidation and subsequent alkaline hydrolysis via royleanone benzoate **195**.

In the beginning of the 90's, Liebeskind and co-workers [144] presented a new approach to synthetize (+/-)-royleanone **1** by construction of the substituted quinone **199** *via* maleoylcobalt complex technology. However, this approach led to low yields. To overcome this difficulty, the quinone **199** was obtained as mixture of regioisomers by traditional but less regioselective cobalt catalysis (5:1 mixture of regioisomers, with the predominant isomer possessing the structure shown). Another key step of this synthesis is the acid induced cyclization of the corresponding hydroquinone methyl ether **201** onto a tethered enone **202**. The synthesis of the racemic **1** was completed by straightforward functional group manipulations (**Erro! A origem da referência não foi encontrada.**2).

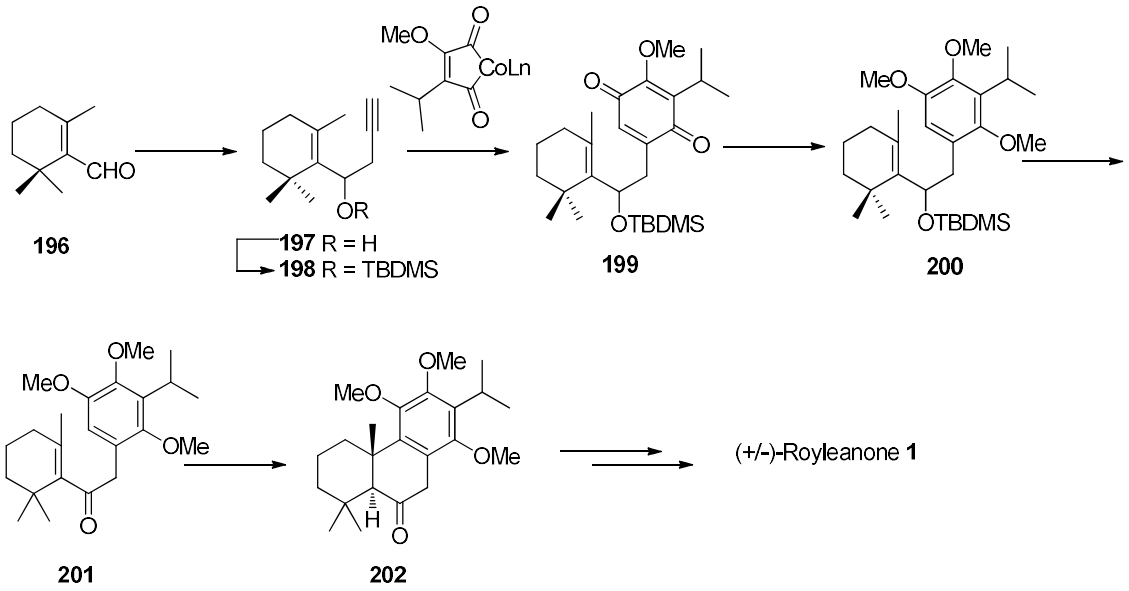

Scheme 2 Synthesis of racemic 1 via maleoylcobalt methodology [144]

Later on, Danheiser and co-workers [145] described the total synthesis of several diterpenoids quinones, namely (+/-)-royleanone by photochemical aromatization annulation from acyclic precursors (**Erro! A origem da referência não foi encontrada.**3). The main strategy involves the irradiation at 254 nm of **203** in the presence of siloxyalkyne **204** to obtain the royleanone precursor **205**. The same strategy was applied to obtain the (+)-neocryptotanshinone **206** using a different siloxyalkyne.

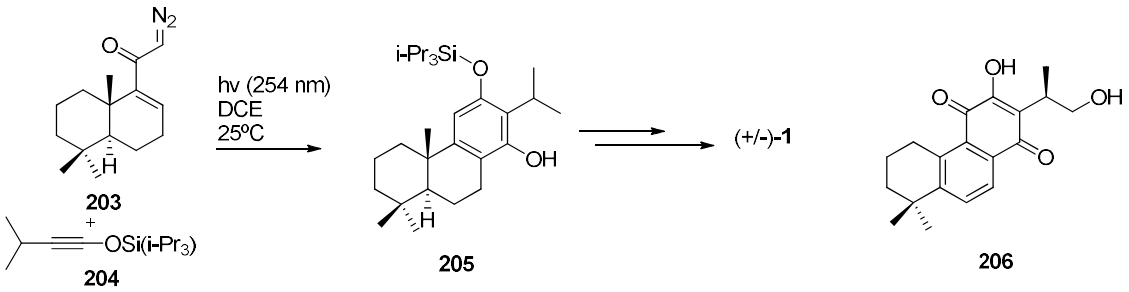

Scheme 3 Photochemical aromatic annulation strategy to obtain (+/-)-1 and 206

In 2000, Toledo and co-workers [146] successfully synthetized the enantiomerically pure (+)-royleanone **1** from sulfinyl quinones. The key precursor, sulfinyl quinone **208**, was synthesized by undertaking the sulfinylation of 2-isoprop-yl-1,3,4-trimethoxybenzene **207** with (*S*)-diacetone glucose *tert*-butylsulfinate (**Erro! A origem da referência não foi encontrada.**4). Afterwards, **208** was employed in the subsequent Diels-Alder reaction with diene **209**. Having

the tricyclic quinone **210** in hand, they were able to successfully reduce the double bond by a normal Pd-C catalyzed hydrogenation and isolate (+)-royleanone **1.**

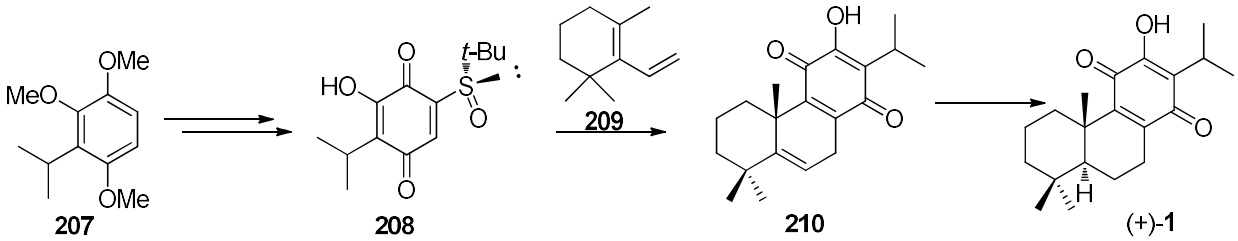

Scheme 4 Synthesis of (+)-royleanone 1 from sulfinyl quinone [145].

In 2001, Tada and co-workers [147] reported the synthesis of twelve natural abietane-type diterpenes, among them **1**.Taking advantage of the asymmetric polyene cyclization, developed by the same authors, **212** was synthesized from acid **211** (Scheme 5). After Friedel-Crafts alkylation and straightforward functional group manipulations it was possible to isolate **1** in seven steps and 17.1% overall yield.

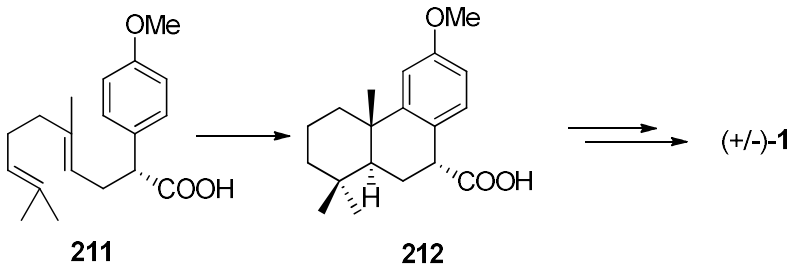

Scheme 5 Synthesis of 1 via polyene cyclization [147]

In 1979, Matsumoto and Harada [54] reported the successful total synthesis of other royleanone family members (+)-taxoquinone **15**, (-)-7α-acetoxyroyleanone **2**, (-)-dehydroroyleanone **3**, (-)-horminone **7** and (-)-7-oxoroyleanone **4**, all from oxidation of (+)-ferruginol **193** and functional group modification (**Erro! A origem da referência não foi encontrada.**6).

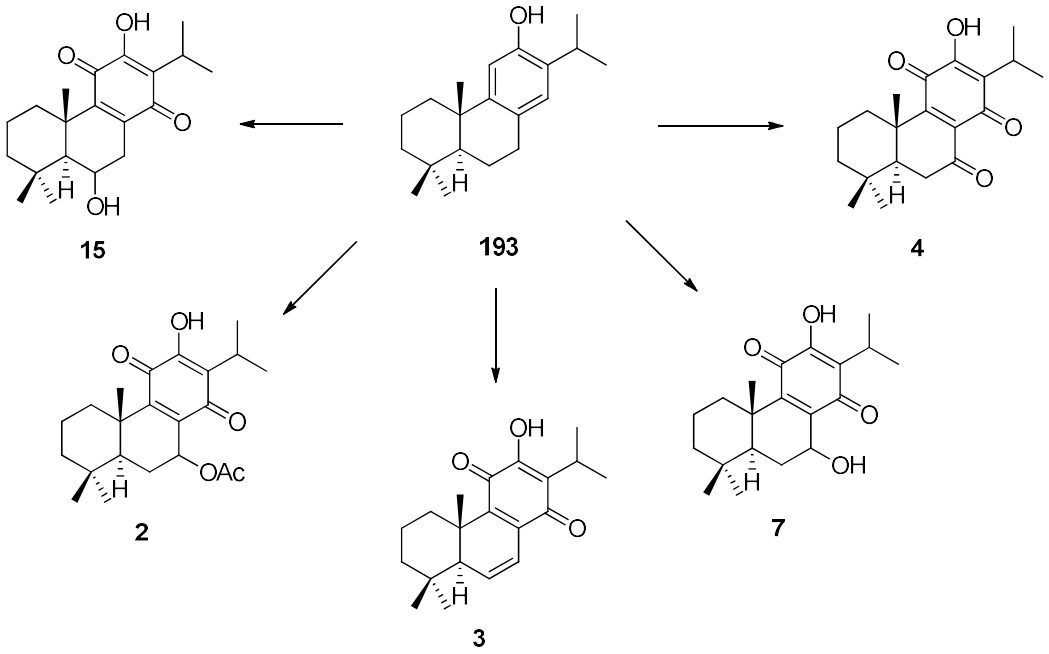

Scheme 6 Products of oxidation and functional group manipulation of (+)-ferruginol 193 [54]

Later on 1990, Quayle and co-workers [148] envisaged and proved that the vinyl carbine complex **213** in the presence of oxygenated acetylene **214** would after oxidative work-up produce 12-*O*-methyl-royleanone **38** (**Erro! A origem da referência não foi encontrada.**7).

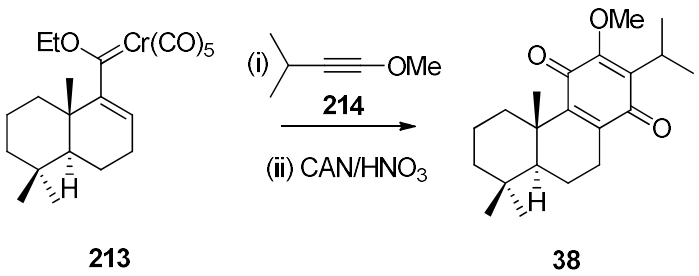

Scheme 7 Synthesis 12-O-methylroyleanone 38 mediated by of Chromium carbine [148]

Other members of royleanone family were successful synthetized, specially taiwaniaquinones and dichroanone that have been widely studied throughout the beginning of this century. All the total synthesis's are summarized in Table 4 with reference to the key transformation. The hydroxyquinone moiety of royleanones presents a remarkable reactivity. The quinones, including hydroxyquinones, constitute one of the most interesting classes of molecules in organic chemistry. Their chemical reactivity is fundamentally reliant on the substituents being either on the quinonic or on adjacent rings.

Generally, the reactivity of hydroxyquinones is associated to the reactivity of quinones with electron donor substituents. Furthermore, the enol-enone moiety provides very interesting versatility allowing transformations such as reductive or oxidative reactions, alkylations or esterification.

The principal pattern of royleanones reactivity is also summarized in Table 4.

Table 1.4 Summary of methods for the synthesis of royleanones and the main reactions used to prepare some derivatives from natural occurring royleanones.

Compound/ Key reaction[ref]	Compound/ Key reaction[ref]
Royleanone 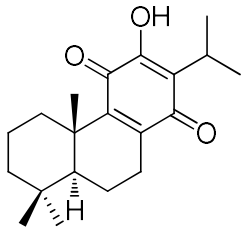 **1** Oxidation of abietic acid **193** [143] Via maleoylcobalt technology [144] Photochemical aromatic annulation [145] Sulfinyl quinones precursors [146] Enantioselective oxidation ferruginol and polyene cyclization [147] Oxidation of ferruginol [54] Methylation [14]	**(-)-7α-Acetoxyroyleanone** 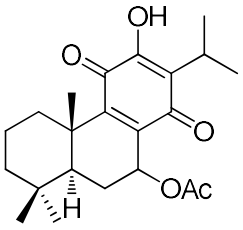 **2** Oxidation of ferruginol **193** [54] Acetylation and basic hydrolysis [14]
(-)-Dehydroroyleanone 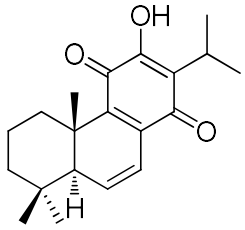 **3** Oxidation of ferruginol **193** [54] Acid-catalyzed rearrangements [149] Hydrogenation [14]	**(-)-7-Oxoroyleanone** 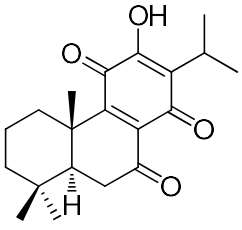 **4** Oxidation of ferruginol **193** [54] Epoxidation to form a epoxyquinone [48]

(-)-Horminone 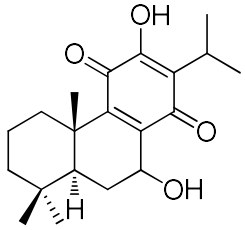 **7** Oxidation of ferruginol [54] Acid-catalyzed rearrangements [149] Hydrogenation [14] Acid-catalyzed dehydroxylation; Acetylation; Esterification; Methylation [81]	**(+)-Taxoquinone** 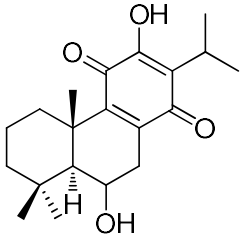 **15** Oxidation of ferruginol [54] Oxidation to 14-hydroxytaxodione [150] Acid-catalyzed rearrangements [149]
7α-Acetoxy-6β-hydroxyroyleanone 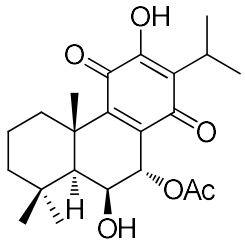 **19** Esterification; acetylation [83], [151]	**7-*O*-Methylconacytone** 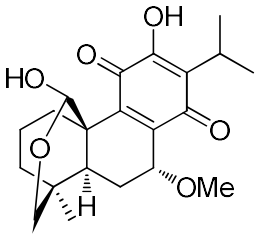 **23** Jones oxidation [27]
Sessein 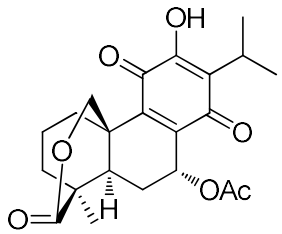 **28** Acetylation, basic hydrolysis and hydrogenolysis [31]	**12-*O*-Methylroyleanone** 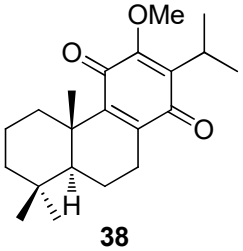 **38** Dotz benzannulation reaction based on chromium carbene complexes [148]
Columbaridione 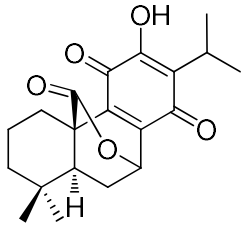 **42** Partial synthesis from available 16-hydroxycarnosol [41]	**16-Hydroxycolumbaridione** 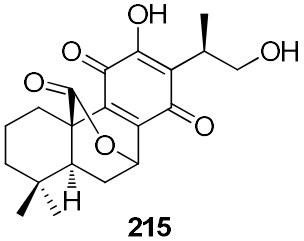 **215** Partial synthesis from relative available 16-hydroxycarnosol; Acetylation [152]

(+/-)-Danshexinkun A 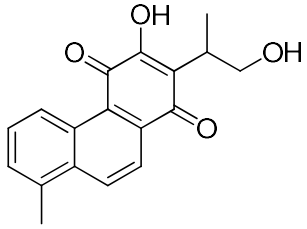 **47** Photocyclization of a highly substituted stilbene [153]	**6β,7α -Dihydroxyroyleanone** 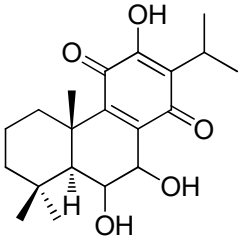 **49** Ring opening of epoxyroyleanone [154]
Coleon-U-quinone 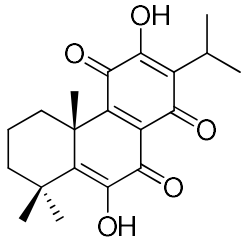 **62** Epoxydation by borate led yieding a epoxyquinone [52]	**12-Deoxyroyleanone** (**33**) **Cryptoquinone** (**69**) **Triptoquinone D** (**216**) and **F** (**217**) 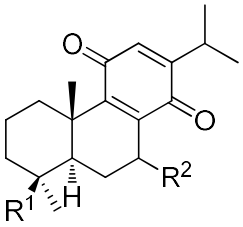 **R¹** **R²** **33** Me H **69** Me =O **216** CH_2OH H **217** COOH H Synthetized from dehydroabietic acid [155]
Salvipisone 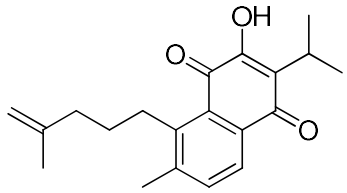 **81** Acid-catalyzed cyclization [156] Partial synthesis from aethiopinone [68] Acid-catalyzed cyclization [156]	**(-)-Taiwaniaquinone A** 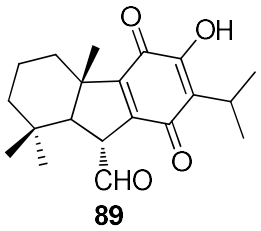 **89** Cleavage C7-C8 bond of (+)-abietic acid **187** [157] Intramolecular aldol condensation of a ketoaldehyde and oxidative cleavage of an isopropylene ketal [158] Bi(OTf)3-cationic cyclization and Wolff-type ring contraction [159] Cycloaddition β-myrcene [4 + 2] cycloadditions of *trans*-ozic acid [120]

(+/-)-Taiwaniaquinone D 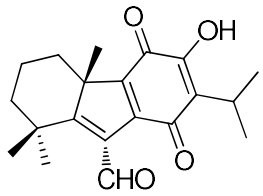 **92** Pd(0)-catalyzed reductive cyclization [160] Ene reaction product from taiwanadduct B [120]	**(-)-Taiwaniaquinone F** 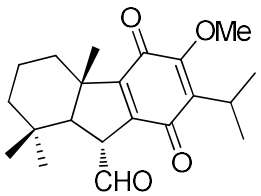 **94** Cleavage C7-C8 bond of (+)-abietic acid **187** [157] Intramolecular aldol condensation of a ketoaldehyde and oxidative cleavage of an isopropylene ketal [158] Wolff ring contraction and aromatic oxidation [161]
Taiwaniaquinone G 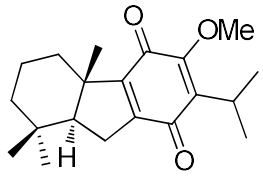 **218** (-)-**218**: Enantiospecific thermal 6π eletrocyclization [162] via Lewis acid catalysed tandem acylation Synthesis of unnatural 5-epi-**218** Nazarov cyclization [163]	**Taiwaniaquinone H** 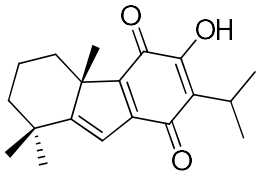 **219** Intramolecular Friedel-Crafts alkylation and degradative oxidation [164] (-)-**219:** Asymmetric intramolecular Heck reaction [165] (-)-**219:** Enantiospecific Benzylic acid intramolecular rearrangement [166] (+)-**219:** Pd(II)-catalyzed asymmetric conjugate addition [167]
Dichroanone 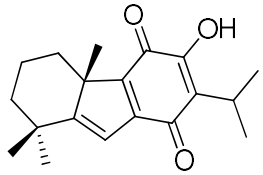 **95** Pd(0)-catalysis reductive cyclization [160], [168] Domino Friedel-Crafts acylation/alkylation [169] Intramolecular Friedel-Crafts alkylation and degradative oxidation [164] (+)-**95**: Enantioselective Tsuji Allylation [170] (+)-**95**: Enantiospecific thermal 6π eletrocyclization [171] (+)-**95:** Pd(II)-catalyzed asymmetric conjugate addition [167] (-)-**95**: Asymmetric intramolecular Heck reaction [165] **(-)-95:** Cleavage C7-C8 bond of (+)-abietic acid [157]	**Komaroviquinone** 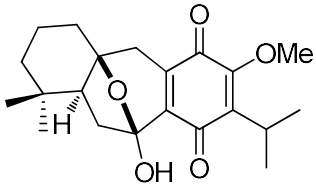 **99** Intramolecular Heck reaction [172] Rh(II) catalysis cycloaddition [173], [174] Negishi coupling reaction [175] Reduction by *Trypanosoma cruzi* old yellow enzyme (TcOYE) to its semiquinone radical [142]

Plectranthon A 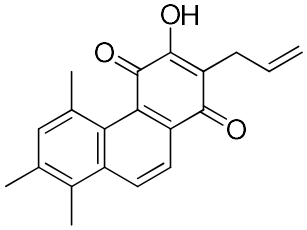 **156** Photocyclization of highly substituted stilbene [176] Esterification of hydroxyl group [109]	**Plectranthon C** 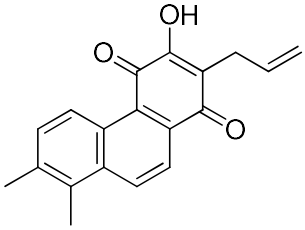 **158** Photocyclization of highly substituted stilbene [176] Ultrasound-promoted and Lewis acid catalysed, highly regioselective cycloadditions of styrenes with substituted 1,4-benzoquinones [177]
Plectranthon D **Danshenxinkun B** **Danshenxinkun C** 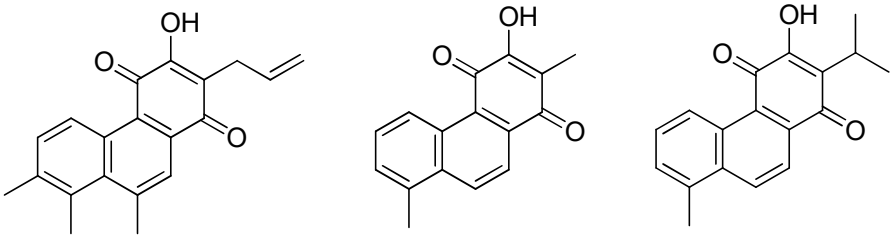 **159** **48** **220** Ultrasound-promoted and Lewis acid catalysed, highly regioselective cycloadditions of styrenes with substituted 1,4-benzoquinones [177]	
(+)-Neocryptotanshinone 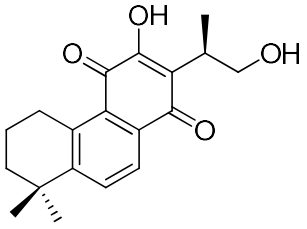 **206** Photochemical aromatic annulation [145] Partial synthesis from relative available 16- hydroxycarnosol [152]	**14-Methoxy-*p*-quinone** (unstable) 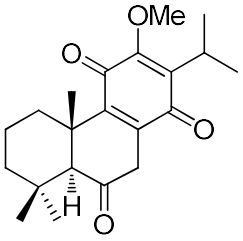 **221** Synthetized from 7-acetoxyroyleanone **2** [178]

1.6 Biological activity

Abietanes are compounds that exhibit a variety of attractive biological activities. Their significant biological properties have medicinal and pharmacological potential for drug development. Several reviews of plants' biological activities have appeared through the 2000s. Bioactivities of diterpenoids isolated from Anatolian Lamiaceae plants [179], and from several Lamiaceae genus, namely compounds from *Salvia* [180], *Isodon* [181], *Hyptis* [182] and *Agastache* [183] species, have been reported in the literature, as well as *Plectranthus* genus'

chemistry [184], [185]. The biological activities of diterpenes described in literature are listed in Table 5.

Table 1.5 Biological activities described for royleanone-related diterpenoids.

Royleanone-related diterpenes	Biological Activity	Reference
Royleanone, **1**	Cytotoxic	[71], [72], [74], [75]
	Gastroprotective	[72]
	Antioxidant	[55]
7α-Acetoxyroyleanone (or 7-*O*-acetylhorminone), **2**	Cytotoxic	[58], [71], [74], [75]
	Antibacterial	[80]
	Antioxidant	[55]
6,7-Dehydroroyleanone, **3**	Antioxidant	[87]
	Gastroprotective	[72]
	Cytotoxic	[72], [86]
7-Ketoroyleanone, **4**	Cytotoxic	[74], [75]
	Antimicrobial	[119]
Horminone, **7**	Antibacterial	[80], [90]
	Antifungal	[89]
	Antimicrobial	[67], [92]
	Cytotoxic	[71], [72], [74], [75]
	Antioxidant	[55]
	Gastroprotective	[72]
Horminone and its derivatives	Antimicrobial	[81]
Taxoquinone, **15**	α-glucosidase and tyrosinase inhibition	[96]
	Antibacterial	[95]
	Antimycotic	[94]
	Gastroprotective	[72]
	Cytotoxic	[72]
6β-Acetoxy-7α-hydroxyroyleanone, **16**	Antioxidant	[98]
	Anti-inflammatory	[97]
6β,7β-Dihydroxyroyleanone, **17**	Antibacterial	[111]
	Butyrylcholinesterase (BuChE) inhibition	[111]
7β-Acetoxy-6β-hydroxyroyleanone, **18**	Antibacterial	[111]
	Butyrylcholinesterase (BuChE) and α-Glucosidase inhibition	[111]
7α-Acetoxy-6β-hydroxyroyleanone, **19**	Antitumour	[110]
	Antimicrobial	[67]
	Immunomodulatory	[101]
7α-Acetoxy-6β-hydroxyroyleanone derivatives	Antimicrobial	[151]
	Antimycobacterial	[83]
Agastaquinone, **39**	Cytotoxic	[38]
	HIV-1 protease inhibition	[103]
Atuntzensin A, **41**	Antioxidant	[105]
6β,7α-dihydroxyroyleanone, **49**	Antitumour	[110]
Grandidone A, **54**	Antitumour	[110]
Coleon U quinone, **61**	Antibacterial	[99], [111]
	Butyrylcholinesterase (BuChE) and α-Glucosidase inhibition	[111]
7α,19-Diacetoxy-royleanone, **64**	Chemopreventive	[53]
7-Oxoroyleanone-12-methyl ether, **67**	Antioxidant	[55]

7,20-Epoxyroyleanone, **68**	Gastroprotective Cytotoxic	[72] [72]
Cryptoquinone, **69**	Antifungal Cytotoxic	[57] [57]
7*β*-Hydroxy-11,14-dioxoabieta-8,12-diene, **70**	Cytotoxic	[58]
12-Methyl-5-dehydrohorminone, **71**	Antituberculous	[59]
12-Methyl-5-dehydroacetylhorminone, **72**	Antituberculous	[59]
Triptoquinone A, **73**	Selective iNOS inhibition Aromatase inhibition iNOS induction inhibition	[186] [187] [112]
Triptoquinone derivatives:	Immunomodulatory Cytotoxic	[188] [188]
Dracocequinone A, **75**	Trypanocidal	[61]
Dracocequinone B, **76**	Trypanocidal	[61]
7α-Acetoxyroyleanone-12-methyl ether (or 7-acetylhorminone-12-methyl ether), **78**	Antioxidant	[55]
16-Acetoxy-7α-hydroxyroyleanone, **79**	Antibacterial Antiviral	[66]
Salvipisone, **81**	Anti-amoebic Antibacterial	[116] [117]
12-Deoxy-salvipisone, **82**	Antifungal	[89]
2,3-Dehydrosalvipisone, **83**	Antimicrobial	[119]
Sahandinone, **84**	Cytotoxic Antifungal	[75] [89]
Coleon A, **86**	Antibacterial	[111]
Coleon A lactone, **87**	Antibacterial	[111]
Komaroviquinone, **99**	Trypanocidal	[61], [123], [142]
Fruticulin A, **100**	Chemopreventive	[53]
Demethyl-fruticulin A, **101**	Chemopreventive	[53]
7α,12-Dihydroxy-17(15→16)-*abeo*-abieta-8,12,16-triene-11,14-dione (horminone derivative), **169**	Antimicrobial	[92]
Taiwaniaquinoid derivative Abietane quinone derivative	Leishmanicidal Trypanocidal	[189]

1.7 Conclusions

This review covers a highly bioactive group, royleanones. An extensive description of the naturally occurring abietanes covering 1962 to 2014 is presented. Is interesting to notice that royleanone derivative structures contains rearranged compounds with seco ring A structures, *abeo*-abietanes 6-5-6 ring and also 6-7-6 ring skeletons. Other royleanone-related diterpenoids have been found among the new isolated structures. It also includes synthetic studies, covering the total syntheses of royleanone and a summary of different methods for the synthesis of royleanones is described. The royleanone reactivity was outlined describing the main reactions used to prepare royleanone derivatives. Finally, the biological activities presented show the wide range of biological properties involving this group of royleanones.

The study of the availability of natural diterpenoids in large amounts, may enable a boost for further semisynthetic studies. The importance of bioactive royleanones to chemists will warrant more studies towards the development of new lead compounds. This work emphasizes the chemistry of these bioactive compounds and will justify their potential in the discovery of new pharmaceutical drugs.

1.8 Hypothesis and objectives

The increasing prevalence of drug-resistant pathogenic bacteria represents an alarming global threat to public health, which has been worsened by the lack of development of new antibacterials. The natural products constitute an inexhaustible source of new molecules being the source of many of the therapeutic forms commercialized and is the main source for new antibiotics. The *Lamiaceae* family concerns numerous species with special interest by its use in traditional medicine. Diterpenes with abietane structure, with special interest in the royleanone skeleton, demonstrated high antibacterial activity in resistant species and a reduced cytotoxicity.

Nanoparticles combined with a therapeutical drug can be developed as an important strategy of drug delivery. Their use could result in several advantages, such as low side effects, increased therapeutic efficiency or reduced therapy time.

According to the previous information, we propose that:

- Since royleanones are natural compounds whose structures is associated with high ativity such as antibacterial, the study of one of the most active structures could provide important data such as:
    - Determination of their physicochemical properties may provide important information about its structure and conformation;
    - Define of its mechanism of action on the cell wall and cellular membrane of a type of resistant bacteria provide data about their structure activity interaction;

- If we conjugate different types of nanoparticles with a natural therapeutic form, it may result in formulations with significant advantages for a more effective treatment. This approach can be done through:
    - Use of plants extracts with biological activity encapsulated into bio-polymeric nanoparticles;
    - Use of one natural compound with high antibacterial activity and silver nanoparticles;

Through the hypotheses introduced, I propose the following objectives for this work:

1. Study physico-chemical properties of 7α-acetoxy-6β-hydroxyroyleanone
2. Study the antibacterial mechanism against an MRSA strain.
3. Develop and characterize polymeric nanoparticles containing a biological active extracts a test their release over time.

4. Develop and characterize silver nanoparticles functionalized with antibiotics for a topical application.

Chapter 2

Extraction optimization, structural and thermal characterization of the antimicrobial abietane 7α-acetoxy-6β-hydroxyroyleanone

Extraction optimization, structural and thermal characterization of the antimicrobial abietane 7α-acetoxy-6β-hydroxyroyleanone

2.1 Introduction

The growing incidence of infections caused by bacterial pathogens resistant to multiple classes of antibiotics has developed into a serious health problem [190]. This fostered the search for new antibacterial agents from natural resources [191], such as plant extracts, which have traditionally been used to treat human infections [192, 194]. The biological activities described for royleanone-related diterpenoids are extensive and include antimicrobial properties [195]. Previous *in vitro* antimicrobial studies showed that 7α-acetoxy-6β-hydroxyroyleanone (7α-acetoxy-6β,12-dihydroxy-abieta-8,12-diene-11,14-dione, AHR, **Figure 1**) obtained from *Plectranthus* species [196, 197] exhibits better activity against specific strains of methicillin-resistant *Staphylococcus aureus* (MRSA), vancomycin-resistant *Enterococcus faecalis* (VRE) [151, 198], or multidrug-resistant *Mycobacterium tuberculosis* (MDR-TB) [197], than some of the presently used reference drugs. Besides antibacterial action, other interesting biological activities were evidenced by several works, such as proven cytotoxicity at low concentrations against different types of human cancer cell lines [110] and immunomodulatory effects related to antiproliferation of human lymphocytes [101]. All these results suggest that 7α-acetoxy-6β-hydroxyroyleanone can be an interesting lead for future drug development.

When attempting to isolate a compound from a plant matrix, the choice of the extraction method is of the utmost importance to attain the highest possible yield. Available methods can be divided into three categories: (i) traditional methods, like aqueous infusions and decoctions; (ii) conventional solvent extraction methods, which make use of abundant quantities of organic solvents; and (iii) non-conventional methods, such as microwave and ultrasound techniques (which use water or an organic solvent as the extracting medium) or supercritical fluid extraction (SFE). The solvent in SFE is a substance that is gaseous at ambient pressure and temperature, and has enhanced solvent properties above the critical point (supercritical fluid state). A supercritical solvent can, therefore, easily release the extract by a simple pressure-temperature reduction. The supercritical solvent most often used is carbon dioxide which is largely abundant and can be obtained with high purity at a relatively low cost [202 - 204]. Carbon dioxide has several advantages for the extraction of nutraceutical compounds: it is non-toxic, non-flammable, chemically inert, it has no smell or taste, and it has a low critical point (T_c = 304.13 K; p_c = 7.38 MPa) [201].The latter facet is very important for extraction of thermolabile compounds. Furthermore, extracts obtained by SFE have been considered of superior quality in terms of reproducibility and for keeping flavors and aromas

true to themselves, when compared to those obtained by conventional methods [205 – 209]. In this study, all types of methods mentioned above were tested for the optimization of AHR extraction.

Besides optimization of the extraction process from the selected natural resource, two critical aspects that need to be considered as early as possible when the development of pharmaceutical products based solid forms is in view are the structural and thermal characterization of the lead compound, so that phenomena such as polymorphism or chemical decomposition can be identified. The characterization of the crystal structure and thermal behaviour of AHR was, therefore, performed in this work by using single crystal X-ray diffraction and differential scanning calorimetry.

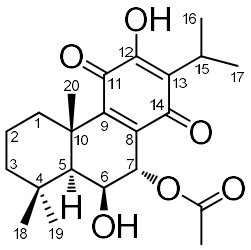

Figure 2.1 Molecular structure of 7α-acetoxy-6β-hydroxyroyleanone (AHR)

2.2 Material and methods

2.2.1 Plant Material

Plectranthus grandidentatus Gürke was cultivated in the Faculty of Pharmacy Hortum, Lisbon University from seeds provided by the National Botanic Garden, Kirstenbosch, Claremont, South Africa. The aerial parts of this species were collected in July – October 2003, and an voucher specimens (ref. C. Marques S/N° LISC) were deposited in the Herbarium of the ‘‘Instituto de Investigacão Científica Tropical’’, Lisbon. Previously to the extraction processes, the dried plant material was finely grinded using a grinder mill. The resultant powder was then used in the different extractions processes.

2.2.2 Chemicals

HPLC grade water, acetone, methanol and trifluoroacetic acid were obtained from Merck (Darmstadt, Germany). $CDCl_3$ from Aldrich 99.80%, <0.01% H_2O, were used in the NMR studies. Carbon dioxide (N48-99.998%) for supercritical fluid extraction was supplied in cylinders by Air Liquide (Lisbon, Portugal).

2.2.3 Extraction Methods

Supercritical fluid extraction was carried out in an experimental apparatus, equipped with a sample cell of 500 cm^3, which as been described elsewhere [198]. A sample of 100 g of the powdered plant was extracted with supercritical CO_2 for 4h at 40ºC and 230 bar, using a fixed CO_2 flow rate of 0.3 kg/h. The SCF extract was recovered by washing the collection vessel and tubing expansion line with acetone.

Acetone maceration extraction was performed using 100 g of dried plant and 1L of the solvent, at room temperature, under strong magnetic stirring for 1h. The resulting extract was filtrated and solvent taken to dryness in a rotatory evaporator.

Acetone ultrasonic-assisted extraction was carried out using 100 g of dried powdered leaves and 1L of solvent. The ultrasonic bath (Sonorex Super RK 510 H; Bandelin, Berlin, Germany) was operated for 1h, at 35 Hz with maximum input power of 320 W. The obtained extract was filtrated and the solvent removed by rotatory evaporation.

Aqueous plant extracts were prepared as decoctions, infusions or using microwave or ultrasound techniques. In all procedures, 10 g of dried and powdered plant material was extracted using 100 mL of water and filtered through Whatman paper nº 5 paper (Whatman, Inc., Clifton, New Jersey, USA). For infusions, the plant material was immersed in freshly boiled distilled water for 10 min and for decoction, the plant material was boiled in distilled water for 10 min. In the microwave method, extracts were prepared using the same amount of plant material, immersed in distilled water and placed inside a conventional microwave oven at 800 W power for 2 min [210, 211].

The AHR content in the extracts obtained from the different extraction methods was evaluated by HPLC-DAD according to Rijo *et. al.* [209].

2.2.4 Extraction quantification of AHR by HPLC-DAD

The HPLC analysis was carried out in an Elite LaChrom® VWR Hitachi Liquid Chromatograph equipped with a Column Oven L-2300 and Diode Array Detector L-2455 (VWR, USA). A column LiChroCART® 250-4 LiChrospher® 100 RP-8 (5 µm) was used. The extracts were analyzed by HPLC injecting 25 µl (1 $mg.mL^{-1}$) with an auto injector, and using a gradient composed of solution A (0.05% trifluoroacetic acid), and solution B (methanol) as following: 0 min, 80% A, 20% B; 20 min 20% A, 80% B; 25 min, 20% A, 80% B. The flow was 1 $mL.min^{-1}$ and the detection was carried out between 200 and 500 nm with a diode array detector. AHR was detected using chromatograms at 270nm, and the quantity in the plant extracts were estimated

comparing the peak areas to a calibration curves using authentic samples standard previously isolated [67].

2.2.5 Preparation and Characterization of the 7α-Acetoxy-6β-hidroxyroyleanone Sample Used in the Structural and Thermal Studies

The 7α-Acetoxy-6β-hidroxyroyleanone sample used in the structural and thermal studies was isolated from the supercritical fluid extract (section 2.2.3) through chromatographic methods as described elsewhere [92] and recrystallized from *n*-hexane:dichloromethane (1:9). Yellowish crystals, suitable for SCXRD and DSC, studies were obtained. HPLC analysis gave a purity of 99.4%. ^{1}H-NMR and ^{13}C-NMR analysis were carried out in $CDCl_3$ (Aldrich 99.80%, <0.01% H_2O), at ambient temperature, on a Bruker Ultrashield 500 MHz for ^{1}H-NMR and 125.7 MHz spectrometer for ^{13}C-NMR (supporting information, **Table 2.5**). These results are in agreement with previously reported data [92]. Chemical shifts were given in parts per million (ppm, δ), referenced to the $CDCl_3$ peaks at δ = 7.26ppm (^{1}H-NMR) and δ = 77.16 (^{13}C-NMR). The X-ray powder pattern, recorded at 298±2 K, on a Philips Analytical X'Pert PRO apparatus, using previously described conditions [210], was indexed as orthorhombic, space group $P2_12_12$, a = 1420.4±2.1 pm, b = 2076.3±3.0 pm, c = 743.1±1.4 pm (supporting information, **Table 2.6**). This indicated that the overall sample corresponded to the orthorhombic phase characterized in this work by single crystal diffraction (see below) for which the following parameters were obtained: space group $P2_12_12$, a = 1411.8±0.4 pm, b = 2073.0±0.5 pm, c = 742.2±0.2 pm.

2.2.6 Single Crystal X-ray Diffraction.

Single crystal X-ray diffraction data for AHR was collected on a Bruker AXS-KAPPA APEX II area detector diffractometer with graphite-monochromated MoKα (λ = 71.073 pm) radiation at 167±2 K and 296±2 K. The X-ray generator was operated at 50 kV and 30 mA and the X-ray data collection was monitored using the APEX2 program [211]. All data were corrected for Lorentzian, polarization and absorption effects using SAINT [212] and SADABS [213] programs. SHELXS [214] and SHELXL [215], both included in WINGX-Version 1.1.2 [216], were used for structure solution and was used for full-matrix least-squares refinement on F^2, respectively.

Non-hydrogen atoms were refined with anisotropic thermal parameters. In the low temperature structure, most hydrogen atoms were located in a Fourier map and their positions and isotropic displacement parameters, Uiso(H), were refined freely, except for the hydrogens bonded to C5 and C7 atoms that were inserted in idealized positions and allowed to refine riding in the parent carbon atom. In the ambient temperature structure, most of the hydrogen atoms

were placed in idealized positions and allowed to refine riding in the parent carbon atom. The hydrogen atoms linked to C1, C5, C6, C7, C15 and to O5 atoms were localized from the electron density map and allowed to refine freely. Graphical representations were prepared using Mercury 3.1.1. [217]. PLATON [218] was used for hydrogen bond interactions. A summary of the crystal data, structure solution, and refinement parameters is given in **Table 2.1**.

Table 2.1 Crystal Data and Structure Refinement Parameters for 7α-acetoxy-6β-hidroxyroyleanone (AHR) ($C_{22}H_{30}O_6$) at 167 K and 296 K.

***T*/K**	167±2	296±2
Crystal size/mm	0.50×0.25×0.20	0.20×0.16×0.10
Crystal system	Orthorhombic	Orthorhombic
Space group	$P2_12_12$	$P2_12_12$
***a*/Å a c**	14.0964(12)	14.118(4)
***b*/Å**	20.5705(18)	20.730(5)
***c*/Å**	7.3873(7)	7.4220(17)
***V*/Å^3**	2142.1(3)	2172.2(9)
Z	4	4
d_{calcd}/g·cm^{-3}	1.211	1.194
μ/mm^{-1}	0.087	0.086
F(000)	840	840
θ **limits/deg**	2.451 to 26.404	2.438 to 26.425
Limiting indices	$-17 \le h \le 13$ $-25 \le k \le 18$ $-9 \le l \le 9$	$-16 \le h \le 17$ $-25 \le k \le 18$ $-9 \le l \le 8$
Reflections collected/ unique	10019 / 4352 (R_{int} = 0.0467)	12300 / 4422 (R_{int} = 0.0688)
Completeness to ϑ/deg, (%)	99.7	99.7
Data / restraints / parameters	4352 / 0 / 366	4422 / 0 / 289
GOF on F^2	0.993	0.959
Final *R* indices [$I>2\sigma(I)$]	R_1 = 0.0485; wR_2 = 0.0843	R_1 = 0.0520; wR_2 = 0.0956
***R* indices (all data)**	R_1 = 0.0840; wR_2 = 0.0961	R_1 = 0.1475; wR_2 = 0.1244
Absolute structure parameter	-	0(2)
Largest diff. peak and hole×10^6/e.pm^{-3}	0.186 and -0.190	0.133 and -0.158

2.2.7 Differential Scanning Calorimetry (DSC)

The DSC analysis of the obtained AHR sample was carried out on a Perkin-Elmer DSC 7 apparatus (Massachusetts, USA). The runs were performed in the range 298-513 K under a flow of nitrogen (Air Liquide N45) of 25 cm^3·min^{-1}. The samples with masses of 1.3-5.2 mg were sealed in aluminum crucibles and weighed with a precision of ± 0.1 μg on a Mettler XP2U ultramicro-balance (Ohio, USA). The heating rate was β = 5 K·min^{-1}. The temperature scale of the apparatus was calibrated at the same heating rate by taking the onsets of the fusion peaks of benzoic acid (NIST SRM 39j, mass fraction 0.999996, T_{fus} = 122.37 ºC), indium (Perkin Elmer,

mass fraction 0.99999, T_{fus} = 156.63 ºC), lead (Goodfellow, mass fraction 0.99995, T_{fus} = 327.46 ºC) and zinc (Perkin Elmer, mass fraction 0.99999, T_{fus} = 419.50 ºC). The heat flow scale was calibrated based on the enthalpy of fusion of the indium standard ($\Delta_{fus}h^{o}$ = 28.45 J·g^{-1}).

2.3 Results and Discussion

The biological significance of AHR had been proved[151, 198, 199] and its isolation from *P. grandidentatus* had already been described [67]. However, to obtain higher amounts of this diterpene, an extraction optimization was performed in this study. The structural and thermal characterization were also carried out for the first time by single crystal X-ray diffraction and DSC, respectively, since these are basic requirements when dealing with a potential lead compound.

2.3.1 Extraction optimization of 7α-acetoxy-6β-hydroxyroyleanone (AHR) by HPLC-DAD

To optimize the extraction of AHR from *P. grandidentatus* seven procedures were tested: maceration in acetone, supercritical fluid extraction with CO_2, ultrasound-assisted extraction in acetone and water, microwave-assisted extraction in water, decoction in water and infusion in water. The extraction yields of AHR were evaluated by HPLC-DAD according to Rijo *et. al.* [209] and the obtained results are summarized in **Table 2.2**.

The most efficient method was by far supercritical fluid extraction (57.351 µg.mg^{-1}) and the poorest yields (1-2 µg.mg^{-1}) were obtained for the aqueous extractions. Maceration and sonication in acetone led to approximately the same amount of AHR (8-10 µg.mg^{-1}).

Table 2.2 Quantification of 7α-acetoxy-6β-hidroxyroyleanone (AHR) of different *P. grandidentatus* extracts.

Method	Solvent	Amount of AHR in *P. grandidentatus* (µg.mg^{-1})
Maceration extraction	Acetone	9.77
Ultrasound	Acetone	8.04
Supercritical fluid extraction	CO_2	57.35
Decoction	H_2O	2.00
Infusion	H_2O	0.95
Microwave	H_2O	0.93
Ultrasound	H_2O	0.93

2.3.2 Single Crystal X-ray Diffraction (SCXRD)

Well-formed yellowish crystals (**Figure 2.2**) suitable for a single crystal X-ray diffraction determination of the molecular and crystal structure of AHR could be produced by recrystallization of the SCE product from *n*-hexane:dichloromethane (see experimental section). The SCXRD study was carried out at 167 K and 296 K. The molecular structure of AHR obtained at 296 K, with its corresponding atom labelling scheme is shown in **Figure 2.3**. The geometrical parameters determined at the two temperatures are given as supplementary information (**Tables 2.6** and **2.7**) along with corresponding data previously reported, at 100 K, for royleanone [219] and for 7α-hydroxyroyleanone [220]. The comparison indicates that analogous bond distances and angles are similar for the three compounds.

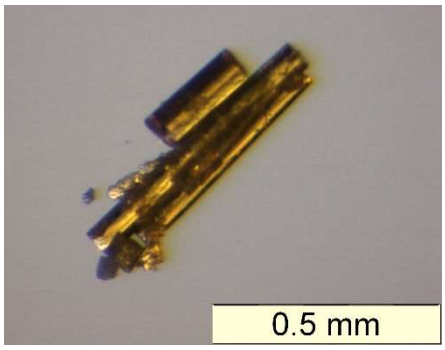

Figure 2.2 Optical microscopy image of the orthorhombic crystals of 7α-acetoxy-6β-hydroxyroyleanone used in the single crystal X-ray diffraction studies.

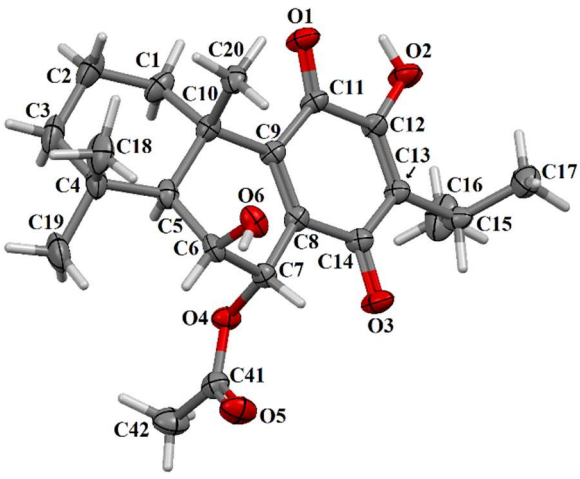

Figure 2.3 Molecular structure of 7α-acetoxy-6β-hidroxyroyleanone (AHR) with the atom labelling scheme. Ellipsoids are set at 50% probability.

The molecule includes the three fused six membered rings typical of abietane diterpenoids. Two of them are *trans* fused cyclohexane rings. One cyclohexane ring (C1–C5/C10)

is in a standard chair conformation with the puckering parameters [221] Q = 0.5588 Å, ϑ = 5.79° and φ = -28.18°, whereas the other (C5–C10) is in half chair conformation, with the puckering parameters Q = 0.5146 Å, ϑ = 51.18° and φ = 28.12°. These values are similar to those found in royleanone [219] and 7α-hydroxyroyleanone [220]. The benzoquinone ring (C8–C9/C11–C14/) is slightly twisted with atoms C9 and C11 deviated from the plane by −0.032(3) and 0.041(3) Å, respectively. An intramolecular O−H···O1 hydrogen bond (**Table 2.3**) generates a *S*(5) [226, 227] ring motif ($d_{O2-H\cdots O1}$ = 2.13 Å at 167 K and $d_{O2-H\cdots O1}$ = 2.15 Å at 296 K). Relevant intermolecular hydrogen bond (H-bond) interactions are listed in **Table 2.3**.

Table 2.3 Hydrogen Bond Distances and Angles for 7α-acetoxy-6β-hydroxyroyleanone (AHR) at 167 K and 296 K (D = donor; A = acceptor).

	D−H	H···A	D···A	D−H···A
			296±2 K	
O(2)−H(2O)···O(1)	0.80	2.15	2.5984(7)	116
(intramolecular)				
O(2)−H(2O)···O(3)	0.80	2.20	2.8467(8)	139
O(6)−H(6O)···O(5)	0.82	2.02	2.7963(8)	158
C(15)−H(15)···O(1)	0.96	2.48	3.3278(9)	148
			167±2 K	
O(2)−H(2O)···O(1) (intramolecular)	0.83	2.13	2.6112(2)	117
O(2)−H(2O)···O(3)	0.83	2.10	2.8111(3)	144
O(6)−H(6O)···O(5)	0.85	1.96	2.7860(3)	163
C(15)−H(15)···O(1)	1.00	2.45	3.3473(3)	150

Even though the crystalline packing of AHR at the two temperatures has similar motifs, the hydrogen bonds are slightly smaller at low temperature, reflecting the shrinkage of the unit cell volume. As illustrated in **Figure 2.4a**, the molecules in AHR originate $R_2^2(14)$ synthons sustained by O6−H···O5 hydrogen bonds ($d_{O-H\cdots O}$ = 1.96 Å at 167 K and $d_{O-H\cdots O}$ = 2.02 Å for at 296 K). The packing also exhibits $C_1^1(6)$ chains along the *a* axis (**Figure 2.4b**) involving O2−H···O3 hydrogen bonds ($d_{O-H\cdots O}$ = 2.10 Å at 167 K and $d_{O-H\cdots O}$ = 2.20 Å at 296 K). These two types of motif

are interconnected, yielding $R_6^6(46)$ patterns (**Figure 2.4c**) that link to each other originating a wave structure along the *b* axis (**Figure 4**). Adjacent wave patterns interact through weak C–H···O type interactions ($d_{C19–H···O6}$ = 2.62 Å and $d_{C42–H···O3}$ = 2.62 Å). The $C_1^1(6)$ motif is reinforced by a weak C15–H···O1 intermolecular interaction ($d_{C–H···O}$ = 2.45 Å for structure at 167 K and $d_{C–H···O}$ = 2.48 Å for structure at 296 K).

Overall, only a small expansion of the unit cell volume (1.4 %, **Table 2.1**) without significant changes in the supramolecular structure, is observed when the temperature increases from 167 K to 296 K. Thus, no polymorphism was evidenced by the SCXRD analysis in the 167-296 K temperature range.

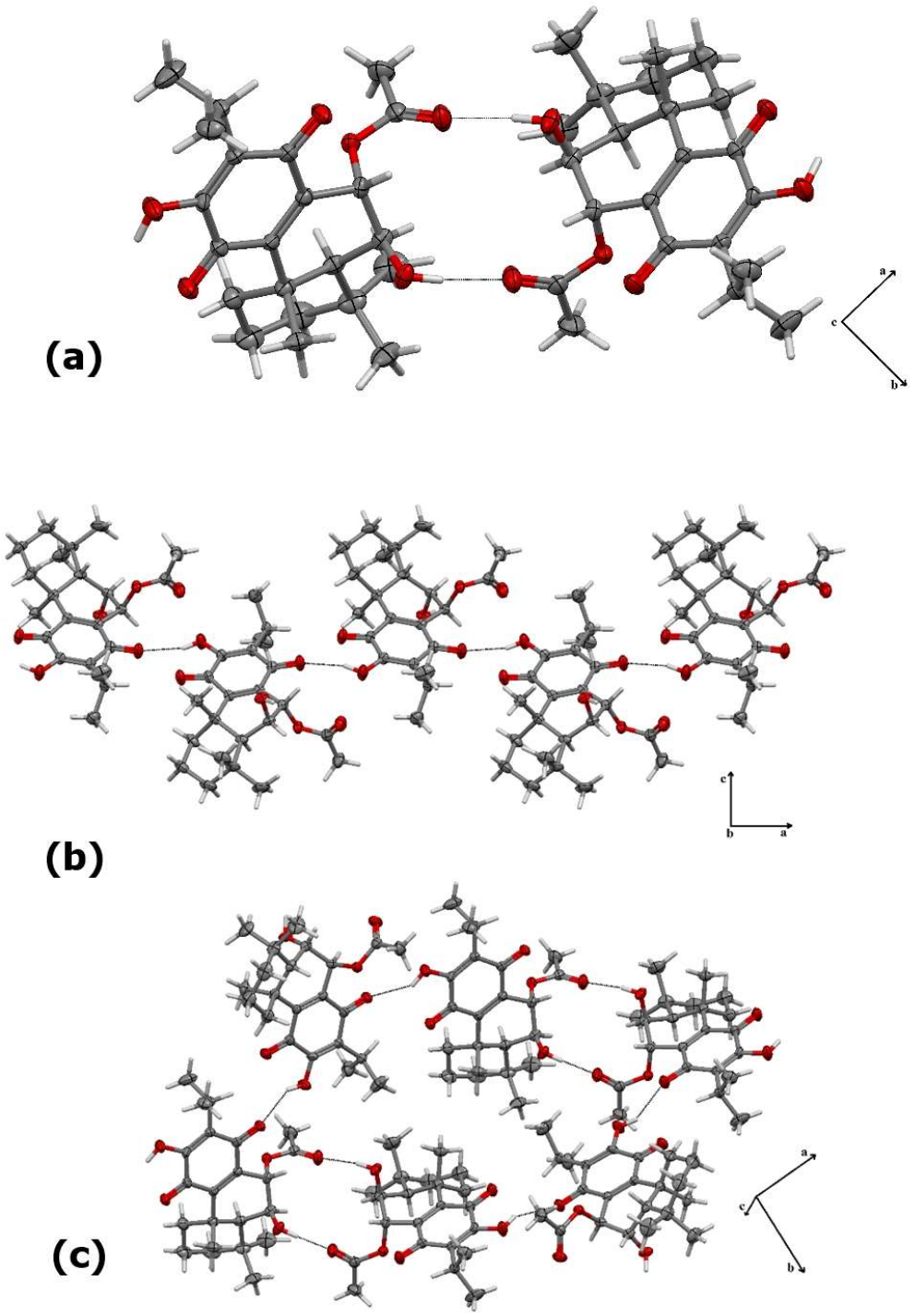

Figure 2.4 Synthon motifs in 7α-acetoxy-6β-hidroxyroyleanone (AHR):(a) $R_2^2(14)$, (b) $C_1^1(6)$; (c) $R_6^6(46)$.

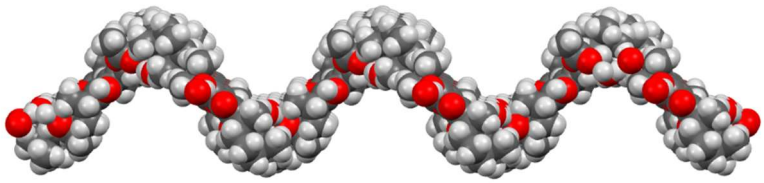

Figure 2.5 Crystal packing of 7α-acetoxy-6β-hidroxyroyleanone (AHR) showing the wave pattern defined by the chain and ring motifs formed by the hydrogen bonds.

2.3.3 Differential Scanning Calorimetry (DSC)

As shown in **Figure 2.6**, on heating the AHR sample from 298 K to 513 K, three thermal events are observed. The first two correspond to solid-solid phase transitions and the third one to fusion. The onset (T_{on}) and maximum (T_{max}) temperatures of the corresponding peaks, and the associated molar enthalpies are summarized in **Table 3**, where the assigned uncertainties correspond to twice the standard error of the mean of six independent determinations. Both solid-solid phase transitions were reversible, as demonstrated by submitting a sample to a series of heating-cooling cycles in the range 298-368 K (**Figure 2.6**). This suggests that the crystal phase initially prepared in this work, here dubbed phase III, is the stable phase bellow 333.5 K, and undergoes a phase transition to polymorph II at 336.4 K. Phase II is stable between 333.5 K and 352.0 K, where it transforms into the high temperature form I. The fact that both phase transitions are reversible, indicates that the three polymorphs are enantiotropically related i.e. there is a transition temperature before fusion at which the stability order of a polymorph pair is reversed. After the II→I solid-solid phase transition, the sample decomposes on fusion. The fusion temperature taken at the onset of the fusion peak (T_{fus} = 500.8±0.8 K) is in good agreement with that previously obtained for a sample recrystallized from acetone (500.2-501.2 K)[110]. It is, however, considerably higher than those reported for samples recrystallized from CCl_4 (487.2-490.2 K)[6] or hexane/CH_2Cl_2 (482.4-483.6 K [224] and 485.7-485.9 K [225]). This suggests that the present material has higher purity than those recrystallized from CCl_4 and hexane/CH_2Cl_2 or that different polymorphs can be obtained when different solvents are employed in the recrystallization processes.

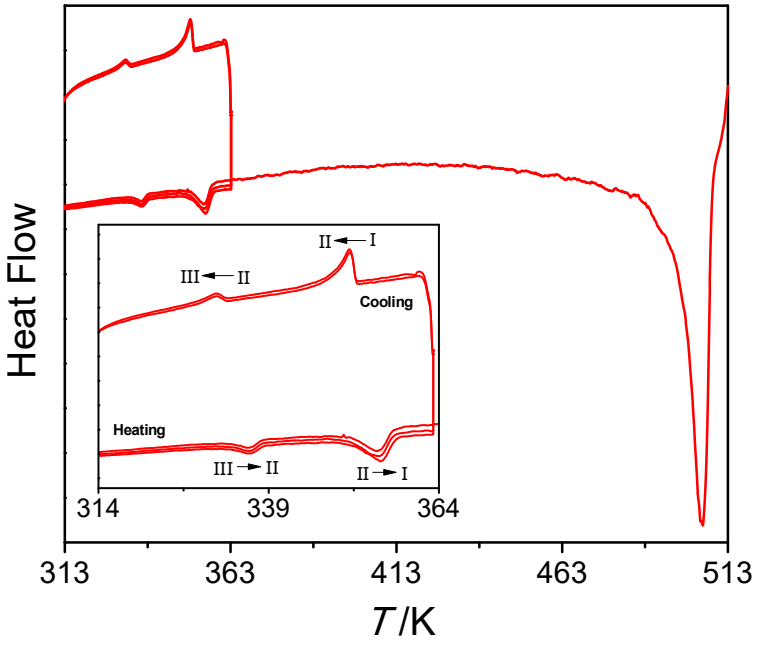

Figure 2.6 Differential scanning calorimetry measured curves obtained for 7α-acetoxy-6β-hidroxyroyleanone (AHR) in the range 298-513 K at a scanning rate of 5 K·min^{-1}. The inset corresponds to an expansion of the heating cooling cycles performed in the III → II and II → I phase transition ranges, before increasing the sample temperature up to fusion.

Table 2.4 Onset (T_{on}) and maximum (T_{max}) temperatures, and molar enthalpies ($\Delta_{trs}H^{o}_{m}$) of the phase transitions detected by DSC for 7α-acetoxy-6β-hidroxyroyleanone (AHR) in the range 298-513 K.

Phase Transition	T_{on}/K	T_{max}/K	$\Delta_{trs}H^{o}_{m}$/kJ·mol^{-1}
Form III → Form II	333.5±1.6	336.4±0.8	0.1±0.1
Form II → Form I	352.0±1.6	355.5±0.8	1.4±0.2
Fusion	500.8±0.8	506.4±0.6	34.3±1.8

2.4 Conclusions

Supercritical fluid extraction has proved to be the method of choice for extraction of the abietane AHR from *P. grandidentatus* (yield = 57.351 μg/mg). The combined results of single crystal X-ray diffraction and differential scanning calorimetry experiments evidenced the presence of three enantiotropically related polymorphic forms: form III (orthorhombic space group $P2_12_12$), whose crystal structure was obtained at 167±2 K and 296±2 K, and which is the most stable phase up to 333.5 K; form II stable in the range 333.5-352.0 K; and form I stable between 352.0 K and the fusion temperature (500.8 K) where it decomposes on melting. The

fact that the solid-solid phase transitions relating the three phases are reversible is a good indication that polymorphism may not perturb the development pharmaceutical formulations based on ARH, since once at ambient temperature forms I and II will quickly transform into form III. Melting should, however, be avoided if, for example, strategies to improve solubility based on the production of glassy materials or solid dispersions are considered.

2.5 Supporting information

Table 2.5 ^{1}H and ^{13}C NMR data for AHR.

Position	δH (ppm)	Position	δC (ppm)
12´-OH	7.19	14	185.74
7β	5.65	11	183.29
6α	4.31	7	169.60
15	3.14	12	150.90
1β	2.62	9	149.91
6-OH	~2.03*	8	137.12
7α-OAc	2.02	13	124.69
2β	1.83	7	68.75
Me-20	1.59	6	67.00
2α	1.55	5	49.76
3β	1.46	3	42.28
5α	1.32	10	38.63
Me-19	1.21	1	38.37
Me-17#	1.20	4	33.67
3α	~1.20*	18	33.52
Me-16#	1.17	15	24.17
1α	~1.17*	19	23.81
Me-18	0.93	20	21.51
6β-OAc	---	7	20.93
12-OAc	---	16	19.84
		17	19.70
		2	19.00

#Interchangeable assignments, *Overlapped signals

Table 2.6 Indexation of the Powder Pattern of the 7α-acetoxy-6β-hydroxyroyleanone sample used in the DSC study: orthorhombic, space group $P2_12_12$, a = 1420.4±2.1 pm, b = 2076.3±3.0 pm, c = 743.1±1.4 pm.

h	*k*	*l*	2θ(Obs)/º	2θ(Calc)/º	$\Delta 2\theta$/º
1	1	0	7.60	7.53	0.07
0	2	0	8.46	8.51	-0.05
1	2	0	10.59	10.55	0.05
0	0	1	11.94	11.90	0.04
2	0	0	12.39	12.45	-0.06
0	1	1	12.55	12.64	-0.09
2	1	0	13.19	13.16	0.03
1	1	1	14.12	14.10	0.02
0	2	1	14.62	14.65	-0.03
2	2	0	15.05	15.10	-0.05
1	2	1	15.92	15.93	-0.01
0	3	1	17.52	17.50	0.02
2	3	0	17.98	17.88	0.10
1	3	1	18.56	18.59	-0.02
3	1	0	19.24	19.21	0.03
3	2	0	20.49	20.60	-0.11
0	4	1	20.76	20.86	-0.10
2	4	0	21.23	21.18	0.05
1	4	1	21.76	21.79	-0.02
3	1	1	22.66	22.66	0.01
3	2	1	23.89	23.86	0.03
0	2	2	25.44	25.44	0.00
2	5	1	27.59	27.61	-0.01
4	1	1	28.15	28.16	-0.01
1	6	1	29.08	29.13	-0.05
0	5	2	32.41	32.31	0.10
1	7	1	33.13	33.10	0.03

Table 2.7 comparison between the bond distances and angles obtained in this work for AHR (296 K and 167 K) and those reported for royleanone (100 K), and 7α-hydroxyroyleanone (100 K).

	7α-Acetoxy-6β-hydroxyroyleanone		Royleanone	7α-hydroxyroyleanone
	296±2	167±2	100 K[219]	100 K [220]
			Bond Distances/Å	
C(1)-C(2)	1.532(7)	1.536(5)	1.537 (2)	1.5322 (19)
C(2)-C(3)	1.500(7)	1.518(6)	1.513 (3)	1.522 (2)
C(3)-C(4)	1.529(7)	1.535(5)	1.533 (3)	1.538 (2)
C(4)-C(5)	1.546(6)	1.551(4)	1.558 (2)	1.5547 (18)
C(4)-C(18)	1.545(6)	1.535(5)	1.539 (3)	1.534 (2)
C(4)-C(19)	1.538(7)	1.541(6)	1.538 (2)	1.534 (2)
C(5)-C(6)	1.506(6)	1.520(5)	1.534 (3)	1.526 (2)
C(6)-C(7)	1.517(6)	1.517(4)	1.514 (2)	1.5178 (19)
C(7)-C(8)	1.500(5)	1.497(4)	1.495 (2)	1.5082 (19)
C(8)-C(9)	1.333(5)	1.352(4)	1.348 (3)	1.344 (2)
C(9)-C(10)	1.536(5)	1.533(4)	1.536 (2)	1.5394 (18)
C(10)-C(1)	1.542(6)	1.552(5)	1.542 (2)	1.543 (2)
C(10)-C(5)	1.553(6)	1.562(5)	1.548 (3)	1.5570 (19)
C(10)-C(20)	1.544(6)	1.541(5)	1.542 (2)	1.546 (2)
C(11)-C(9)	1.477(6)	1.485(4)	1.481 (2)	1.4874 (19)
C(11)-C(12)	1.485(6)	1.506(4)	1.501 (2)	1.4931 (19)
C(12)-C(13)	1.334(5)	1.343(4)	1.341 (3)	1.348 (2)
C(13)-C(14)	1.460(5)	1.464(4)	1.481 (3)	1.476 (2)
C(14)-C(8)	1.494(6)	1.503(4)	1.506 (2)	1.5066 (19)
C(13)-C(15)	1.498(6)	1.510(4)	1.519 (2)	1.5098 (19)
C(15)-C(16)	1.499(7)	1.519(5)	1.535 (2)	1.530 (2)
C(15)-C(17)	1.502(7)	1.522(5)	1.532 (2)	1.530 (2)
C(41)-C(42)	1.502(7)	1.496(5)	-	-
O(6)-C(6)	1.423(5)	1.424(4)	-	-
O(4)-C(41)	1.343(5)	1.346(4)	-	-
O(4)-C(7)	1.453(5)	1.461(4)	-	1.4488 (18)
O(5)-C(41)	1.180(5)	1.197(4)	-	-
O(3)-C(14)	1.228(4)	1.229(4)	1.225 (2)	1.2288 (18)
O(2)-C(12)	1.349(5)	1.341(4)	1.349 (2)	1.3461 (17)
O(1)-C(11)	1.220(4)	1.219(3)	1.224 (2)	1.2266 (17)
			Bond Angles/degrees	
C(2)-C(1)-C(10)	110.9(4)	111.1(3)	112.12 (15)	112.22 (12)
C(3)-C(2)-C(1)	112.6(5)	112.6(4)	111.93 (18)	111.88 (12)
C(2)-C(3)-C(4)	115.1(4)	114.7(3)	114.57 (15)	114.40 (12)
C(3)-C(4)-C(5)	107.6(4)	107.7(3)	108.09 (14)	108.26 (11)
C(3)-C(4)-C(18)	111.2(5)	111.2(3)	107.69 (15)	107.13 (12)
C(3)-C(4)-C(19)	107.0(4)	107.2(3)	111.12 (16)	110.61 (12)
C(18)-C(4)-C(19)	107.2(5)	106.3(3)	106.43 (16)	107.48 (12)
C(18)-C(4)-C(5)	114.7(4)	115.3(3)	108.58 (15)	108.58 (11)

C(19)-C(4)-C(5)	108.9(4)	108.8(3)	114.68 (13)	114.52 (12)
C(6)-C(5)-C(4)	115.5(4)	115.4(3)	114.94 (15)	115.24 (11)
C(6)-C(5)-C(10)	112.7(4)	112.6(3)	109.26 (13)	110.17 (11)
C(4)-C(5)-C(10)	117.0(4)	117.2(3)	116.62 (16)	116.38 (11)
C(7)-C(6)-C(5)	108.7(4)	108.6(3)	109.12 (15)	109.42 (12)
O(6)-C(6)-C(5)	113.4(4)	113.5(3)	-	-
O(6)-C(6)-C(7)	107.9(3)	107.5(2)	-	-
C(8)-C(7)-C(6)	112.5(4)	112.8(3)	113.02 (17)	111.93 (12)
O(4)-C(7)-C(6)	108.9(3)	109.0(2)	-	108.07 (12)
O(4)-C(7)-C(8)	105.9(3)	105.6(2)	-	107.49 (11)
C(9)-C(8)-C(7)	123.4(4)	123.2(3)	122.99 (14)	123.18 (12)
C(9)-C(8)-C(14)	122.4(4)	122.2(3)	121.79 (15)	122.44 (12)
C(7)-C(8)-C(14)	114.2(3)	114.6(3)	115.20 (15)	114.35 (12)
C(8)-C(9)-C(10)	124.3(4)	124.3(3)	123.65 (15)	124.29 (12)
C(8)-C(9)-C(11)	116.1(4)	116.3(3)	116.69 (14)	116.29 (12)
C(11)-C(9)-C(10)	119.6(3)	119.3(3)	119.60 (16)	119.34 (12)
C(1)-C(10)-C(5)	107.0(4)	106.5(3)	107.17 (13)	107.24 (11)
C(20)-C(10)-C(1)	109.3(4)	109.0(3)	110.27 (16)	109.94 (11)
C(9)-C(10)-C(1)	110.1(4)	110.4(3)	109.58 (13)	110.91 (11)
C(9)-C(10)-C(5)	107.3(3)	107.4(3)	106.69 (14)	106.92 (11)
C(20)-C(10)-C(5)	116.1(4)	116.4(3)	115.45 (14)	115.00 (12)
C(9)-C(10)-C(20)	106.9(3)	107.1(3)	107.53 (12)	106.82 (12)
C(9)-C(11)-C(12)	120.0(4)	120.1(3)	119.46 (16)	120.26 (12)
O(1)-C(11)-C(9)	123.3(4)	123.6(3)	123.94 (15)	123.52 (13
O(1)-C(11)-C(12)	116.7(4)	116.3(3)	116.59 (16)	116.22 (13)
C(13)-C(12)-C(11)	124.2(4)	123.3(3)	122.80 (16)	123.13 (12)
O(2)-C(12)-C(11)	114.6(4)	114.7(3)	113.40 (16)	114.03 (12)
O(2)-C(12)-C(13)	121.2(4)	121.9(3)	123.80 (15)	122.83 (12)
C(12)-C(13)-C(14)	114.9(4)	116.0(3)	116.67 (14)	116.18 (12)
C(12)-C(13)-C(15)	126.0(4)	125.3(3)	125.48 (17)	124.46 (13)
C(14)-C(13)-C(15)	119.0(4)	118.7(3)	117.82 (16)	119.36 (13)
C(13)-C(14)-C(8)	121.9(4)	121.7(3)	120.41 (16)	120.78 (12)
O(3)-C(14)-C(8)	118.3(4)	117.3(3)	118.62 (15)	118.62 (13)
O(3)-C(14)-C(13)	119.8(4)	121.0(3)	120.92 (15)	120.59 (13)
C(13)-C(15)-C(16)	112.5(5)	111.5(3)	109.82 (14)	110.95 (12)
C(13)-C(15)-C(17)	113.0(4)	113.0(3)	113.86 (15)	112.84 (12)
C(16)-C(15)-C(17)	112.3(5)	111.8(4)	110.11 (15)	110.82 (12)
O(5)-C(41)-C(42)	110.2(4)	111.0(3)	-	-
O(5)-C(41)-O(4)	123.1(5)	123.2(3)	-	-
O(4)-C(41)-C(42)	126.7(5)	125.8(3)	-	-
C(41)-O(4)-C(7)	116.5(3)	116.6(3)	-	-
		Torsion Angles/degrees		
C(10)-C(1)-C(2)-C(3)	-57.3(7)	-57.3(5)	−56.7 (2)	−56.85 (16)
C(1)-C(2)-C(3)-C(4)	54.5(7)	54.2(5)	54.2 (2)	54.11 (17)
C(5)-C(4)-C(3)-C(2)	-49.0(6)	-48.9(4)	−49.9 (2)	−49.87 (16)
C(18)-C(4)-C(3)-C(2)	77.4(6)	78.3(4)	−167.00 (15)	−166.79 (12)
C(19)-C(4)-C(3)-C(2)	-165.9(5)	-165.8(4)	76.8 (2)	76.36 (15)

C(6)-C(5)-C(4)-C(3)	-171.9(4)	-171.5(3)	-177.96 (16)	−176.51 (12)
C(10)-C(5)-C(4)-C(3)	51.8(5)	52.3(4)	52.25 (18)	52.23 (16)
C(6)-C(5)-C(4)-C(18)	63.8(6)	63.7(4)	−61.40 (19)	−60.53 (17)
C(10)-C(5)-C(4)-C(18)	-72.5(6)	-72.5(4)	168.81 (14)	168.22 (12)
C(6)-C(5)-C(4)-C(19)	-56.3(6)	-55.6(4)	57.5 (2)	59.57 (16)
C(10)-C(5)-C(4)-C(19)	167.4(4)	168.2(3)	−72.3 (2)	−71.68 (16)
C(4)-C(5)-C(6)-C(7)	156.1(4)	156.3(3)	158.12 (15)	157.64 (12)
C(10)-C(5)-C(6)-C(7)	-65.8(5)	-65.5(3)	−68.58 (19)	−68.21 (14)
C(4)-C(5)-C(6)-O(6)	-83.9(5)	-84.2(3)	-	-
C(10)-C(5)-C(6)-O(6)	54.2(5)	53.9(4)	-	-
C(8)-C(7)-C(6)-C(5)	45.2(5)	45.9(3)	40.90 (19)	44.75 (16)
O(4)-C(7)-C(6)-C(5)	-72.0(5)	-71.1(3)	-	−73.43 (14)
C(8)-C(7)-C(6)-O(6)	-78.2(4)	-77.3(3)	-	−73.43 (14)
O(4)-C(7)-C(6)-O(6)	164.6(3)	165.7(3)	-	-
C(6)-C(7)-C(8)-C(9)	-12.5(6)	-14.1(4)	−4.3 (2)	−10.8 (2)
C(6)-C(7)-C(8)-C(14)	166.4(3)	165.0(3)	-	171.12 (12)
O(4)-C(7)-C(8)-C(9)	106.4(5)	104.8(4)	-	107.73 (15)
O(4)-C(7)-C(8)-C(14)	-74.7(4)	-76.1(3)	177.17 (14)	−70.35 (15)
C(10)-C(9)-C(8)-C(7)	-3.7(7)	-2.1(5)	−7.2 (2)	−2.6 (2)
C(11)-C(9)-C(8)-C(7)	174.5(4)	175.2(3)	169.78 (13)	174.19 (13)
C(10)-C(9)-C(8)-C(14)	177.5(4)	178.9(3)	171.21 (13)	175.36 (13)
C(11)-C(9)-C(8)-C(14)	-4.3(6)	-3.8(5)	−11.8 (2)	−7.9 (2)
C(8)-C(9)-C(10)-C(1)	-129.7(5)	-130.2(4)	−134.34 (17)	−134.70 (14)
C(11)-C(9)-C(10)-C(1)	52.1(5)	52.7(4)	48.77 (19)	48.64 (17)
C(8)-C(9)-C(10)-C(5)	-13.6(6)	-14.4(4)	−18.63 (19)	−18.10 (19)
C(11)-C(9)-C(10)-C(5)	168.3(4)	168.5(3)	164.48 (13)	165.24 (11)
C(8)-C(9)-C(10)-C(20)	111.7(5)	111.3(4)	105.79 (19)-	105.50 (16)
C(11)-C(9)-C(10)-C(20)	-66.5(5)	-65.8(4)	−71.10 (19)	−71.16 (15)
C(5)-C(10)-C(1)-C(2)	55.8(6)	55.8(4)	55.2 (2)	55.46 (15)
C(9)-C(10)-C(1)-C(2)	172.1(4)	172.1(3)	170.62 (16)	171.86 (12)
C(20)-C(10)-C(1)-C(2)	-70.8(6)	-70.5(4)	−71.2 (2)	−70.22 (15)
C(1)-C(10)-C(5)-C(4)	-56.2(5)	-56.4(4)	−55.33 (17)	−55.33 (16)
C(1)-C(10)-C(5)-C(6)	166.3(4)	166.2(3)	172.24 (13)	171.09 (11)
C(9)-C(10)-C(5)-C(4)	-174.4(4)	-174.8(3)	−172.64 (13)	−174.34 (12)
C(9)-C(10)-C(5)-C(6)	48.1(5)	47.8(3)	54.93 (16)	52.09 (15)
C(20)-C(10)-C(5)-C(4)	66.1(5)	65.3(4)	67.96 (19)	67.26 (16)
C(20)-C(10)-C(5)-C(6)	-71.4(5)	-72.1(4)	−64.48 (19)	−66.31 (15)
C(12)-C(11)-C(9)-C(10)	-174.3(4)	-175.3(3)	−165.74 (13)	−172.31 (12)
C(12)-C(11)-C(9)-C(8)	7.4(6)	7.3(4)	17.2 (2)	10.76 (19)
O(1)-C(11)-C(9)-C(8)	-172.6(5)	-172.6(3)	−162.38 (16)	−168.73 (14)
O(1)-C(11)-C(9)-C(10)	5.7(7)	4.8(5)	14.7 (2)	8.2 (2)
C(9)-C(11)-C(12)-C(13)	-5.7(7)	-6.2(5)	−10.4 (2)	−5.5 (2)
O(1)-C(11)-C(12)-C(13)	174.3(5)	173.7(3)	169.20 (16)	174.01 (13)
C(9)-C(11)-C(12)-O(2)	176.5(4)	175.8(3)	169.71 (14)	174.85 (12)
O(1)-C(11)-C(12)-O(2)	-3.5(6)	-4.3(4)	−10.7 (2)	−5.63 (19)
C(11)-C(12)-C(13)-C(14)	0.4(6)	1.0(5)	−2.1 (2)	−2.7 (2)
C(11)-C(12)-C(13)-C(15)	-180.0(5)	-179.3(3)	176.03 (14)	177.11 (13)

O(2)-C(12)-C(13)-C(14)	178.2(4)	178.9(3)	177.82 (14)	176.88 (13)
O(2)-C(12)-C(13)-C(15)	-2.2(7)	-1.5(5)	−4.1 (2)	−3.3 (2)
C(8)-C(14)-C(13)-C(12)	2.8(6)	2.6(4)	7.7 (2)	5.73 (19)
C(8)-C(14)-C(13)-C(15)	-176.8(4)	-177.0(3)	−170.58 (13)	−174.11 (13)
O(3)-C(14)-C(13)-C(12)	-175.5(4)	-177.9(3)	−174.92 (15)	−175.35 (15)
O(3)-C(14)-C(13)-C(15)	4.9(6)	2.4(5)	6.8 (2)	4.8 (2)
C(13)-C(14)-C(8)-C(7)	-179.7(4)	179.8(3)	178.12 (13)	177.93 (13)
C(13)-C(14)-C(8)-C(9)	-0.8(6)	-1.2(5)	−0.4 (2)	−0.2 (2)
O(3)-C(14)-C(8)-C(7)	-1.4(6)	0.3(4)	0.68 (19)	−1.0 (2)
O(3)-C(14)-C(8)-C(9)	177.6(4)	179.4(3)	−177.84 (15)	−179.11 (15)
C(12)-C(13)-C(15)-C(16)	-63.8(7)	-68.0(5)	−69.8 (2)	−63.29 (18)
C(14)-C(13)-C(15)-C(16)	115.7(5)	111.6(4)	108.33 (18)	116.53 (14)
C(12)-C(13)-C(15)-C(17)	64.6(7)	59.0(5)	54.2 (2)	61.75 (19)
C(14)-C(13)-C(15)-C(17)	-115.8(5)	-121.4(4)	−127.68 (17)	−118.43 (14)
C(7)-O(4)-C(41)-O(5)	-4.1(6)	-3.9(4)	-	-
C(7)-O(4)-C(41)-C(42)	175.3(4)	175.2(3)	-	-
C(41)-O(4)-C(7)-C(8)	153.4(3)	155.0(3)	-	-
C(41)-O(4)-C(7)-C(6)	-85.3(4)	-83.5(3)	-	-

Table 2.8 Comparison of the Hydrogen Bond Distances and Angles Obtained in this Work for 7α-Acetoxy-6β-hydroxyroyleanone at 296 K and 167 K, with those Reported at 100 K for Royleanone and 7α-Hydroxyroyleanone (D = donor; A = acceptor).

	D–H	H···A	D···A	D–H···A

	7α-Acetoxy-6β-hidroxyroyleanone (296±2 K)			
O(2)–H(2O)···O(1)	0.80	2.15	2.5984(7)	116
(intramolecular)				
O(2)–H(2O)···O(3)	0.80	2.20	2.8467(8)	139
O(6)–H(6O)···O(5)	0.82	2.02	2.7963(8)	158
C(15)–H(15)···O(1)	0.96	2.48	3.3278(9)	148
	7α-Acetoxy-6β-hidroxyroyleanone (167±2 K)			
O(2)–H(2O)···O(1) (intramolecular)	0.83	2.13	2.6112(2)	117
O(2)–H(2O)···O(3)	0.83	2.10	2.8111(3)	144
O(6)–H(6O)···O(5)	0.85	1.96	2.7860(3)	163
C(15)–H(15)···O(1)	1.00	2.45	3.3473(3)	150
	Royleanone (100 K)[219]			
O(2)–H(2O)···O(1)	0.88	2.05	2.5977 (18)	119
O(2)–H(2O)···O(3)	0.88	2.35	3.1079 (19)	145
C(7)–H(7A)···O(1)	0.97	2.51	3.131 (3)	122
	7α-Hydroxyroyleanone (100 K)[220]			
O(2)–H(2O)···O(1)	0.83 (2)	2.075 (19)	2.5892 (14)	119.8 (19)
O(4)–H(2O)···O(1)	0.88 (2)	2.24 (3)	2.9502 (15)	137 (2)
O(4) –H(1O4)···O(3)	0.88 (2)	2.52 (3)	2.9399 (14)	109.8 (19)
O(2)–H(2O)···O(3)	0.83 (2)	2.42 (2)	3.1635 (14)	148.8 (18)
C(7)–H(7A)···O(1)	0.98	2.42	3.0998 (17)	126
C(15)–H(15)···O(1)	0.98	2.38	2.8549 (17)	109
C(1)–H(1A)···O(1)	0.97	2.33	2.9493 (18)	121

Chapter 3

Effect of 7α-acetoxy-6β-hydroxyroyleanone on an MRSA/VISA strain: membrane and cell wall interaction

Effect of 7α-acetoxy-6β-hydroxyroyleanone on an MRSA/VISA strain: membrane and cell wall interaction

3.1 Introduction

The resistance to antibiotics is one of the biggest health problems in the world. Since this is a phenomenon in continuous growth, new aprproachest and new options as antibacterial agents appear for to control of this health problem [226].

Multidrug resistant strains such as Methicillin-resistant *Staphylococcus aureus* (MRSA) have been spreading at alarming rates. Its multidrug resistant profile is determined by the presence of the penicillin-binding protein 2a (PBP2a) *mecA* gene, which results in a low tropism to all *β*-lactams [227]. Adverse outcomes, such as associated increased morbidity and mortality, are issues of high concern among healthcare and community facilities. Surveillance and control strategies are necessary interventions towards a decreased prevalence of such pathogen [228], however discovering and/or developing new antibacterial agents are also of great matter.

The treatment of human infections resorting to plants is long established in traditional medicine. The demonstrated therapeutic effects of some plants have attracted researchers to discover which compounds are responsible for such bioactivity [151].

Secondary metabolites, such a diterpenes, have been the focus of a series of scientific studies due to their acknowledged bioactivity [229]. Many royleanone diterpenes, including 7α-acetoxy-6β-hydroxyroyleanone (AHR), are documented for their antibacterial ascertain activity [151, 195]. AHR is frequently found in *Plectranthus grandidentatus* and its optimized isolation has been documented [195]. Along with other similar diterpenes, this compound has revealed activity against Gram-positive bacteria, and more importantly, against MRSA strains [67, 151, 230].

However, to the best of our knowledge, its mechanism of action is not entirely known [151]. In the hopes of unveiling the mechanism behind bacterial death, the effect of AHR on MRSA bacterial cell membrane and cell wall was studied.

3.2 Materials and Methods

3.2.1 Reagents

1,2-dioleoyl-*sn*-Glycero-3-phosphocholine (DOPC), 1-palmitoyl-2-oleoyl-*sn*-glycero-3-phosphocholine (POPC) and *N*-palmitoyl-sphingomyelin (PSM) were purchased from Avanti Polar Lipids (Alabaster, AL). Cholesterol, 5,6-carboxyfluorescein (CF), 8-hydroxypyrene-1,3,6-trisulfonic acid (HPTS) trisodium salt (pyranine), Sephadex G-25 and Triton X-100 were acquired from Sigma-Aldrich Química, S.L. (Sintra, Portugal). Solvents for lipid and Royleanone derivative (AHR) stock solutions were of spectroscopic grade. Methicillin, ampicillin and vancomycin were obtained from Sigma-Aldrich.

3.2.2 Extraction, isolation and purification of AHR

Three extraction processes were performed to obtain extracts with different AHR context from *Plectranthus grandidentatus*. Supercritical fluid (SCF) extraction was carried out in an experimental apparatus equipped with a sample cell with 100 dm^3. Air-dried leaves (100.45g) were powdered extract with CO_2 for 4h at 40ºC and 230 bar. After extraction, the extract was recovered with acetone. Acetone maceration extraction was carried out using 100.88g of dried plant and 1L acetone at room temperature and strong agitation for 1h. The resulting extract was then filtrated and the solvent evaporated in a rotary evaporator. Acetone ultrasonic-assisted extraction was carried out using 100.13g of dried powdered leaves with 1L acetone. The suspension was maintained in an ultrasonic bath for 1h at room temperature. After extraction, the suspension was filtrated and the solvent evaporated. The content of AHR present in the extract was evaluated by HPLC-DAD according to the method developed and published previously [231]. The isolation of AHR was conducted through different chromatographic methods previously described by our group [73, 92, 198, 200, 237, 238].

3.3 Liposome preparation

To obtain a final lipid concentration of 5mM in the liposomal suspensions, the appropriate volume of a stock solution of lipid in chloroform was mixed and the solvent removed by evaporation under a mild flow of nitrogen. Then, samples were placed in vacuum overnight to ensure the complete elimination of organic solvent. The lipid film was hydrated with 10mM Tris-HCl, 20mM NaCl 0.1mM EDTA buffer to a final lipid concentration of 5 mM. After that, seven freeze/thaw cycles (liquid nitrogen/water bath) were performed. Subsequently, 100 nm large unilamellar vesicles (LUVs) were prepared by the extrusion method as described previously [233].

The stock solution of AHR (10 mg.mL^{-1}) was prepared in DMSO and stored at -18ºC. During each experiment, a fresh aliquot solution was used and diluted in the corresponding buffer. The concentration of DMSO on experiment solution was under 1%.

3.3.1 Absorption measurements

The absorption spectra were obtained with a Shimadzu UV 560 double beam spectrophotometer, in the absence and presence of LUV suspension, in Tris-HCl, pH 7.4 buffer. DOPC LUVs were prepared at a total lipid concentration of 1 mM and AHR at 20µM. The light scattering due to LUVs in suspension was corrected with the subtraction of an appropriate blank.

3.3.2 Strains and growth conditions

The MRSA/VISA strain CIP 106760, from Faculdade de Farmacia da Universidade de Lisboa, was used in this study. It was routinely grown in mannitol salt agar (Chapman medium, Merck, USA) at 37ºC with aeration. All experiments were performed in Mueller-Hinton broth or Mueller-Hinton agar (Merck, USA).

3.3.3 Synergy studies

Antibiotic synergy effect between AHR with methicillin, vancomycin and ampicillin were evaluated through well-diffusion method. The synergy was evaluated by measuring the inhibition halos in Mueller-Hinton agar plates. AHR (1 mg.mL^{-1}) was combined with an antibiotic (1 mg.mL^{-1}), at well concentration of 0.5 mg.mL^{-1}. The results were deliberated after plates were incubated at 37ºC for 24h. DMSO, AHR and antibiotic inhibition were performed as controls. The study was conducted at least three independent assays.

3.3.4 Bacterial Growth curve

The bacterial growth was observed over time when combined to different concentrations of AHR. An 100µL inoculum (≈ 10^5 CFU) was incubated at 37ºC with stirring in 9 mL of Mueller-Hinton broth with 1 mL AHR solution to a final concentration of [MIC]/2, [MIC] and 2[MIC]. Bacterial growth was determining at 15-min intervals by measuring the optical density at 620nm.

3.3.5 Cell leakage assay

For the cell leakage analysis, an overnight culture of CIP 106760 strain was centrifuged and resuspended in 0.9% sterile sodium chloride solution to yield a final OD (λ=620nm) of 3. Then, AHR was added at different inhibitory concentrations and the cell suspensions were

incubated at 37ºC. The cell supernatants were monitored by measuring the OD (λ=260nm) for 4h.

3.3.6 Membrane interaction and Leakage assay

The AHR effect on lipid bilayers passive permeability was monitored by measuring the leakage of intraliposomal CF, through the concomitant increase of fluorescence intensity [234]. LUV suspensions were prepared in buffer Hepes 10 mM, pH 7.4, containing CF at a concentration of 40 mM. Afterwards, non-encapsulated CF was separated from vesicles suspension through a gel filtration in a Sephadex G-25 column equilibrated with buffer Hepes 50 mM, pH 7.4. 500 µL fractions were collected and only the third one, containing the LUVs with encapsulated CF, was used for the leakage assay. Then, LUV suspension was distributed into a 96-well standard opaque microplate to a final lipid concentration of 0.5 mM, in a final volume of 250 µL. The minimum inhibitory concentration (MIC) of AHR (20 µM), 2MIC (40 µM) and MIC/2 (10 µM) were tested. Liposome suspensions containing CF in the presence of 0.9% of DMSO were used as a control.

The variation of fluorescence intensity was measured at excitation and emission wavelengths of 492 and 530 nm, respectively, with a cut off filter of 515 nm, using a microplate reader (Gemini EM Microplate Reader, Molecular Devices), at 25 °C. The fluorescence intensity measurements were performed initially only with the LUV suspension, then in the presence of different AHR concentrations, and, finally, by adding Triton X-100 to a final concentration of 0.5% (v/v) to obtain the value corresponding to the complete release of CF. Quantification of leakage was determined according to the following equation 1 [234]:

$$Leakage\ (\%) = \frac{F_p - F_0}{F_{100} - F_0} \times 100$$

where F_p corresponds to fluorescence value over time, F_0 is the initial fluorescence of the vesicle suspension, and F_{100} is the fluorescence value after the addition of Triton X-100. The values were converted considering the control measurements.The phospholipid concentration in the final LUV suspensions was confirmed by quantification of inorganic phosphate following the colorimetric method of Rouser [235].

3.3.7 Proton leakage assay

The effect of AHR on ion exchange through lipid bilayers was followed by ratiometric fluorimetric measurements using a pH-sensitive probe, HPTS, following procedures described in [236]. LUVs of POPC/SM/cholesterol, in the proportions of 59.7:26.3:14 (26% liquid ordered

phase, l_o) and 34:32.7:33.3 (83% l_o phase), were prepared in citrate phosphate buffer (citric acid 100 mM, Na_2HPO_4 200 mM, pH 5.0) containing 0.5 mM of HPTS. Those two lipid composition are referred further ahead as low-cholesterol and high-cholesterol. The excess HPTS was separated from LUVs with encapsulated HPTS by gel filtration in a Sephadex G-25 column equilibrated in buffer Hepes 10 mM, NaCL 150 mM, pH7.4 and 1.0 mL fractions were collected.

Then, LUV suspension was distributed into a 96-well standard opaque microplate to a final lipid concentration of 0.2 mM, in a final volume of 250 µL per well. AHR concentrations employed and the control were the same as in the CF leakage assay.

The pH measurements inside the liposomes were performed using the ratio of fluorescence at two excitation wavelengths, 405 and 450 nm, and a fixed emission wavelength of 510 nm ($IF_{450/405}$), with a 495 nm cut off filter, in the microplate reader referred above, at 25 °C. Finally, Triton X-100 was added to a final concentration of 1% (v/v) to acquire the intensity ratio corresponding to the total dissipation of pH gradient. The dissipation percentage of pH gradient (%ΔpH), considering as appropriate a linear relation with $IF_{450/405}$ in the pH range covered, was determined according to equation 1 [234].

3.3.8 Cell surface charge

The influence of AHR in bacterial surface charge was determined by cytochrome c binding, as described by Palacios and Mukhopadhyay [232, 243]. Bacteria cells were grown to mid-exponential phase, recovered and washed twice in PBS buffer (pH 7.2) by centrifugation for 5 min at 3000 rpm. A cellular suspension with OD 600nm of 7.0 in buffer was incubated with 0.5 $mg.mL^{-1}$ of cytochrome c and with the combination with AHR at MIC/2, MIC and 2.MIC. The suspension was allowed to incubate for 10 min at room temperature and the supernatant recovered by centrifugation. The supernatant cytochrome c was quantified at 530 nm and compared with controls. The experiment was made in triplicate on different days. The quantity of bound molecule was calculated from the difference between these values.

3.3.9 Lysis assay

Lysis assays were performed in sterile nontreated 96-well microplates at 37°C with shaking (80 rpm) and measured during 2 h. Heat-inactivated cells of MRSA/VISA strain was prepared as described by Grilo *et al.* [238]. Bacteria were incubated in Mueller-Hinton medium until begin exponential phase. Cells were recovered and washed twice with PBS pH 7.2 and autoclaved during 20 min at 121ºC. After autoclaving, cells were washed and resuspended in PBS to an initial OD600 of 0.3. AHR at [MIC]/2, [MIC] and 2[MIC] concentrations were added to

the wells at the beginning of the assay at different concentrations and different time points at 30min, 1h and 2h. The assay was performed in triplicate.

3.3.10 Analysis of peptidoglycan composition

Isolation of cell wall was performed as previously described [244, 245]. Briefly, cells were harvested by centrifugation, washed twice with cold double-distilled water, resuspended in 10% sodium dodecyl sulfate and boiled for 20 min, to remove the cell wall-associated proteins. After the sodium dodecyl sulfate was washed off, the cells were disrupted using 106 mm glass beads (Sigma) and FastPrep FP120 apparatus (Bio 101, La Jolla, California, USA), purified and washed. After centrifugation, the cell wall fragments were resuspended in 0.1 M Tris-HCl (pH 7.5) and incubated with 0.5 $mg.mL^{-1}$ trypsin to degrade cell-bound proteins. Purified cell walls were washed with double-distilled water and lyophilized. To isolate the peptidoglycan fraction, the cell walls were next incubated with 49% hydrofluoric acid, in order to remove teichoic acids. The purified peptidoglycan was washed with water several times to remove all traces of hydrofluoric acid and then lyophylised. Identical amounts of peptidoglycan were digested with mutanolysin (1 $mg.mL^{-1}$; Sigma). The resulting muropeptides were reduced with sodium borohydride and separated by reverse phase-high performance liquid chromatography (RP-HPLC) using a Hypersil ODS (Runcorn Cheshire, UK) column (3 mm particle size, 25064.6 mm, 120 A ° pore size) and a linear gradient from 5% to 30% MeOH in 100 mM sodium phosphate buffer pH 2.5 at a flow rate of 0.5 $mL.min^{-1}$ as described [245, 247].

3.3.11 Electron microscopy analysis

High-resolution imaging of bacteria treated with AHR was performed by scanning electron microscope (SEM) (JEOL 5200LV, JEOL Ltd., Tokyo, Japan). Bacteria were incubated overnight in Mueller-Hinton broth at 37ºC. Cells were centrifuged at 3000 rpm for 10min and washed twice in PBS buffer pH 7.4. The remaining cells were resuspended in PBS buffer, the OD 600 nm measured and diluted to obtain an OD of 2.0. AHR was added at different inhibition concentrations and allowed to incubate for 30min at room temperature with cell suspension. The preparation of different samples for imaging was prepared as described by F. He *et al.* [242]. A positive control was considered with cell suspension untreated.

3.4 Results and Discussion

Optimization of AHR extration

The *Plectranthus* species are known for their predominance in diterpenes with royleanone scaffold. According to a recent study [209], to optimize AHR extraction, this was carried out resorting to three different methods. The content of AHR in all three extracts was evaluated through HPLC-DAD. The results are shown in **Table 3.1**. A higher extractive capacity was evident using the supercritical fluid process and acetone as solvent. Extraction using ultrasonic-assisted and maceration resulted in very similar yields.

Table 3.1. Quantification of AHR in different *P. grandidentatus* extracts.

Extraction method	AHR index (μg mg^{-1} extract)
Acetone maceration	9.77
Acetone ultrasonic-assisted	8.04
Supercritical fluid	57.35

Effect of AHR on the growth rate of CIP106760 strain

Royleanone was added at multiple values of the MIC [67] for three different concentrations, twice the MIC (15.6 μg.mL^{-1}), MIC (7.8 μg.mL^{-1}) and half the MIC (3.9 μg.mL^{-1}), to a growing culture the MRSA strain CIP106760 (**Figure 3.1**). The growth profile of the strain in the presence of AHR was compared to its growth rate in the absence of compound. The growth rate of CIP106760 (0.00143 min^{-1}) decreased to almost half its value (0.00084 min^{-1}) at the MIC concentration of AHR and growth was almost completely impaired at twice the MIC concentration. For the lower AHR concentration tested, half the MIC, although the decrease of the growth rate was lower than 10% (0.00132 min^{-1}), the OD value attained in the stationary phase was approximately half the OD value of CIP106760, suggesting a strong effect on cell viability.

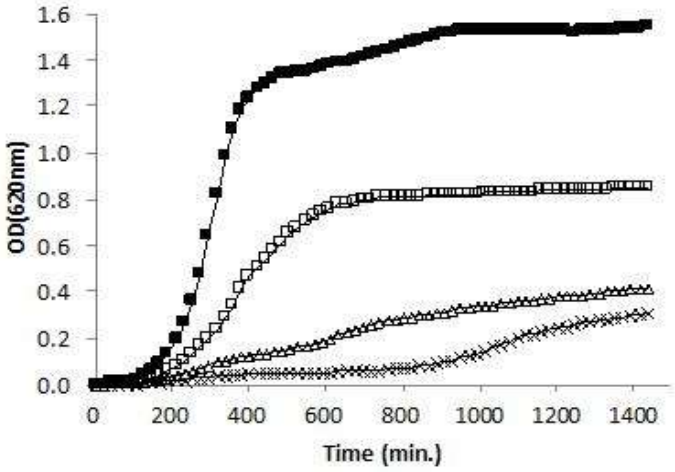

Figure 3.1 Growth curves of MRSA CIP106760 (■) and CIP106760 challenged with different concentrations of 7α-acetoxy-6β-hydroxyroyleanone; (□) half the MIC (3.9 μg.mL^{-1}); (Δ) MIC (7.8 μg.mL^{-1}); (✕) double the MIC (15.6 μg.mL^{-1}). Growth was monitored by measuring the OD_{620nm} for 24h in a microplate reader.

Effect of AHR on the viability of CIP106760 strain

To determine the bacteriostatic and bactericidal properties of AHR, the antibacterial activity of AHR was evaluated by monitoring the number of viable cells (c.f.u./ml) in paralell with the culture turbidity, over time (Figure 2). The bacterial growth curve was followed for 300 min from the addition of the compound, to the beginning of exponential phase. For half the MIC concentration (3.9 μg.mL^{-1}), the reduction observed in the growth rate of the bacterial culture was not accompanied by a loss in viability, suggesting a bacteriostatic effect. However, for higher compound concentrations, at the MIC and double MIC values (7.8 μg.mL^{-1} and 15.6 μg.mL^{-1}, respectively), the steadiness of the culture turbidity was accompanied by a continuous decrease in cell viability, suggesting a bactericidal effect.

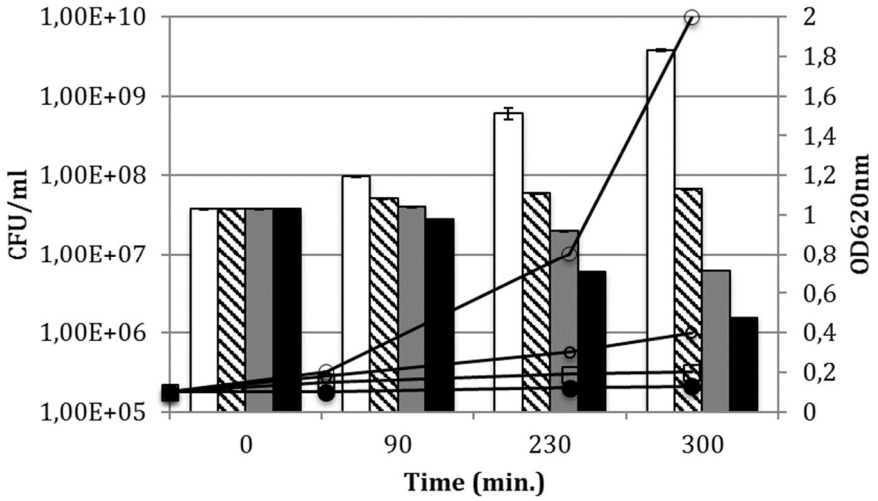

Figure 3.2 Comparison of the effect of AHR on the culture turbidity and on the cell viability. The optical density (OD_{620nm}) and c.f.u..ml^{-1} were measured at discrete time points and represented as a line chart and a column chart, respectively. The growth profiles were determined MRSA CIP106760 (■; white bar) and CIP106760 challenged with different concentrations of 7α-acetoxy-6β-hydroxyroyleanone; (□; striped bar) half the MIC (3.9 µg.mL^{-1}); (Δ; grey bar) MIC (7.8 µg.mL^{-1}) and (✕; black bar) double the MIC (15.6 µg.mL^{-1}).

Effect of AHR on the cell integrity of CIP106760 strain

To determine if AHR mode of action involves the disruption of cellular integrity, cell leakage assays were performed (**Figure 3.3**). CIP106760 cells were incubated with AHR at the MIC, half MIC and double MIC concentrations, and the supernatant of the cell suspension was analysed at discrete time points for 16 hours the after challenge. The monitorization of the optical density value of the cell supernatant at a wavelength of 260nm (OD_{260nm}), allows to obtain a relative quantification of the nucleic acid contents, result of cytoplasmic contents leakage from compromised cells.

The endopeptidase lysostaphin was used as a positive control, as it specifically disrupts the pentaglycine bridge of the peptidoglycan of certain Staphylococcus species, leading to rapid cell lysis [244, 245]. As a negative control, cells were incubated with DMSO. All tested concentrations of AHR caused no significant cell disruption until 180 min of incubation, presenting OD_{260nm} values similar to the negative control and much lower than the positive control, for which cell lysis was observed. However, from 240 min of incubation, a modest increase of the OD_{260nm} value of the supernatant of cells treated with any of the concentrations of AHR tested, suggests that a moderate leakage of nucleic acids occurs, possibly resulting from a controlled disruption of the membrane and/or cell wall.

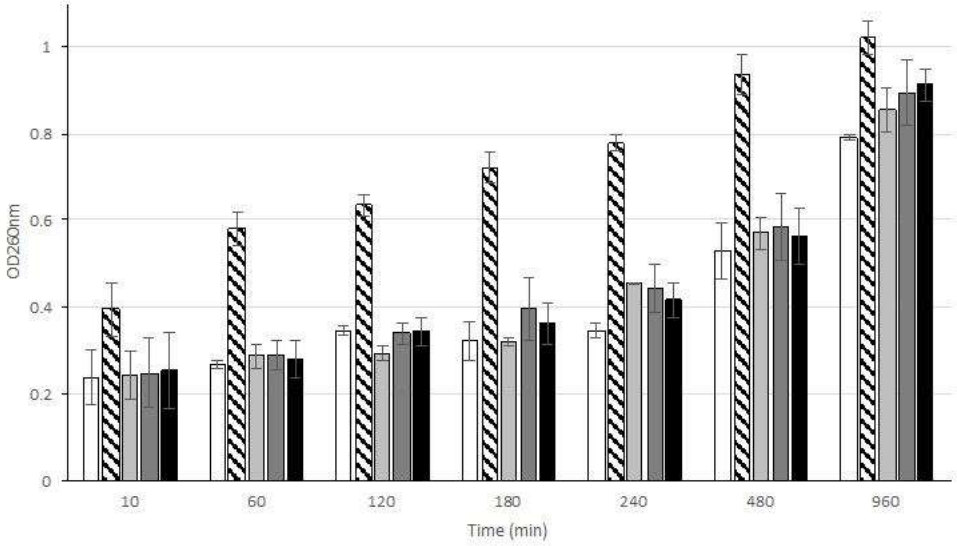

Figure 3.3 Cell leakage assay of MRSA CIP 106760 strain challenged with 7α-acetoxy-6β-hydroxyroyleanone. The optical density (OD_{260nm}) of the cell supernatant was measured at discrete time points for MRSA CIP106760 in the presence of DMSO (white bar), CIP106760 challenged with 100 $\mu g.mL^{-1}$ of lysostaphin (striped bar) and CIP106760 challenged with different concentrations of 7α-acetoxy-6β-hydroxyroyleanone; (light grey bar) half the MIC (3.9 $\mu g.mL^{-1}$); (dark grey bar) MIC (7.8 $\mu g.mL^{-1}$) and (black bar) double the MIC (15.6 $\mu g.mL^{-1}$).

Assessment of AHR cell wall lytic activity

To determine if the AHR could directly mediate hydrolysis of the cell wall of *S. aureus*, cells of CIP106760 strain were heat-inactivated by autoclaving, washed from growth medium and ressuspended in PBS buffer. After normalization of the optical density, the inactivated cell suspension was incubated with AHR at the MIC, half MIC and double MIC concentrations, and the optical density of the cell suspension was analysed at discrete time points for 2 hours the after challenge. Incubation of the heat-inactivated cell suspension with lysostaphin and DMSO, were used as positive and negative controls, as before. All tested concentrations of AHR caused no significant cell degradation as the optical density was unchanged along the incubation time. Lysostaphin treatment resulted in a rapid decrease of the optical density of the cell suspension, indicating efficient cell degradation, as expected (**Figure 3.4**).

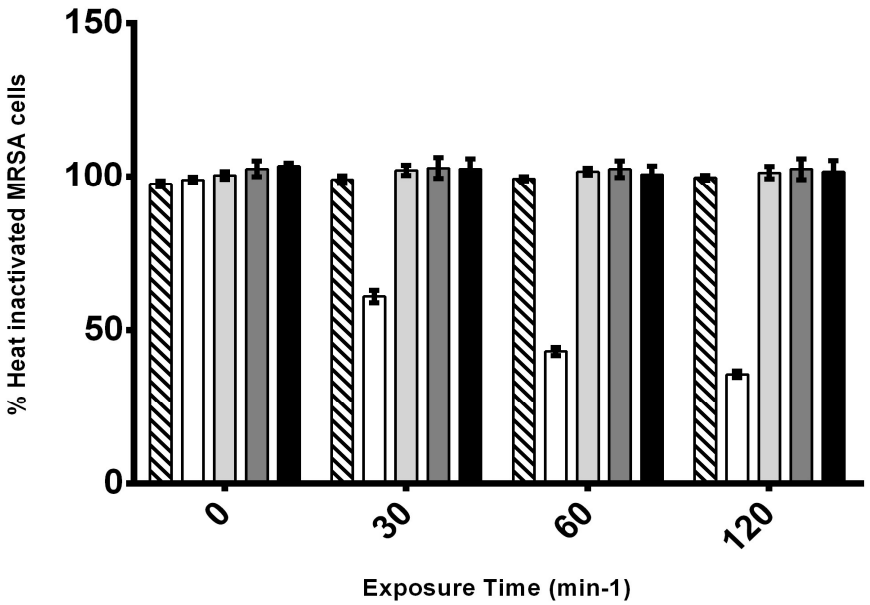

Figure 3.4 Lysis assay of heat-inactivated cells with different concentrations of AHR. The percentage of the cell supernatant was measured at discrete time points for MRSA CIP106760 in the presence of DMSO (striped bar), CIP106760 challenged with 100 μg.mL^{-1} of lysostaphin (white bar) and CIP106760 challenged with different concentrations of 7α-acetoxy-6β-hydroxyroyleanone; (light grey bar) half the MIC (3.9 μg.mL^{-1}); (dark grey bar) MIC (7.8 μg.mL^{-1}) and (black bar) double the MIC (15.6 μg.mL^{-1}).

Cell morphological alterations upon challenge with AHR

The morphological changes of the surface of CIP106760 cells challenged with AHR at the MIC and half the MIC concentrations, were observed by SEM microscopy (**Figure 3.5**). Treatment of cells with the double MIC concentration of AHR did not allow to perform SEM analysis. During the cell attachment process to the support, intact cells were no longer visible. At MIC and MIC/2 concentrations, the images showed the formation of large clusters of cells and lack of cell lysis, consistent with the previously described results on the lack of cell wall lytic activity. Furthermore, most cells present obvious deformation of their native structure, losing the coccoid shape and adopting a more elongated aspect. Also, the surface of the cells lost its native

smooth aspect, which may be related with the production of an aggregation matrix, or incorrect trimming of cell surface-associated polymers.

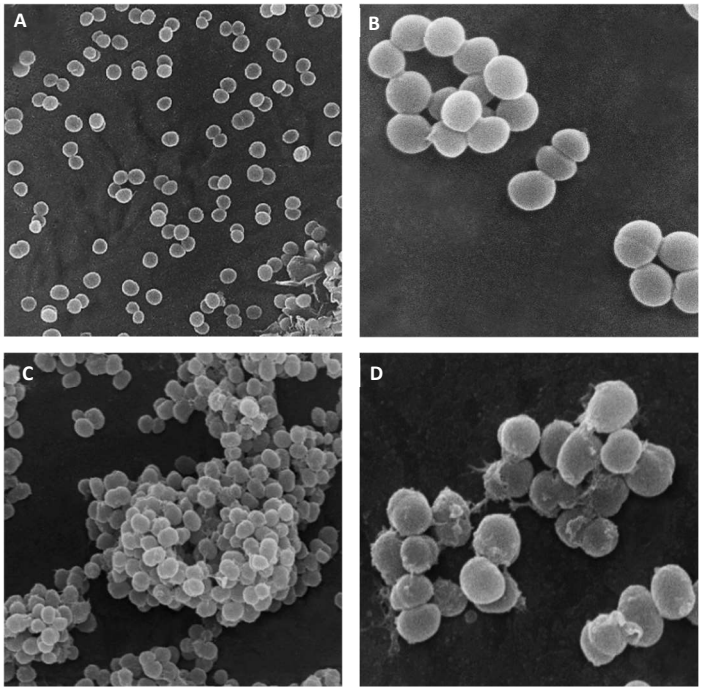

Figure 3.5 SEM microphotography of MRSA / VISA CIP 106760 strain. A, B - Control bacteria. C - bacteria treated with AHR at MIC/2, D - Bacteria treated with AHR at MIC. Scale Bars: 4 µm (A, C); 1 µm (B, D).

Effect of AHR on cell wall synthesis and peptidoglycan composition

Although the cell integrity and heat-inactivated cells lytic assays demonstrate that AHR bactericidal effect does not involve cell lysis, the mode of action of AHR results in severe changes in the cell morphology and cell surface. This observation suggests that the AHR interferes with cell wall synthesis, or with its major component, peptidoglycan. To explore this hypothesis, whole cell wall was extracted and peptidoglycan was purified for CIP106760 and CIP106760 challenged with the MIC, half the MIC and double MIC concentrations. Significant differences were observed in the amount of total cell wall retrieved from the different cell cultures. The cell wall dry weight per gram of cell wet weight was 27.26 (±5.4) mg for CIP106760 and decreased continuously as the AHR concentration increased; 22.08 (±4.8) mg for CIP106760 grown in the presence of 3.9 $\mu g.mL^{-1}$ of AHR, 15.36 (±3.9) mg for CIP106760 grown in the presence of 7.8 $\mu g.mL^{-1}$ of AHR and finally 9.12 (±2.7) mg for CIP106760 grown in the presence of 15.6 $\mu g.mL^{-1}$ of AHR. These results demonstrate that the cell wall thickness of the cell must be drastically reduced in the presence of AHR.

Regarding the peptidoglycan recovery yield, always representing 40-50% of the total cell wall amount. However, for AHR concentrations of MIC and double MIC, we detected a significant increase in the relative amounts of some muropeptide structures, which corresponding peaks are identified in Figure 6 as peaks a, b, c and d. By comparing the HPLC profiles with previously reported studies, in which the muropeptide structures were identified by mass spectrometry [239], the muropeptides of peaks a, b, c and d correspond to the monomeric pentapeptide without the pentaglycine bridge, the monomeric pentapeptide with only a tetraglycine bridge, the dimeric pentapeptide with one pentaglycine bridge and one tetraglycine bridge, respectively. These results suggest a relative increase in muropeptide structures that usually exist in very small amounts in the native S. aureus peptidoglycan. All these structures have less pentaglycine bridges or incomplete bridges, suggesting the inhibition of one, or more than one, of the steps of peptidoglycan biosynthesis that are responsible for the bridge formation. Such biosynthetic steps are mediated by FemA, FemB and FemX aminoacyltransferases that catalyze the sequential addition of the glycine residues to the lipid linked muropeptide, in a membrane-associated reaction.

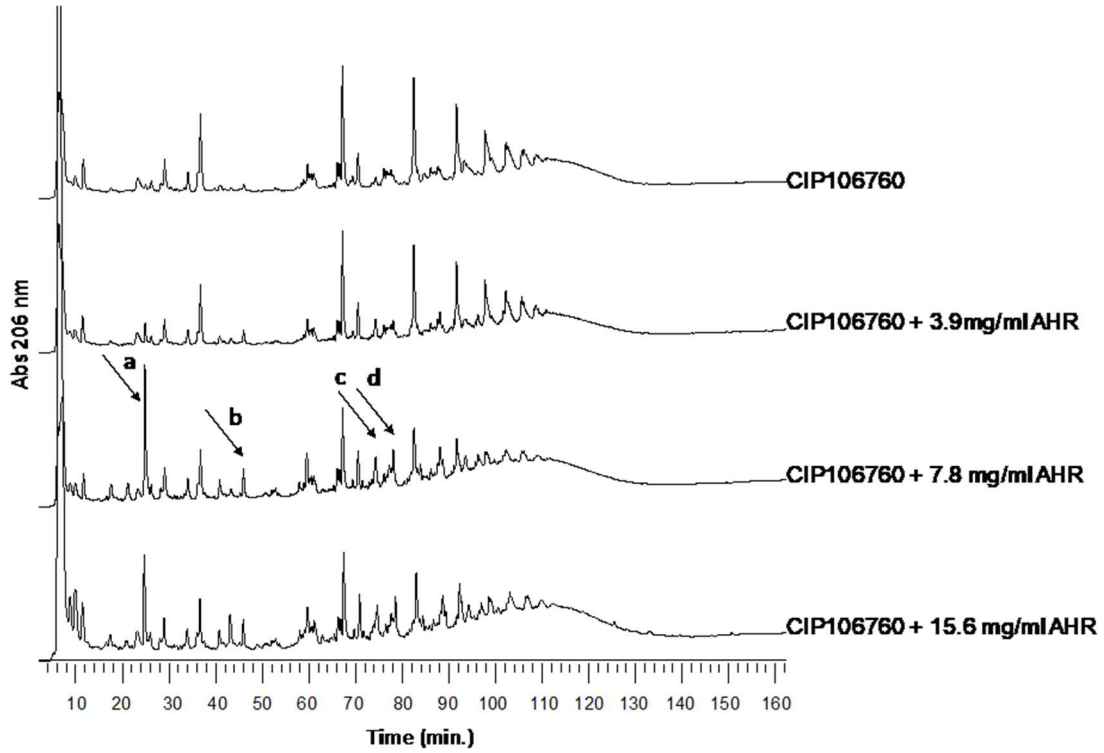

Figure 3.6 RP-HPLC peptidoglycan profiles. The purified peptidoglycan was digested with mutanolysin, reduced and analyzed by RP-HPLC. Muropeptide profiles of CIP106760 strain grown with 3.9 µg.mL^{-1} (MIC/2), 7.8 µg.mL^{-1} (MIC) and 15,6 µg.mL^{-1} (2MIC) of AHR. Muropeptide structures corresponding to peaks a, b, c and d are over-represented in the peptidoglycan of CIP106760 challenged with MIC and double MIC concentrations of AHR.

Assessment of AHR effect on the cell surface net charge

Cytochrome c is a cationic protein that has been used to estimate the relative surface charge of the cell envelope of *S. aureus* strains [245]. It is also known that the less the linking percentage of this protein, the higher relative positive surface charge of the cell [246]. Therefore, according to the results obtained (**Figure 3.7**), 2MIC concentrations decreased significantly the binding of this externally added cationic protein, thus suggesting an alteration of the usual negative surface charge of the bacterial strain used [247]. Accordingly, AHR at such concentration is able to affect the cell envelope. However, the inability o alter significantly surface charge at MIC suggests that this is a crucial step in AHR mode of action.

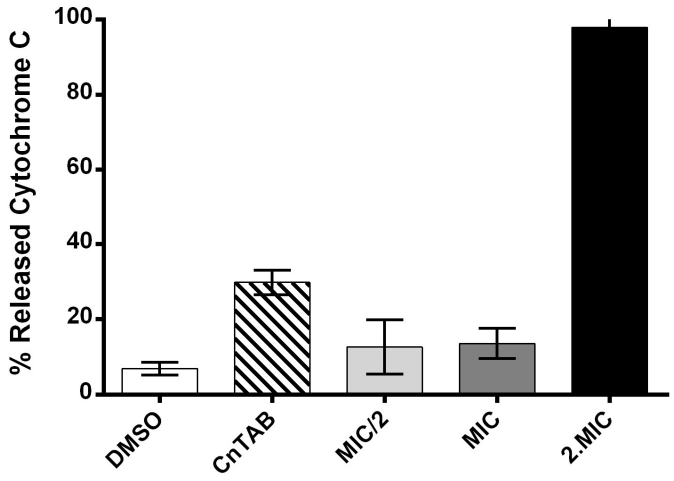

Figure 3.7 Percentage of cytochrome C that is not linked to cell was measured in the presence of DMSO (white bar), CnTAB (striped bar) and different concentrations of AHR; (light grey bar) half the MIC (3.9 $\mu g.mL^{-1}$); (dark grey bar) MIC (7.8 $\mu g.mL^{-1}$) and (black bar) double the MIC (15.6 $\mu g.mL^{-1}$).

To further understand the mechanism of action of AHR at the bacterial membrane level, the interaction of this antimicrobial diterpene with artificial lipid bilayers was carried out. DOPC at room temperature spontaneously forms a disordered phospholipid bilayer, representative of the fluid bilayers that are found in living organisms, with the additional advantages that it is available with very high purity and presents a very low turbidity compared to other phospholipids. This fact allows a complete correction of the absorption spectra. Since AHR has a good chromophore, the interaction between the compound and the lipid membrane can be

easily tested using the absorption bands of the antibacterial compound. Afterwards, the interaction of AHR with DOPC bilayers in suspension was first studied by UV-visible absorption spectroscopy.

As shown in **Figure 3.8 A**, the electronic absorption spectrum of AHR in aqueous buffer has one band in the near UV with maximum at 275 nm, and a broad band in the visible centered at ca. 520 nm, which is responsible for the yellow colour of the compound aqueous solution buffered at pH 7.4. In the presence of LUV changes in the absorption bands were clearly observed. On one hand, the lipid bilayer induced hyperchromism of the band at 275 nm possibly accompanied by a small hypsochromic shift. On the other hand, the band centered at 520 nm underwent a hypochromic effect. The differences encountered clearly indicate that AHR is surrounded by a less polar environment when in the presence of 1 mM LUV, i.e., a significant fraction of the compound partitions into the membrane, where it becomes less accessible to highly polar water molecules [248].

After confirming that AHR interacts with DOPC bilayers at typical lipid concentrations used in biophysical experiments and at relevant concentrations of the compound at which it displays antibacterial activity, its effect on membrane stability was tested. The effect of AHR on membrane leakiness was studied in lipid bilayers composed by DOPC and monitored by measuring the increase in fluorescence intensity as consequence of the release of encapsulated CF. Release of this probe may occur as consequence of strong perturbation of membrane order and other events such as (hemi)fusion, pore formation and detergent-like action. Representative curves of CF leakage kinetics from DOPC LUV suspension in the presence of different concentrations of AHR are shown in **Figure 3.8 B**. The presence of AHR at MIC and 2MIC led to ~ 10% of CF maximum leakage (**Figure 3.8 B**). At the compound: lipid molar ratio of 1:25 (MIC), AHR had a small effect in the passive permeability of lipid bilayers, when compared, e.g., with a fusion peptide $SARS_{FP}$ which induced ~ 60% CF leakage for the same 1:25 molar ratio [234].Furthermore, no differences between 2MIC and MIC concentrations of AHR were detected. AHR at the MIC/2 presented at the most ~ 3% of CF leakage, which is quite low compared to the effect of $SARS_{FP}$ (~ 50% CF leakage) [234] and antimicrobial peptides (~ 90-100% CF leakage) [249] at the same compound: lipid molar ratio of 1:50. In sum, AHR does not affect the integrity of fluid membranes.

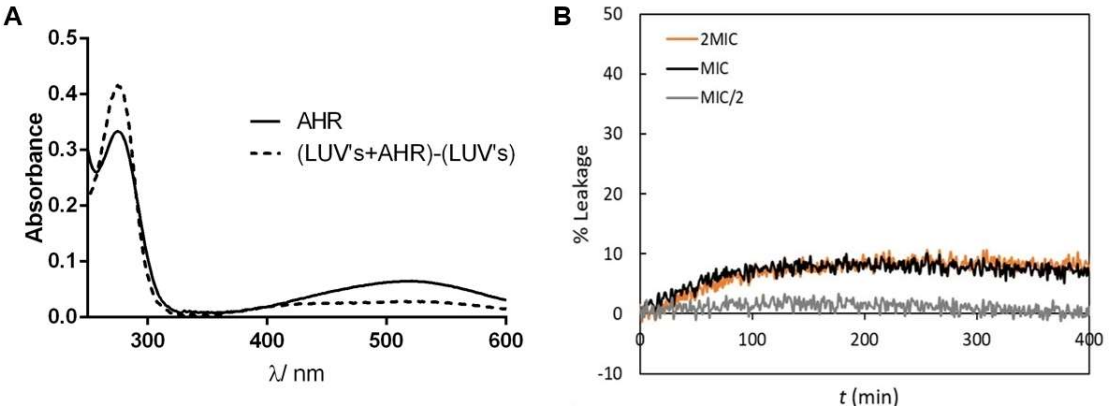

Figure 3.8 AHR at relevant antimicrobial concentrations interacts with phospholipid bilayers without compromising its integrity. (A) Electronic absorption spectrum of AHR at 20 μM in buffer Tris-HCl, pH 7.4 in the absence and presence of 1mM DOPC LUV suspension. (B) Representative curves (median behavior from 6 independent experiments) of the effect of AHR on CF leakage from DOPC LUVs in suspensions with a total lipid concentration of 0.5 mM, in the presence of different AHR concentrations: 40 μM (2MIC), 20 μM (MIC), and 10 μM (MIC/2). This experiment was performed at 25 °C

Since CF is a small organic molecule, it could still be possible that AHR is able to induce the formation of very small pores or defects that would not be stable and large enough to allow the release of the probe, but could, for example, lead to the dissipation of ionic gradients. Therefore, the effect of AHR on membrane passive permeability to protons was evaluated through the variation of fluorescence intensity ratio of encapsulated HPTS, a pH-sensitive probe, at two excitation wavelengths. The liposomes were subjected to a proton gradient, i.e., the internal solution has a pH of 5.0 and the external solution of 7.4. As can be seen in **Figure 3.9**, AHR does not greatly influence the passive permeability to protons in both model systems used. In fact, only ~ 5% and ~ 1.5% of pH gradient dissipation for bilayers with low and high concentration of cholesterol, respectively, were obtained.

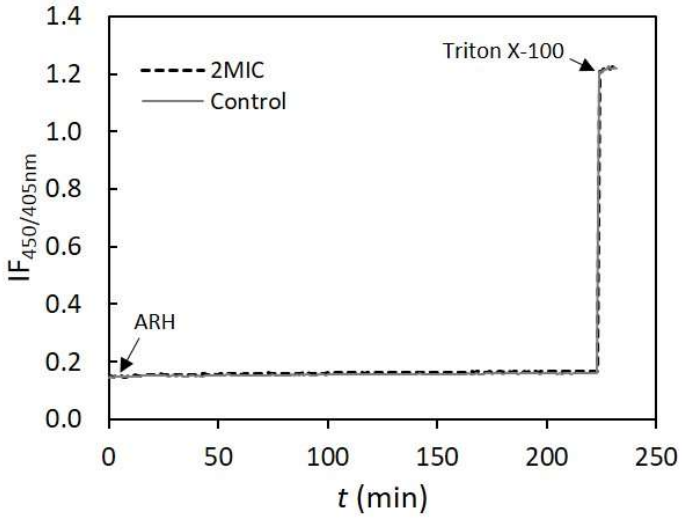

Figure 3.9 Effect of AHR at 2MIC on lipid bilayer passive permeability to protons**.** Representative curves of the time-dependence of fluorescence intensity ratio of HPTS at the excitation wavelengths of 405 and 450 nm ($IF_{450/405}$), at 25 °C. The experiments were conducted with high-cholesterol LUVs at total lipid concentration of 0.2 mM. Triton X-100 (1%) was added at 220 min to obtain the value of $IF_{450/405}$ corresponding to total pH gradient dissipation.

Moreover, no significant differences between the different AHR concentrations used were observed. Also, the presence of DMSO led to a small %ΔpH, allowing us to conclude that DMSO does not affect passive permeability, and the effect of AHR is almost negligible taking into account the values for the control (**Table 3.3**). These results obtained with the low cholesterol liposomes which resemble in biophysical properties mammalian intracellular membranes or bacterial membranes, are concomitant with those obtained in CF leakage assays. Thus, AHR at MIC does not have any noticeable effect on passive permeability and, as stated above, AHR does not disturb membrane structure. Furthermore, regarding the results presented above, and considering that the lipid mixtures containing a high concentration of cholesterol mimics the plasma membrane of mammalian cells, it is quite possible that AHR will display a low toxicity towards human cells .

Table 3.2 Effect of different concentrations of AHR on lipid bilayer passive permeability to protons. monitored through HPTS ratiometric fluorimetry, at 25 °C. The experiments were conducted in lipid mixtures containing low and high concentrations of cholesterol. The percentage of pH-gradient dissipation (% ΔpH) presented is related to the outwards movement of protons trough the lipid bilayer before the total dissipation of pH gradient. The values are the mean ± S.D. of 3 independent experiments.

AHR concentration	% ΔpH	
	Low cholesterol LUVs	High cholesterol LUVs
2MIC	5.1±0.1	1.4±0.2
MIC	4.8±0.3	1.5±0.3
MIC/2	4.6±0.7	1.6±0.2
Control	3.6±0.2	1.3±0.1

AHR does not provide a synergistic effect with cell wall antibiotics

Antimicrobial combination therapies are often used with the intention of providing broad-spectrum coverage and preventing the emergence of resistant strains [250]. Having this in mind, the synergic effects of AHR with other antibiotics active against Gram-positive (methicillin, ampicillin and vancomycin) were studied (**Table 3.2**). As expected, when testing methicillin and ampicillin without coupling AHR, no visible effect was seen on bacterial growth. These results are in accordance with the fact that these two antibiotics are both β-lactams, to which this MRSA strain is resistant. Regarding the effect of vancomycin, since this antibiotic is not a β-lactam (glycopeptide) - hence why it is used to treat MRSA caused infections - visible effect on MRSA bacterial growth was observed (inhibition zone of 17±1 mm).

Table 3.3 Synergy effect of AHR and three different antibiotics against MRSA CIP 106760 strain.

Compound	Zone inhibition (mm)			
	DMSO	MET	AMP	VANC
AHR	21±2	20±2	20±2	19±3
No AHR	5	5	5	17±1

3.5 Conclusions

AHR is not only an effective antibacterial agent as also exerts promising activity against multidrug resistant strains, such as MRSA. Having in mind that the purpose of this study was to unveil its mechanism of action, it seems that this abietane diterpene does not affect the bacterial cell membrane but rather its cell wall. However, its ability to interact with a fluid phospholipid membrane without significantly perturbing it suggests that it is able to permeate the bacteria cell membrane and exert intracellular actions, which may result in some of the alterations observed at the cell wall.

The results showed that AHR is able to disrupt the cell wall without causing the lysis of the bacteria. Therefore, its antibacterial mechanism resembles the one of daptomycin. Daptomycin is an antibiotic with rapid bactericidal effect but with absence of cell lysis. Instead, it causes potassium efflux, disturbing the ion-concentration and consequently membrane depolarization. Also, like daptomycin, the lack of lysis consequently does not comprise the release of proinflammatory bacterial compounds, which is in itself an asset regarding potential clinical use.

The herein presented results suggest that further studies should be made in order to further assess AHR antibacterial effect, toxicity and possible clinical use.

Chapter 4

Production and characterization of polymeric nanoparticles containing methanol extracts of Portuguese Lavenders

This chapter is based on the following article:

Pereira, F., Baptista, R., Ladeiras, D., Madureira, A.M., Teixeira, G., Rosado, C., Fernandes, A.S., Ascensão, L., Silva, C.O., Reis, C.P., Rijo, P. Production and characterization of nanoparticles containing methanol extracts of Portuguese Lavenders. 2015, *Measurement*, 74: 170-177.

Production and characterization of nanoparticles containing methanol extracts of Portuguese Lavenders

4.1 Introduction

Lavenders are aromatic evergreen shrubs from *Lamiaceae* family that have been traditionally used as culinary herbs and medicine for headaches, digestive troubles, burns, skin sores and insect bites. Nowadays, these plants are extensively cultivated as ornamental plants for garden, landscape use, potpourris and essential oil production to fragrance, cosmetic, pharmaceutical, food and flavor industries [251]. *Lavandula stoechas* ssp. *luisieri* (Rozeira) Rozeira (Syn: *L. luisieri*; *L. stoechas* var. *luisieri*) and *Lavandula pedunculata* (Mill.) Cav. (Syn: *L. pedunculata* ssp. *sampaiana*; *L. stoechas* ssp. *pedunculata*) are two common *Lavandula* species growing wild in Portugal [252]. In the last decade, the essential oils from *L. stoechas* ssp. *luisieri* were analyzed and their antifungal, anti-inflammatory and antioxidant activities studied [253], [254]. The essential oils from *L. pedunculata* were also analyzed and their antifungal activity demonstrated [255]. In addition, several extracts of both species showed antibacterial activity [256], anticholinesterase inhibition and antioxidant capacity [257]. Taking into account these reports, we found reasonable to foresee, in the present study, an application for these lavender extracts as skin anti-aging and antioxidant agents, for topical and cutaneous treatment.

Naturally, the skin acts as an efficient barrier to external environment factors, against toxic substances, pathogens and other organisms [258]. Some of these aggressive conditions, such as ultraviolet or ionizing radiation, are related with the formation and accumulation of free radicals in cells, damaging or modifying the proteins and nucleotides structure and, as a consequence, resulting in cancer or other pathologies [259]. The interaction of antioxidant and anti-inflamatory compounds with radical species results in a decrease of cellular damage and oxidative stress [260], playing and important function against several pathologies. However, many active compounds have the disadvantage of showing toxicity, which is one of the main challenge in skin diseases treatment [266, 267].

It is now well known that nanotechnology provided new approaches and alternatives for diseases treatment [263]. The encapsulation into nanoparticles of a wide range of drugs resulted in significant advances in the treatment efficiency for topical acne and anti-aging, anti-inflammatory, antimicrobial or antifungal drugs [264]. *Poly (lactic-co-glycolic) acid* (PLGA) nanoparticles were commonly used to encapsulate selected extracts, to enhance their antioxidant activity by protecting them from instability. In addition, PLGA has been extensively employed in drug delivery applications, since it decomposes through hydrolysable ester bonds in the body, it is excreted as CO_2 [270, 271] and it is biodegradable and biocompatible [267].

This study aimed to encapsulate methanol extracts of *Lavandula stoechas* ssp. *luisieri* and *L. pedunculata* that previously have shown to have a high antioxidant activity into PLGA nanoparticles. In this way, we would improve the stability of the active compounds and provide a better efficiency for treatment of cutaneous diseases.

4.2 Materials and methods

4.2.1 Chemicals

PURASORB PDLG 5002 - PLGA (Poly-DL-Lactide/Glycolide copolymer) with Ratio L/G in % of 50:50 (MW 45,000-75,000 Da) was obtained from PURAC. Pluronic® F68 was obtained from Sigma-Aldrich™ (USA). All other reagents were of analytical grade.

4.2.2 Plant Material

The aerial parts of *Lavandula stoechas* ssp. *luisieri* (Rozeira) Rozeira and *Lavandula pedunculata* (Mill.) Cav. were collected from natural populations occurring throughout the Center and Southwestern regions of Portugal. The plant material was identified and vouchers specimens deposited in the Herbarium of the Lisbon Botanical Garden (LISU 236672) and in the Lisbon Agronomic Institute Herbarium (LISI 164/2011), respectively. The plant material was air-dried at room temperature and powdered. Several extractions (during 24h at room temperature) with organic solvents of increasing polarity were performed to obtain the essential oils and n-hexane, dichloromethane, ethyl acetate, methanol and water extracts.

4.2.3 Determination of total phenol content

Total phenol content (TPC) was determined using Folin-Ciocalteu reagent according with the method modified describe by Singleton and Rossi [268] and Cheung *et al.* [269]. In summary, 0.2 mL of Folin-Ciocalteu reagent was added to 0.1 mL of sample (2 $mg.mL^{-1}$), 1 mL of sodium carbonate (15%) and 2 mL of distilled water. After incubation for 2h, the absorbance was measured at 765 nm. Gallic acid was used as the standard and the results were expressed in $mg.mL^{-1}$ of gallic acid equivalents (GAE).

4.2.4 Determination of total flavonoids content

Total flavonoids content (TFC) was determined according to Dowd method modified by Zhishen *et al.* [270]. A 0.5 mL of sample solution (2 $mg.mL^{-1}$) was added 2 mL of distilled water and 150 µL of sodium carbonate (5%). After incubation for 5 min in the dark at room temperature, 150 µL of $AlCl_3$ 10%, 1.0 mL of sodium chloride (1M) and 2 mL of distilled water

was added to solution and incubated for more 10 min in the dark at room temperature. The absorbance was measured at 510 nm against blank sample. Rutin was used as the standard and the results were expressed in mg.mL^{-1} of rutin equivalents (RE).

4.2.5 Antioxidant activity

4.2.5.1.1 Lipid peroxidation inhibition

The lipid peroxidation inhibition capacity (LPIC) was realized according to Liegeois *et al.* [271]. Briefly, 30 µL of linoleic acid (16 mM), 2.81 mL of phosphate buffer (50 mM, pH 7.4) and 20 µL of sample (0.3 mg.mL^{-1}) were added to 150 µL of 2,2'-azobis(2-amidinopropane) dihydrochloride (AAPH) solution. The absorbance measurement at 234 nm was carried out after incubation for 20 min in the dark at room temperature. Butylated hydroxytoluene (BHT) was used as positive control.

4.2.5.1.2 Free radical scavenging activity (DPPH)

The antioxidant activity was evaluated according with Sarikurkcu *et al.* [272]. Different concentrations samples (1.5 mL at 50, 200 and 400 µg.mL^{-1}) were incubated with 9.0 mL of 2,2-diphenyl-1-picrylhydrazyl (DPPH) in methanol for 30 min at room temperature. The absorbance was measured at 520 nm. Butylated hydroxytoluene (BHT) and ascorbic acid were used as positive controls.

4.2.6 Cytotoxicity

The cytotoxicity of the extracts of *L. stoechas* ssp. *luisieri* and *L. pedunculata* was characterized in HaCat cells (human adult low-calcium high-temperature keratinocytes). HaCat cells were maintained in DMEM supplemented with 10% fetal bovine serum, 100 U mL^{-1} penicillin, and 0.1 mg.mL^{-1} streptomycin. Approximately 5 x 10^5 cells were cultured in 200 µL of culture broth per well, in 96-well plates, and incubated 24h at 37°C under a 5% CO_2 atmosphere. Cultures were then treated with the extracts (1-15 µg.mL^{-1}) for a 24 h-period. Afterwards, the crystal violet assay was carried out as previously described [273]. Two independent experiments were performed and four replicate cultures were used in each independent experiment.

4.2.7 *Lavandula* ssp. extract methanol nanoparticles

4.2.7.1.1 Production of poly(lactic-co-glycolic) acid (PLGA) nanoparticles

The encapsulation process of methanol extracts in PLGA nanoparticles was prepared according a modified-spontaneous emulsification solvent diffusion method (mSEDM) described by Reis *et al.* [266]. An organic solution was prepared using 5 mL of a solvent mixture of acetone/ethanol (8:2, v:v). Extract (25 mg) and PLGA (50 mg) were slowly added to the organic solution, under constantly stirring to 10 mL aqueous solution of Pluronic F®-68 (0.1%) and at room temperature. Nanoparticles suspension was formed immediately. Organic solvents were then removed by evaporation (IKA RV06-ML 1-B, Staufen, Germany) under reduced pressure at 30ºC and stored at 4ºC.

4.2.7.1.2 Characterization of nanoparticles

The mean particle size and zeta potential of PLGA empty and loaded nanoparticles were measured in DelsaTM Nano C (Beckman Coulter, Brea, CA, USA), by photon correlation spectroscopy (PCS) and electrophoretic mobility, respectively. Each analysis of zeta potential was carried out at 25ºC with an angle of detection of 90º. Polydispersity index (PI) was also determined; higher particle stability is associated with a PI close to zero. Measurements were made after the evaporation process and in triplicate. The size of NP was also confirmed by scanning electron microscopy (SEM). The batches were analyzed before the centrifugation procedure (Hermle Labortechnik, Wehingen, Germany). An aliquot of each methanol extracts of both lavenders was placed in a glass coverslip and leave to dry in a desiccator. Then, the material was coated with a thin layer of gold (with 500 nm of thickness) and observed with a JEOL 5200LV scanning electron microscope (JEOL Ltd., Tokyo, Japan) at an accelerating voltage of 20 kV. Images were digitally recorded.

4.2.7.1.3 High-Performance Liquid Chromatography (HPLC) analysis:

The HPLC analysis was carried out in a Liquid Chromatograph Agilent Technologies 1200 Infinity Series LC System equipped with diode array detector (DAD), using a ChemStationSoftware and a LiChrospher® 100 RP-18 (5 mm) column from Merck (Darmstadt, Germany). Rosmarinic acid, the main component of both *Lavandula* species methanol extracts were determined and quantified by injecting 20 µL of each sample at 1 $mg.mL^{-1}$, using a gradient composed of Solution A (methanol), Solution B (acetonitrile) and Solution C (0.3% trichloroacetic acid in water) as follows: 0 min, 15% A, 5% B and 80% C; 20 min, 80% A, 10% B and 10% C; 25 min, 80% A, 10% B and 10% C. The flow rate was set at 1 $mL.min^{-1}$. The standards were run under

the same conditions in methanol, and the detection was carried out between 200 and 600 nm with a diode array detector (DAD). All analyses were performed in triplicate.

4.2.7.1.4 HPLC analysis of encapsulation efficiency:

The encapsulation efficiency (EE, %) was quantified by using high-performance liquid chromatography (HPLC) analysis [209] using rosmarinic acid as the major component in both extracts. A standard of rosmarinic acid was used.

The encapsulation efficiency of polymeric PLGA nanoparticles methanol extracts of both *Lavandula* species was determined in triplicate. The supernatant obtained in the preparation of nanoparticles was injected directly in the HPLC-DAD using the method described previously. Rosmarinic acid concentration was used as the indicator of encapsulation efficiency using the following formula:

$$EE\% = \frac{(C_i - C_f)}{C_i} \times 100$$

where EE% corresponds to the encapsulation efficiency, C_i to the initial concentration of rosmarinic acid and C_f to the final concentration of rosmarinic acid (non-encapsulated or free rosmarinic acid) present in the supernatant.

4.2.8 Permeation studies

Human abdominal skin tissue from cosmetic surgery, obtained following informed consent, was used to produce epidermal membranes [274]. Ethical approval was provided by the Ethics Committee of the *Escola de Ciências e Tecnologias da Saúde da Universidade Lusófona*. After removal of the adipose tissue by blunt dissection, the epidermis was separated by immersing the skin in water at 60˚C for 1 min. It was then pinned on a cork-board, the epidermis was carefully peeled away from the dermis and mounted on filter paper, after which it was stored in a freezer at −20˚C until use. Prior to the diffusion experiments, the epidermis was defrosted and cut to an appropriate size. Permeation experiments (n = 3) with epidermal membranes were conducted on glass Franz type diffusion cells with a receptor volume of approximated 4 mL and a diffusional area of 0.95 cm^2. The continuously stirred receptor medium was isotonic phosphate buffered saline (PBS, pH 7.4). The receptor compartment was thermostated at 37˚C. A solution of extract of *L. stoechas* ssp. *luisieri* or *L. pedunculata* in ethanol:water (80:20, v/v) was placed in the donor compartment. The diffusion experiments were performed under occluded conditions by sealing the donor compartment with microscope

coverslips. At designated time intervals (3, 9 and 24h), 200 µL samples were collected from the receptor compartment and immediately replaced with fresh and pre-thermostated PBS. Quantitative analysis of rosmarinic acid was performed by HPLC-DAD as described above.

4.3 Results and discussion

4.3.1 Total phenol and flavonoids contents

The results obtained on the TPC and TFC assays are presented in **Table 4.1**. Methanol and water extracts of both *Lavandula* species displayed the highest phenols content. Methanol extracts of both plants also presented the highest flavonoids content (482.4 mg and 360.0 mg RE for *L. stoechas* ssp. *luisieri* and *L. pedunculata,* respectively). As expected, neither of lavenders' essential oils revealed a significant flavonoid rate.

Table 4.1 Total phenol content (TPC) and total flavonoids content (TFC) of lavenders extracts and essential oils.

Extracts	**TPC[a]/ QTP[a]**	**TFC[b]/ QTF[b]**
L. stoechas* subsp. *luisieri		
Essential oils	201.2[c]	8.2[d]
n-hexane	381.4	196.8
Dichloromethane	67.4	390.6
Ethyl acetate	102.3	227.4
Methanol	1387.2	482.4
Water	1654.7	451.8
L. pedunculata		
Essential oils	50.0[c]	3.1[d]
n-hexane	474.4	314.1
Dichloromethane	148.8	339.6
Ethyl acetate	102.3	237.6
Methanol	1044.2	360.0
Water	631.4	242.7

Legend: [a] $mg_{GAE}\ g_{sample}^{-1}$; [b] $mg_{RE}\ g_{sample}^{-1}$; [c] The unit is $mg_{GAE}\ mL^{-1}$; [d] The unit is $mg_{RE}\ mL^{-1}$

4.3.2 Antioxidant activity

The determination of the antioxidant activity through lipid peroxidation inhibition assay was evaluated in a concentration range between 0.01 – 0.4 $mg.mL^{-1}$ (**Figure 4.1**) and using BHT as the positive control. Methanol and water extracts of both lavenders species displayed higher ability to neutralize AAPH. In addition, DPPH radical scavenging capacity assay (results presented in **Figure 4.2**) confirmed their antioxidant action. As can be inferred from the analysis of **Figure 4.2**, essential oils, dichloromethane and methanol extracts of *L. stoechas* ssp. *luisieri* showed

higher radical scavenging capacity and in a dose-dependent pattern. The results obtained for *L. pedunculata* essential oils were also similar. With exception of both aqueous extracts, all the extracts displayed an inhibition percentage in the same range observed with the BHT for a concentration of 40 µM. This apparent discrepancy on lower phenolic and flavonoids content, as well as the high percentage of radical inhibition in essential oils of both extracts, may be attributed to the linalool and linalyl acetate compound presence on these extracts [254]. According with the results obtained for the antioxidant activity and phenolic and flavonoids content, the both methanol extracts were selected for encapsulation.

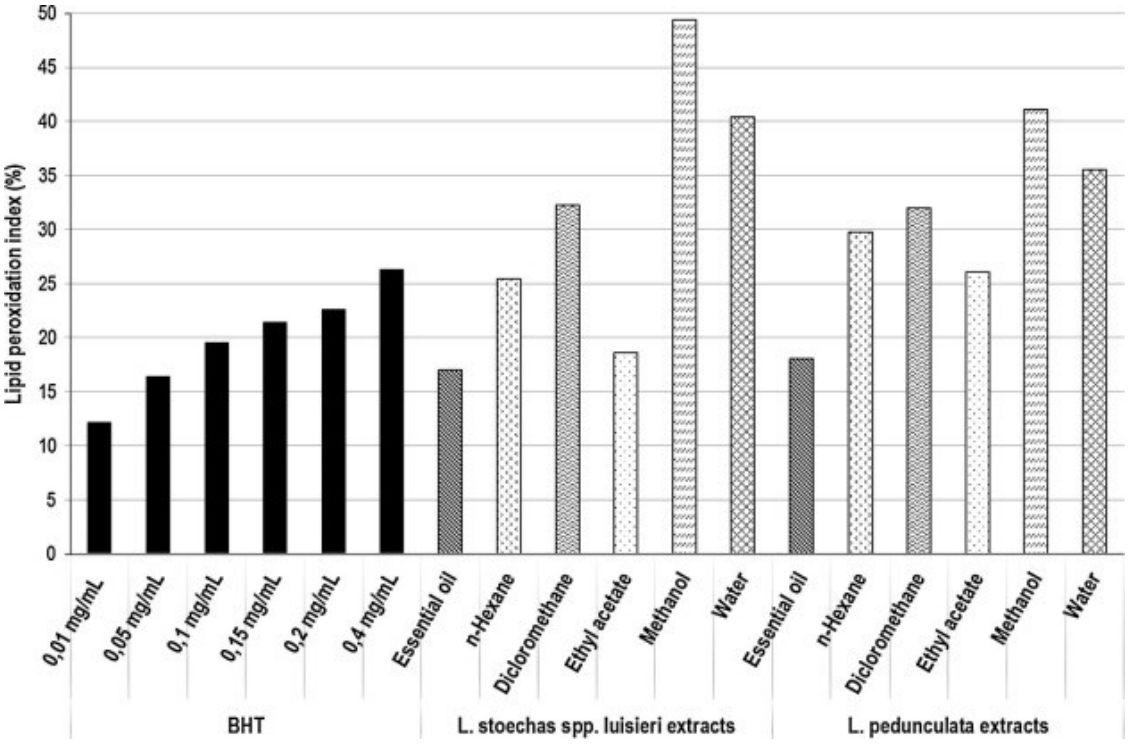

Figure 4.1 Lipid peroxidation index (%) of the extracts and essential oils of *Lavandula stoechas* ssp. *luisieri* and *L. pedunculata.*

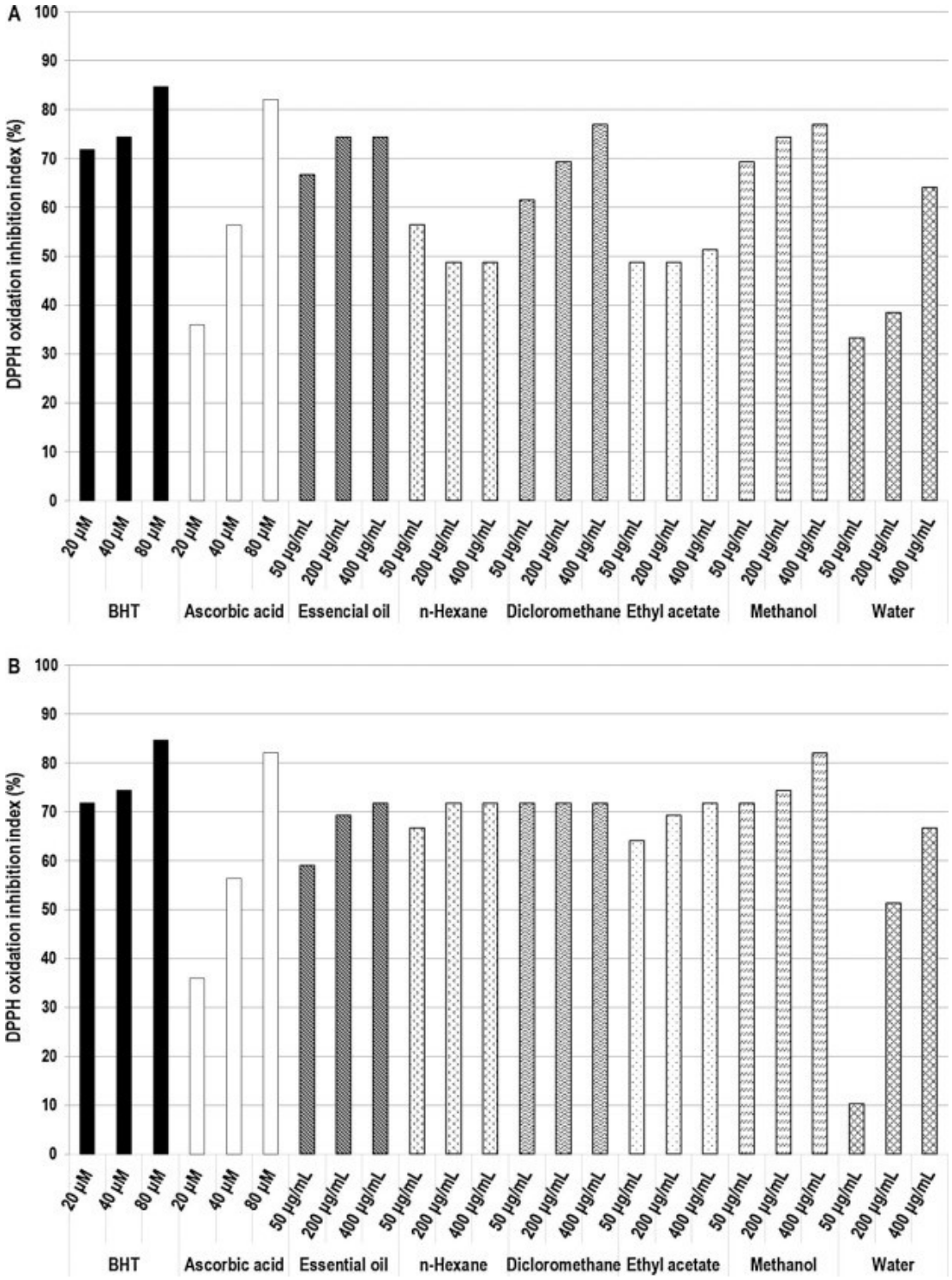

Figure 4.2 *DPPH oxidation inhibition index (%) of the extracts and essential oils of* Lavandula stoechas ssp. luisieri *(**A**) and* Lavandula pedunculate *(**B**).*

4.3.3 Cytotoxicity

The results obtained with *L. stoechas* ssp. *luisieri* and *L. pedunculata* suggest that these extracts could be potentially used in skin care products. For concentrations up to 15 µg.mL^{-1} and an incubation period of 24h, no relevant cytotoxic effects were observed (**Figure 4.3**). DMSO 5% (v/v) was used as positive control and decreased cell viability to 38.7 ± 0.8%. Since the studied lavender extracts did not decrease cell viability, their use in cutaneous formulations is not expected to be limited by safety concerns [273].

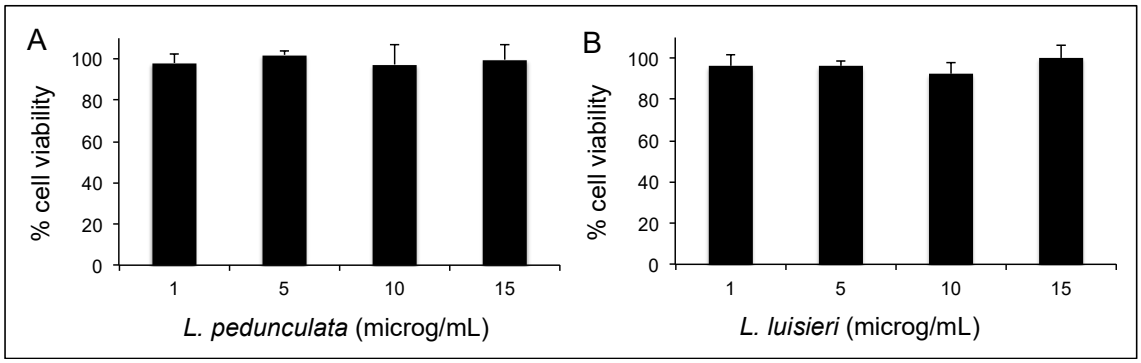

Figure 4.3 *Effect of* L. stoechas ssp. luisieri *and* L. pedunculata *extracts on the viability of human keratinocytes HaCat, as evaluated by the crystal violet assay. Results are average values ± SD of two independent experiments, each comprising four replicate cultures.*

4.3.4 Permeation studies

Rosmarinic acid is the main component of *Lavandula* spp., and it was quantified in *Lavandula stoechas* ssp. *luisieri* and *L. pedunculata* methanol extracts as 2.95 mM and 3.78 mM using the HPLC-DAD method described before. The permeation through human epidermis of rosmarinic acid, from methanolic extracts of *L. stoechas* ssp. *luisieri* and *L. pedunculata* was determined. After 24h of assay and using the described HPLC method, no measureable amount of this compound was detected in the receptor compartment of the diffusion cells, which is indicative of low permeation. These results are suggestive of low risk of toxicity of lavender extracts.

4.3.5 Nanoparticles Characterization

Particle mean sizes were 301.8 ± 87.1 nm with PI of 0.117 for methanol extract of L. stoechas ssp. luisieri and 303.9 ± 87.0 nm with PI of 0.142 for methanol extract L. pedunculata. The surface zeta potential values were −15.74 ± 9.93 mV and −19.35 ± 8.42 mV, respectively. In fact, this negative charge of nanoparticles may increase interactions between them and the

external skin barrier, which could result in an uptake increase, especially in inflamed skin [275], [276]. In addition, empty nanoparticles showed a smaller mean size of 221.5 ± 60.2 nm with PI

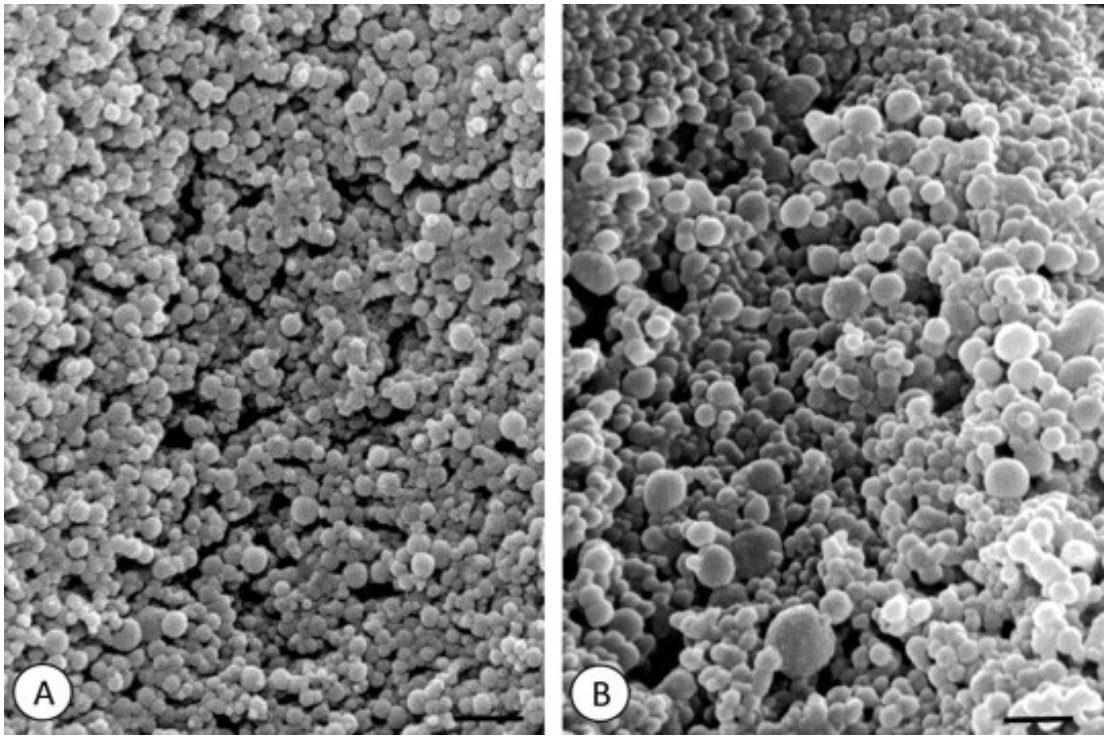

Figure 4.4 SEM micrographs of PLGA nanoparticles produced by modified-spontaneous emulsification solvent diffusion (m-SESD) method. PLGA nanoparticles containing methanol extracts of *Lavandula stoechas* ssp. *luisieri* (**A**), and *Lavandula pedunculata* (**B**). Scale bars = 1μm.

of 0.076 and a zeta potential of −13.93 ± 10.91 mV. Thus, this variation in the physical characteristic of the PLGA nanoparticles may indicate that the extract is effectively associated with and/or within the polymeric matrix. Moreover, the particles observed by SEM showed a well-defined spherical shape (**Figure 4.4**). Furthermore, the encapsulation efficiency (EE) was 95.8% for L. stoechas ssp. luisieri and 96.7% for L. pedunculata, according to the rosmarinic acid concentration. The retention time and spectrum of rosmarinic acid was the same before and after encapsulation process, suggesting preservation of the structures of each extracts. The high encapsulation efficiency value obtained promotes a higher availability of the active substances for therapeutic purpose, as well as, physicochemical protection of sensitive compounds, enhancing their stability [277]. Additionally, the encapsulation strategy was chosen because antioxidants like rosmarinic acid are susceptible to oxidation and isomerization reactions. In fact, in a previous study with Plectranthus (Lamiaceae) extracts [209], we have shown that rosmarinic acid, the major component, maintained its biological activity after encapsulation process [209]. As the nanotechnology field rapidly grows, advantages such as similar treatment efficacy and reduced side effects are important key factors for implementation in the pharmaceutical industry.

4.4 Conclusion

The antioxidant activity of methanol extracts from *L. stoechas ssp. luisieri* and *L. pedunculata* seems to correlate with the high polyphenol and flavonoid contents of these extracts. Polymeric PLGA nanoparticles demonstrated to efficiently encapsulate methanol extracts from both species. In addition, epidermal permeation and *in vitro* cytotoxicity in human keratinocytes studies were suggestive of low risk of toxicity from formulations containing these two lavender extracts. In conclusion, the current study provides data for promising new cosmetic or dermatological formulations for the pharmaceutical industry, as anti-aging and antioxidant agents.

Chapter 5

Antibacterial effect of nanoparticles for treatment of topical infections

Antibacterial effect of nanoparticles for treatment of topical infections

5.1 Introduction

The diseases associated to infections by different pathogens are one of the main worldwide health problems and one type of infection with high prevalence is the skin infection. Anatomical, physiological or environmental factors can be some of the causes for the development of skin infections [278]. The skin is constantly exposed to environmental agents and different pathogenic organisms. Thus, the treatment of skin infections is still a high challenge mainly due to the lack of effective and available therapies [279]. Because of the outbreak of skin infectious diseases caused by different pathogenic bacteria and the development of antibiotic resistance, worlwide research groups are now focused in searching new antibacterial agents with low resistance and low cost. In fact, antibiotic resistance is a type of drug resistance in which a microorganism has developed the ability to survive exposure to an antibiotic. The 4 main mechanisms by which microorganisms exhibit resistance to antibiotics are (1) drug inactivation or modification; (2) alteration of the target site; (3) alteration of the metabolic pathway; (4) reduced drug accumulation by decreasing drug permeability and/or increasing active efflux (pumping out) of the drugs across the cell surface [302–304].

The treatment with antibiotics is the most effective way to control and treat skin infections. Due to their wide and in some cases incorrect (misuse) use, the currently available antibiotics have a lower therapeutic effect. The use of conventional antimicrobial agents against these infections is always associated with problems such as the development of multiple drug resistance and adverse side effects. Conventional antimicrobial therapy or antibiotics treat the infectious diseases by either killing of the microbes, or interfering with their growth but more than 70% of bacteria causing infections are now resistant to at least one of the drugs most commonly used for the treatment [283]. As a response to the absence of therapeutic alternatives, new molecules have been introduced in the market [259, 260]. Our previous work had focused on the use of plant as source of new therapeutic forms, particularly in species from *Plectranthus* family. Particularly, some diterpenes with abietan scaffold have been demonstrate a relevant antibacterial activity in some bacteria strains resistant to the antibiotics [67, 151].

On the other hand, in some cases, the reduced efficacy of some new antibiotics is mainly due to some issues related reduced to inadequate therapeutic index, their low solubility, bioavailability, high toxicity, among others [288, 289]. In response, developments in different nanotechnology fields have provided new tools to improve their effectiveness of drugs. Nanosized drug delivery carriers and antimicrobial nanoparticles have emerged as potent effective agents against the infections. Nanoparticles have unique properties owing to their ultra

small and controllable size such as high surface area, enhanced reactivity, and functionalizable structure. The use of nanoparticles associated with drugs can promote their stability and improve its bioavailability.

Moreover, the development of a reliable green chemistry process for the biogenic synthesis of nanomaterials is also an important aspect of current nanotechnology research. Silver nanoparticles (AgNP) constitute one of the most studied forms for aplications in biomedicine, bioengineering or related areas [288]. Silver-based compounds and silver ions are known for their broad spectrum of antimicrobial properties. Silver is used in different forms such as metals, nitrates, and sulfadiazine. By decreasing the particle size to nanometer range, antibacterial activity of silver can be increased. Due to the enormous capacity to change properties, silver nanoparticles also can be easily synthesized with different shapes (spheres, rods, tubes, wires, ribbons, plates, cubes, hexagons, triangles, etc.) by the selection of formulation and processes parameters. This enormous diversity of methodology results in high variation of resultant physical characteristics and consequent variation in its therapeutic applications [262, 263]. Their spectrum of applications in therapeutics has many benefits as multilevel antibacterial agent, multidrug resistant and low toxicity compared to other approaches [288].

In the present work, we performed the synthesis of silver nanoparticles through different reducing agents, conjugate them with different antibiotic models and fully characterize those nanosystems. The high efficiency of 7α-acetoxy-6β-hydroxyroyleanone when conjugated with silver nanoparticles could found a promising nanosystem model to treat infections associated with bacterias resistante to antibiotics.

5.2 Materials and Methods

5.2.1 Materials

Polycaprolactone (MW 80,000 Da), ampicillin (AMP) anhydrous (≥96.0%), silver nitrate ($AgNO_3$, ≥99.0%), sodium citrate and sodium borohydride were purchased from Sigma-Aldrich (Missouri, USA). Carbopol 940 was purchased from BF Goodrich Chemical (London, UK). Milli-Q deionized water was applied during all procedures. During the nanoparticle synthesis, all glass material was previously washed with *aqua regia* solution to eliminate possible inorganic contaminants. All chemicals used were of analytical grade.

5.2.2 Extraction and isolation of AHR

The diterpene AHR was extracted from aerial parts and roots of *Plectranthus grandidentatus* using maceration and acetone as solvent. After exhaustive extraction, AHR was isolated by chromatographic procedures as previously described [67, 262]. The structure and purity of AHR were confirmed by NMR spectroscopy.

5.2.3 Synthesis of silver nanoparticles

AgNP were synthesized using two types of reducing agents: sodium citrate and sodium borohydride. The synthesis of nanoparticles with citrate followed the previous protocol developed by Turkevich [291]. Briefly, a solution of 10 mM of $AgNO_3$ was added to boiling 100 mL of sodium citrate solution under reflux. After addition of the silver solution and 15min of reaction, a color change of the solution was verified. Finally, the solution was cooled to room temperature. The preparation of AgNP with borohydride was followed the procedure described by Mulfinger [292]. A 1 mM of $AgNO_3$ solution was added to 30 mL of sodium borohydride solution chilled in ice bath. After synthesis, both nanoparticles were isolated by centrifugation to separate possible unreacted silver and particle aggregates (12500 x *g*, Hermle Labortechnik Gmbh type Z36HK, Wehingen, Germany).

5.2.4 Coating and functionalization of AgNP's

The different synthesized AgNP's were separately functionalized with two types of antibiotics: ampicillin (AMP), a commonly used drug, and 7α-acetoxy-6β-hydroxyroyleanone (AHR), a natural antibacterial compound isolated from *Plectranthus species*. The particle functionalization procedure was made according to the literature [293]. Initially, the AgNP stock solution concentration was adjusted to a concentration of 10mM. A final concentration of 1mM of AgNP was added an aqueous solution of the respective antibiotic. AMP was added to a final concentration of 1 $mg.mL^{-1}$ and added to the AgNP. AHR was added to a final concentration of their isolated MIC value (7.8 $\mu g.mL^{-1}$). The conjugates were left incubated at room temperature for 24h without agitation and analysed through spectroscopic analysis (Thermo Evolution 600 UV/visible spectrophotometer, Massachusetts, USA). The efficiency of association was indirectly calculated by the absorption difference of AMP and AHR. To remove any AMP or AHR that might remain, nanoparticles were centrifuged and washed several times. The amount of AMP and/or AHR in the supernatant was quantified after centrifugation (27,000 × *g*, 20 min, Hermle Labortechnik, Wehingen, Germany) at 19°C. Measurements were done in triplicate by a spectrophotometric method. A calibration curve was performed with a linearity established in the range 50 – 1000 $\mu g.mL^{-1}$ ($R^2 = 0.9999$).

5.2.5 Methods used to characterize nanoparticles pre- and post- functionalization

The UV-vis absorption spectra of synthesized AgNP and their functionalization with both antibiotics were characterized using spectrophotometry (Thermo Evolution 600 UV/visible, Thermo Fisher Scientific, Massachusetts, USA). The mean particle size and polydispersity index (PI) of nanoparticles and conjugated nanoparticles were measured using the photon correlation spectroscopy method in hydrated particulate systems (diluted aqueous solutions, 1:20) with a Coulter Nanosizer Delsa Nano^{TM} C (Coulter Beckman, Fullerton, CA, USA). Topography images of different synthesized nanoparticles were obtained by Atomic Force Microscopy (AFM, Multimode Nanoscope IIIa, Digital Instruments, Veeco, Cambridgeshire, UK). AFM images were taken with silicon cantilevers with force constant 2.7 N/m, tip height <10 nm in contact mode.

5.2.6 *In vitro* antimicrobial activity evaluation

In vitro antimicrobial activity of different AgNP synthesized and functionalized with AMP and AHR (nanoconjugates) were evaluated through agar well diffusion assay, as described by Balouiri *et al.* [294]. Individual plates with *Staphylococcus aureus* (ATCC 25923) and *Staphylococcus epidermidis* (ATCC 12228) species were inoculated in Mueller-hinton agar (MHA). *Candida albicans* (CIP 3153A) and *Saccharomyces cerevisiae* (ATCC 204508) were inoculated in Sabouraud agar (SA) medium. AgNPs, nanoconjugates and free antibiotics were incubated during 24h at 37ºC. After incubation, inhibition halo (mm) was measured with regular rule.

5.2.7 *In vitro* preliminar safety assessment

As preliminar safety assessment, the cytotoxicity of prepared nanoconjugates were evaluated on a eucariotic cell model, *Saccharomyces cerevisiae* (ATCC 204508), as previously developed and reported [302, 303]. Yeast cells, approximately 0.5 x 10^6 cells/mL, in YPD medium were exposed to different amounts of test materials, AgNP with citrate and borohydride, in disposable cuvettes performing a final volume of 2 mL. The cell cultures grow for 5 hours at 30 ºC inside an incubator (Heidolph Incubator 1000 with shaker Heidolph Unimax 1010, Schwabach, Germany). The cuvettes were vortexed (for 2 sec) and the absorbances were measured at minute zero (start of the assay) and at regular intervals of 30 min (Thermo Scientific model Evolution 300 BB, UK). The logarithmic phase from the growth curve was used to evaluate the toxicity, expressed as growth inhibition in percentage of the control cells growth. Three series of assays were performed in different days, each comprising four replicate cultures.

5.2.8 *In vivo* safety assessment

Hairless 42 days-old male SHO-SCID mice (code: 474, Charles River, Barcelona, Spain), immunosuppressed for T and B cells were selected for this study. This study was conducted in accordance to the internationally accepted principles for laboratory animal use and care as found in Directive n. º 2010/63/EU and the project was approved by the Portuguese Veterinary General Division (DGAV). Animals were allowed to adapt to the laboratory for 7 days before testing and then they were maintained with food and water *ad libitum* and kept at 22.0 ± 1.0ºC with controlled relative humidity and 12 h light/dark cycle at Faculty of Pharmacy, University of Coimbra.

5.2.8.1.1 Preparation of a polycaprolactone-based semi-solid formulation

Carbopol hydrogel was prepared using the method described in the literature [297]. Briefly, 2 g Carbopol powder was dissolved in 100 mL of distilled water with stirring (multipoint plate magnetic stirring (Thermo Scientific VARIOMAG® Telesystem Stirrers, Langenselbold, Germany) and slight heating until complete dissolution. Then, a solution of sodium hydroxide was added and led to Carbopol's gelation.

5.2.8.1.2 *In vivo* mice skin irritation

A very viscous semi-solid formulation with AgNP conjugated with AHR was prepared to evaluate skin irritation in hairless mouse models. Chromameter CR300 (Minolta, Tokyo, Japan) was used to determine skin color according CIE color system [300, 301]. Concerning the results of previous section, AgNP with borohydride were functionalized with AHR at MIC value and incorporated into Carbopol gel at 1:10 ratio and applied to dorsal region of mice's. During a period of 21 days, a freshly prepared formulation was once weekly applied and skin coloration measurements were made after 24h of the application. Animals were randomized and distribuited in group: the control group (G0) with only Carbopol gel (n=2), group 1 (G1) dosed with AgNP with Carbopol gel (n=2) and test group (G2) dosed with AgNP functionalized with the AHR (n=3). At end of the study, all animals were sacrificed and skin area was excised for histological analysis. Biopsy specimens from application area of each formulation were collected, fixed in formaldehyde at 10% with phosphate buffer (pH=7.2) andthen post-fixed for 24h, dehydrated and embedded in paraffin. Sections, with 3-4 µm of thickness, were cut with a microtome (Thermo-Shandon AS 325 Microtome, Waltham, MA, USA), then stained with haematoxylin/eosin and observed with a photonic microscope (Nikon Eclipse E600, Tokyo, Japan). In addition, erythema was scored at each site: 0 (absent), 1 (scarcely visible, small

spotted), 2 (mild, large spotted), 3 (pronounced, confluent), and 4 (severe or livid discoloring, homogenous redness) [300].

5.2.9 Statistical analysis

All results are expressed as mean ± standard deviation. One-way ANOVA analysis was applied to demonstrate statistical differences in all tested parameters. All analyses were performed using a software program (GraphPad Prism 5®, GraphPad Software, San Diego, CA, USA) with a statistical significance level of 0.05.

5.3 Results and Discussion

In this study, resultant AgNP with citrate resulted on a clear yellow color solution (**Figure 5.4** in supporting material). In the analyses of SPR spectrum (**Figure 5.1**) it is possible to observe the presence of typical plasmon band with peak at 414 nm of the AgNPs made with citrate [301]. Similarly, AgNPs with borohydride also resulted on a yellow solution and the plasmon band at 402 nm (**Figure 5.1**). The maximum of plasmon band was sensitive to the surface of the particles [308, 309]. When conjugated to AMP and AHR on both particles, there was a change in the maximum of the SPR spectrum. Both AgNP plasmon band shifted to higher wavelengths (± 10 nm). The technique outlined above had proved to be very useful for the analysis of nanoparticles. Since the synthesis with citrate was a slower reaction process than with borohydride, the maximum absorption was at longer wavelength and resulted in larger particles [304].

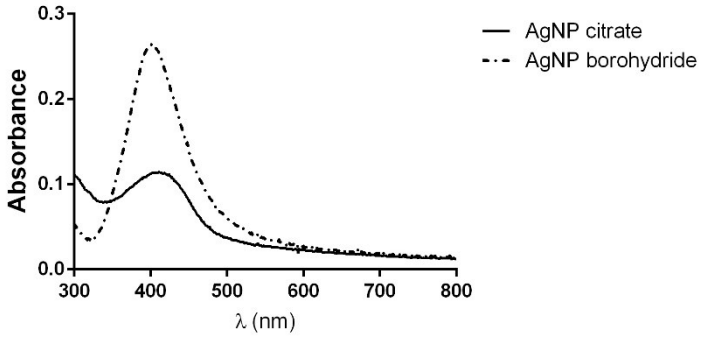

Figure 5.1 SPR spectra of AgNP synthesized with citrate and borohydride as reducing agents.

As shown in **Table 5.1,** after analyzed the mean particle size and size distribution of the

resultant nanoparticles through PCS technique, AgNP with citrate were larger than AgNP with borohydride (21.1nm *vs.* 9.6nm, respectively) but both particles were monodisperse. An increase of nanoparticle size after conjugation with AMP and AHR was observed in both type of nanoparticles, except with AgNP citrate and AHR (similar value before and after conjugation). The images obtained by AFM confirmed previous results (**Figure 5.2**). In general, the AFM images showed spherical nanoparticles using both reducing agents. In the case of AgNP functionalized with AMP, it was observed a larger number of particle agglomerates but no change of particle morphology. This phenomenon may be due to some neutralization of surface charges of nanoparticles and the absence of a stabilizing agent. In fact, AgNPs are highly reactive, allowing different types of bonding with different types of molecules, which makes their surfaces modifiable and a key factor for drug delivery.

Table 5.1 Mean particle size (nm), polydispersity index (PI) and association efficiency (%) of obtained AgNP and functionalized with ampicillin (AMP) and 7α-acetoxy-6β-hydroxyroyleanone (AHR) using PCS.

	Diameter (nm, mean values ± SD)	**Polydispersity index (PI)**	**Association efficiency (%)**
AgNP citrate	21.1 ± 14.1	0.33	n/a
AgNP citrate + AMP	24.8 ± 15.8	0.32	31.8
AgNP citrate + AHR	21.1 ± 14.3	0.33	n/d
AgNP borohydride	9.6 ± 6.4	0.28	n/a
AgNP borohydride + AMP	13.2 ± 8.5	0.14	38.2
AgNP borohydride + AHR	11.1 ± 3.1	0.39	72.5

Note: n/a means not applicable; n/d means not defined.

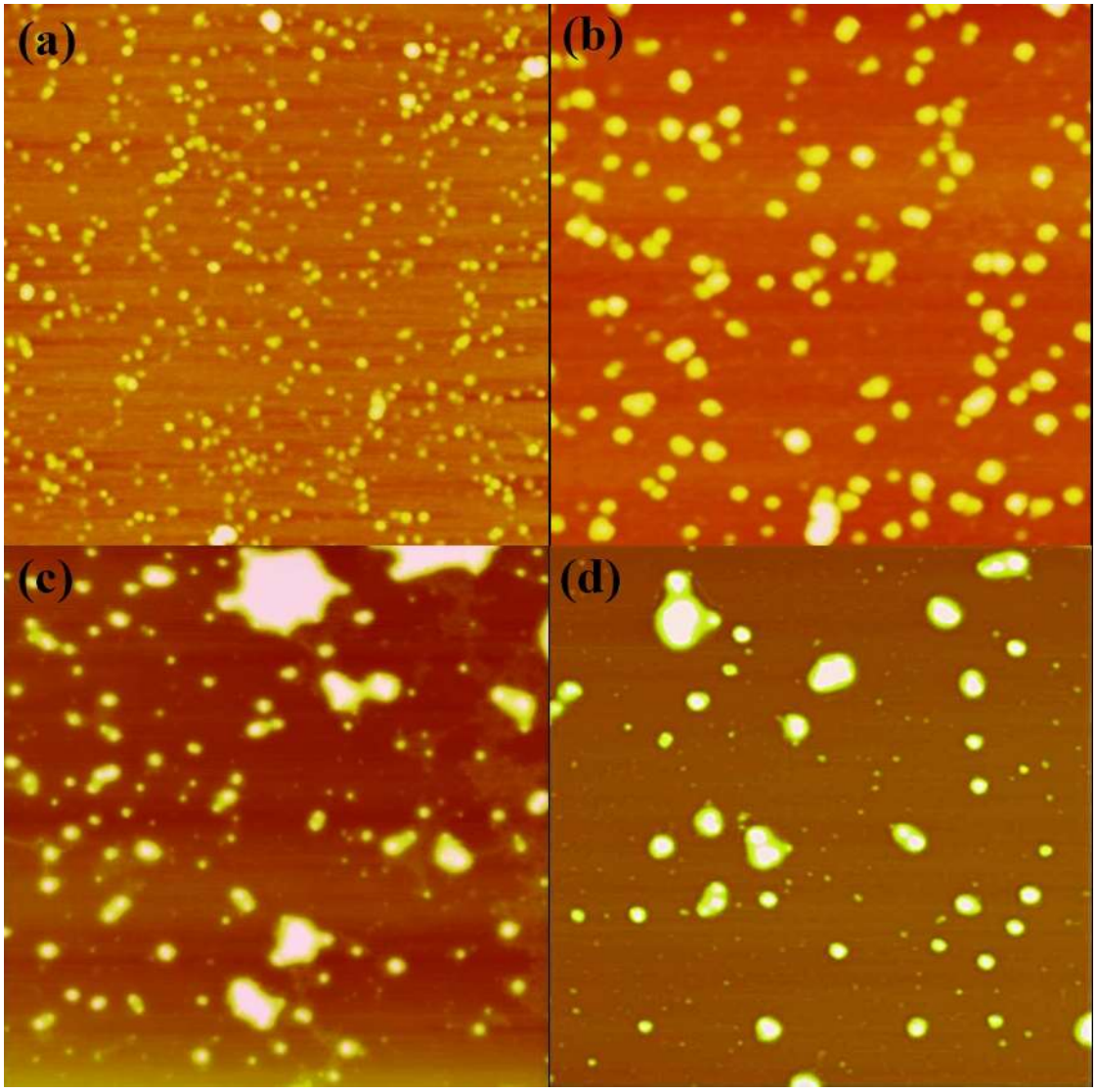

Figure 5.2 AFM images (topography) of different functionalized AgNP: borohydride + AHR (a), citrate + AHR (b), borohydride + AMP (c), citrate + AMP (d).

The association efficiency of AHR and AMP was determined for both AgNPs. As shown in **Table 5.1**, the higher association efficiency (72.5%) was observed with borohydride AgNP and AHR. The efficiency of association between AHR and citrate AgNP particles could not be determined due to the changeability of the particles after association with AHR. When conjugate AMP with both AgNP, results demonstrated a small value of association efficiency, with only 31.8% and 38.2 % for citrate and borohydride, respectively. The efficiency of association of a molecule with AgNP is associated with surface charge of particle and functional groups of each molecule [305]. The interaction with AMP through the thioether moiety are stronger with higher negative groups, showed in association efficiency in borohydride particles.

The antibacterial activity was assessed by measuring the inhibition halos using the well

diffusion method. As shown in the **Table 5.2**, AgNP with citrate showed an high antibacterial activity with a larger inhibition in *S. epidermidis* in comparison to AMP. When compared to AMP, the activity was identical observed with AgNP synthesized with borohydride for both bacterial strains. No activity was observed for *C. albicans* and *S. cerevisiae* strains for all tested samples, except for positive control. In *C. albicans* and *S. cerevisiae,* microbial resistance to silver itself is rare according literature [306] but when conjugated AgNP borohydride with AMP, antibacterial activity slightly increased (± 3%) in *S. aureus* strain and in *S. epidermidis*. Since the chemical group presence on the surface of NP results in different antibacterial activity when conjugated to these molecules, the binding strength and stability may be associated with a synergistic effect. The results with borohydride AgNP and AHR showed no loss of activity, in contrast to AgNP with citrate. This result is highly relevant for its topical application, since the conjugation of AHR with NPs does not result in less therapeutic efficacy. The mechanism of resistance is not completely understood but it is consensual that silver-resistant strains of bacteria are still a continuing problem in wound care despite many claims described in the literature [308, 309].

Table 5.2.- Antibacterial activity of different AgNP and conjugated with AMP and AHR. DMSO was used as negative control, methicillin as positive control for *S. aureus* and *S. epidermidis*, and fluconazole as positive control for *C. albicans* and *S. cerevisiae*.

	S. aureus **(mm)**	***S. epidermidis*** **(mm)**	***C. albicans*** **(mm)**	***S. cerevisiae*** **(mm)**
Negative control	5	5	5	5
Positive Control	15	15	13	20
AMP	34	31	5	5
AHR	15	19	5	5
AgNP citrate	34	34	5	5
AgNP citrate + AMP	34	32	5	5
AgNP citrate + AHR	11	17	5	5
AgNP borohydride	34	31	5	5
AgNP borohydride + AMP	**35**	**32**	5	5
AgNP borohydride + AHR	**34**	**31**	5	5

Our results of AgNP are in agreement with previous studies in the literature [269, 270]. The mechanism by which nanoparticles trigger bacteria's death is not fully demonstrated. In some studies, it is suggested that the interaction of AgNP with some constituents of the cell wall or with other cytoplasmatic components, such as DNA and/or proteins is essential for the cell regulation [311].

At same time, results against *S. cerevisiae* of the *in vitro* antimicrobial activity evaluation

can be also used as preliminary study on toxicity of both nanoconjugates [298]. Both AMP and AHR-loaded AgNP demonstrated a reduced or absence of any inhibition against the yeast model, similarly to previous studies [312]. Our *in vitro* preliminary safety assessment results in *S. cerevisiae* suggested a reduced toxicity of AgNP as seen in **Figure 5.3**. This study was restricted to the concentration of AgNP used in the next *in vivo* assays because higher concentrations could lead to an higher activity due to the antimicrobial properties of silver [317, 318].

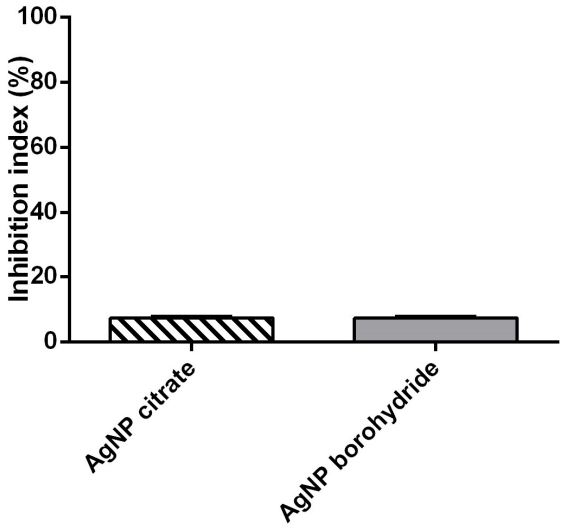

Figure 5.3 Inhibition index observed with AgNP citrate and borohydride in *S. cerevisae* model.

The next step was to evaluate the *in vivo* safety of AgNP conjugated with antibiotics included in a very viscous semi-solid formulation and always following 3R's principles of Animal Experimentation and welfcare. We decided to conduct this study of skin irritation using only AHR as antibiotic and AgNP functionalized with AHR due to several reasons. First, AMP is an antibiotic widely used in the treatment of infections and there is some data that claim possible cutaneous adverse reactions when used [299]. Most of the adverse effects of AMP are well-known and widely described in literature. Moreover, other studies showed some evidence of carcinogenicity of ampicillin [315]. Second, AMP was unsuccessfully associated to AgNP and thus our *in vivo* study was focused on borohydride AgNP funcionalized with AHR. In **Table 5.3/Figure 5.3** showed the average values obtained from the measurement of erythema over time. Per the staining measurement technique, the *L*a*b* colour system was determined in each group. The *L* value is related to color brightness (or lightness) of skin and considerably absorbed by melanin and haemoglobin. The variation of this parameter is directly related to interference with pigmentation and/or erythema. Other parameters also determined, named as *a* and *b*, are

related to coloration skin changes between green (-60) to red (+60) and blue (-60) to yellow (+60), respectively. An decrease of *L* and increase of *b* value's could be related to natural UV and/or artificial chemical tanning [318, 319].

According to the values obtained, none of the tested groups showed an increase in *a* value, i.e, there was no skin irritation. During the experimental period, the *a* value remained the same in all study groups. The last measurement recorded a decrease of the value in all groups, which it is not related to the formulation containing AgNP. From *b* value, the results demonstrated a slight increase over time (**Figure 5.3D**). This increase was not significant for a variation of color skin and was reproduced in all working groups. The skin brightness showed a stable value during the first two weeks and an increase during the third week in all groups (**Figure 5.3B**). This increase in skin brightness may be related to the base formulation used in this study. The measurement of the color of the skin is very difficult to characterize. Although the color is directly related to the amount of melanin and / or haemoglobin in the superficial layers of the skin, factors such as light source, applied pressure or measurement area can be influencing a set of results over time [320, 321].

Table 5.3.- Variation of the skin parameters in mice according chromameter data.

Time (day)	G0			G1			G2		
	L	a	b	L	a	b	L	a	b
0	62.1 ± 1.8	5.5 ± 0.7	-3.6 ± 1.2	63.3 ± 0.4	6.4 ± 0.1	-3.5 ± 0.4	62.6 ± 0.4	6.9 ± 1.0	-2.6 ± 0.9
7	66.8 ± 0.5	5.2 ± 0.2	-4.4 ± 0.4	59.3 ± 0.7	6.0 ± 0.1	-2.9 ± 1.3	62.8 ± 4.1	6.4 ± 0.7	-0.7 ± 2.2
17	60.7 ± 0.0	7.3 ± 0.0	6.9 ± 0.0	63.2 ± 2.1	6.3 ± 0.6	0.6 ± 0.2	63.9 ± 2.7	5.6 ± 1.5	0.6 ± 0.7
21	96.9 ± 0.0	0.2 ± 0.0	1.9 ± 1.0	96.7 ± 0.2	0.3 ± 0.1	1.4 ± 0.6	92.3 ± 6.2	1.9 ± 1.0	1.4 ± 0.4

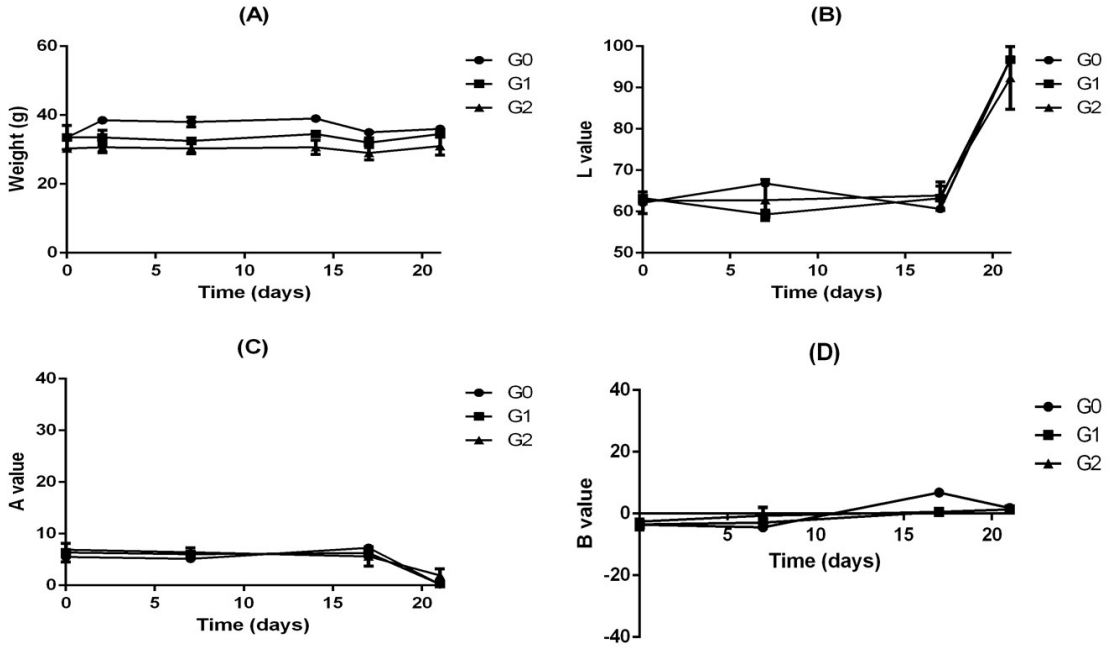

Figure 5.4 Variation of skin parameters over the time in hairless nude mice: control group (G0, n=2), AgNPs (G1, n=2) and test group dosed with AgNPs functionalized with AHR (G2, n=3).

The functionalization of AHR with nanoparticles did not demonstrate skin irritation nor a significant alteration of skin tone (**Figure 5.5**). The results are in agreement with other formulations in the market that use AgNP's as delivery carrier [320]. The functionalization with AHR did not demonstrate any skin irritation or coloring, suggesting a safe topical formulation for the treatment of skin infections. Histological analysis corroborates previous morphological studies (**Figure 5.6**). Samples of positive control showed an high level of anti-inflamatory activity and necrosis (**Figure 5.6a**) meanwhile a normal epidermis was observed in all test groups, including AgNP with AHR (**Figure 5.6e** and **Figure 5.6f**).

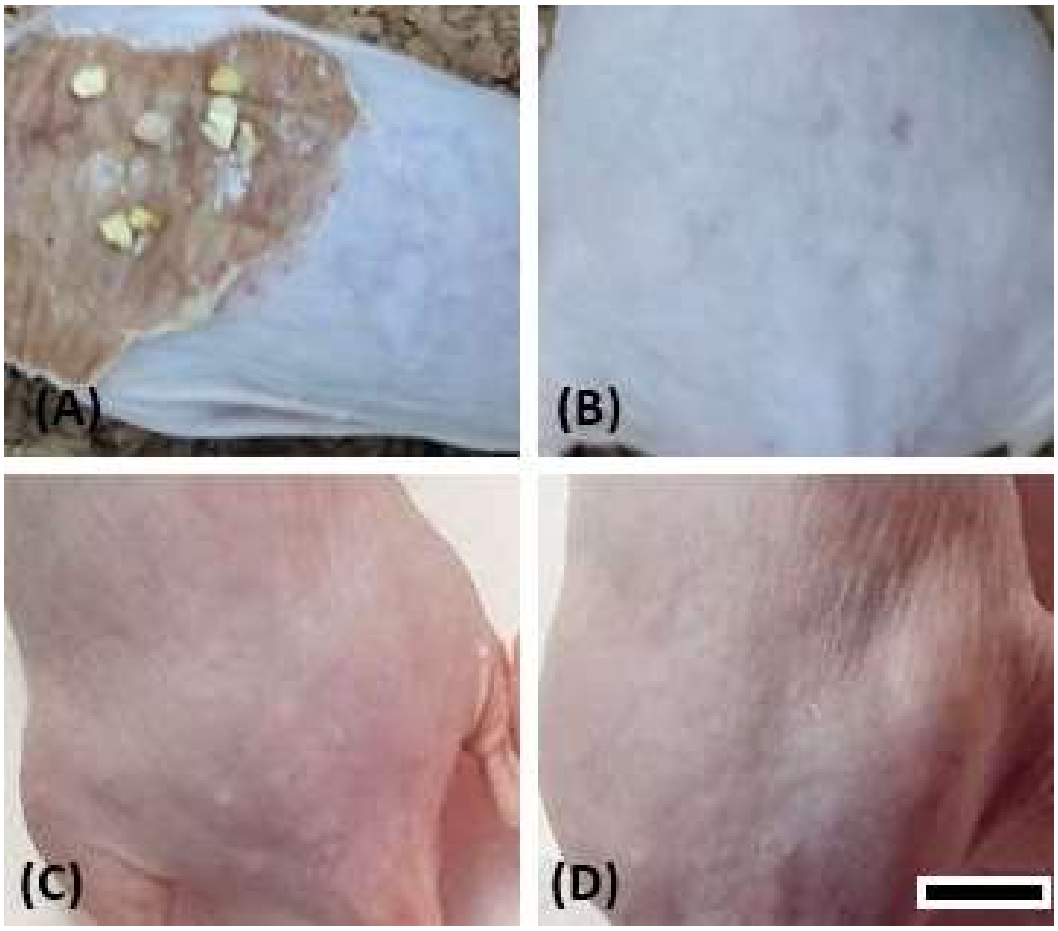

Figure 5.5 Macroscopic observation of the application zone of the formulation in rats after 21 days; **(A)** Positive control; **(B)** specimen from control group G0; **(C)** specimen from group G1; **(D)** specimen from group G2; Scale bar: 1cm.

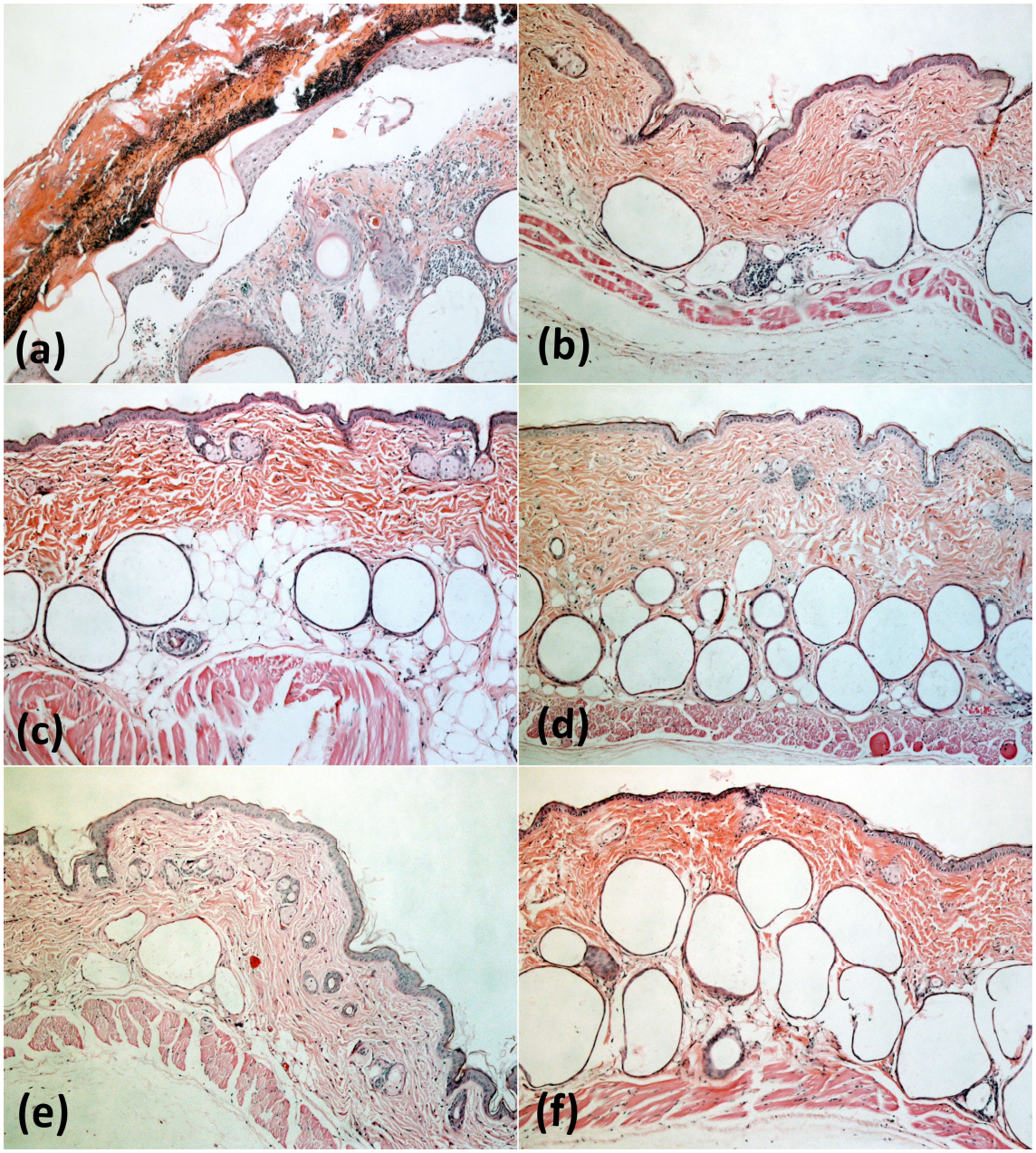

Figure 5.6 Histological images (100x microscopic approach) of skin in mice treated with AHR after 21 days; **(a)** positive control; **(b)** specimen from control group G0; **(c)** and **(d)** specimen from group G1; **(e)** and **(f)** specimen from group G2.

5.4 Conclusion

An effective treatment of resistant skin infections is critical for the general well-being of any patient. Over the last few decades, considerable studies have been done on the development of new drug delivery systems to overcome the limitations caused by the conventional dosage systems of antibiotics. An ideal drug delivery system should lead two importante issues: controlled and targeted delivery. Nanotechnology has proved to achieve these two issues. In design of the NPs, the major goal is to control the particle size and surface properties to achieve the controlled release of the antibiotic at a specific site at the therapeutically optimal rate within the dose regime.

In this study, we observed that the application of borohydride as reducing agent results in a very small particle size, opening a new challenge for the development of novel materials for use in highly advanced technologies. Our silver nanoparticles exhibited remarkable biological properties. Their functionalization with AHR resulted in very stable particles and they were not irritants to the animal skin. But the full potential of this technology has yet to be discovered. The mechanisms underlying the therapeutical properties of those nanoparticles are still not completely understood, and understanding them is a priority for future *in vivo* research.

5.5 Supporting material

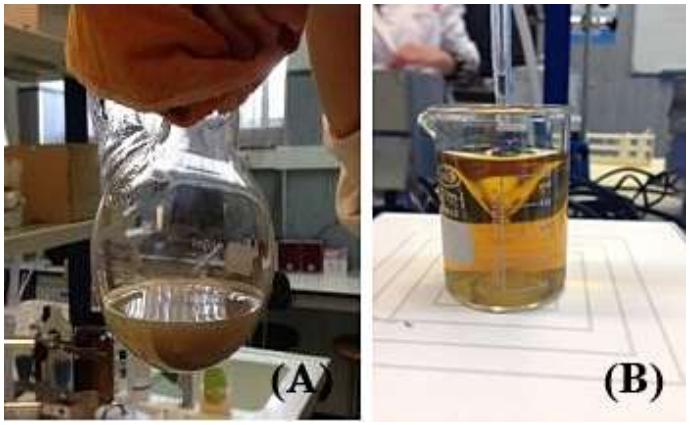

Figure 5.7 Final aspect of AgNP using citrate **(A)** and borohydride **(B)** as reducing agents**.**

Table 5.4 Range of concentrations and linear regressions obtained for association efficiency calculation.

Antibiotic	Concentration range ($\mu g.mL^{-1}$)	Absorvance (λ = 256 nm)	Linear regression	R^2
AMP	50	0.01	Y=0.0009x – 0.0235	0.9991
	100	0.09		
	300	0.27		
	500	0.46		
	700	0.64		
	1000	0.92		
AHR	8	0.08	Y=0.0076x + 0.0766	0.9967
	16	0.18		
	32	0.32		
	42	0.38		
	65	0.59		
	82	0.72		
	128	1.01		

Chapter 6

Conclusions

Conclusions

As established in this work, we aimed to better understand the properties of 7α-acetoxy-6β-hydroxyroyleanone and how it acts on the bacterial cell. We also intended to report the possible application of this compound for topical treatment of infections. For this, we developed two types of nanoparticles, polymeric and metallic, with two different formulations, through the plant extract or the isolated molecule.

The action of 7α-acetoxy-6β-hydroxyroyleanone was studied to a selected strain of MRSA. It has been concluded that at MIC, the compound dramatically reduced growth over time. In a more detailed study, it was verified that its action was dependent on a biochemically active cell, and there was no interaction with the membrane or cell wall structure. The type of action on the bacterial cell was identical to that demonstrated daptomycin.

On two species of Portuguese *Lavandulas* were determined its antioxidant activity in extracts of different polarities. PLGA polymer nanoparticles and selected methanolic *Lavandulas* extracts were successfully encapsulated with high efficiency. These particles showed low cytotoxicity and a high content of flavonoids and antioxidant capacity.

Silver nanoparticles were successfully produced through two procedures. The spherical nanoparticles were functionalized with 7α-acetoxy-6β-hydroxyroyleanone and ampicillin and fully characterized. The biological evaluation in bacterial stains with conjugates demonstrated high activity but no synergistic effect between antibiotics and nanoparticles. The safety assessment evaluation using animal models showed an absence of irritation or any changes on skin coloration.

In conclusion, the developed experiments provided important information about this natural antibacterial compound. To date, no studies have been done on the mode of action of this molecule. It was possible to prepare nanoparticles with plant extracts or the functionalization of silver nanoparticles with AHR. The production of these particles resulted in formulations of low *in vitro* toxicity, biological active for specific bacteria and possible therapeutic application.

In the future, more biochemical studies will be needed to understand possible sites for interaction with AHR. This data will allow to know more about the structure-activity and to improve antibacterial activity in MRSA cells. On the preparation of formulations with silver nanoparticles and AHR, future studies will be necessary on the skin release, as well as their interaction to avoid problems of toxicity.

References

[1] Atta-ur-Rahman and V. U. Ahmad, *13C-NMR of Natural Products*, vol. 2: Diterpe. Springer US, 1992.

[2] R. Firn, *Nature's Chemicals: The Natural Products that Shaped Our World*. Oxford, U.K: Oxford University Press, 2010.

[3] A. Srikrishna and B. Beeraiah, "An enantiospecific synthesis of a komarovispirane," *Tetrahedron Asymmetry*, vol. 18, no. 21, pp. 2587–2597, 2007.

[4] J. R. Hanson, "Diterpenoids of terrestrial origin," *Nat. Prod. Rep.*, vol. 29, p. 890, 2012.

[5] J. R. Hanson, "Diterpenoids.," *Nat. Prod. Rep.*, vol. 24, no. 6, pp. 1332–1341, 2007.

[6] J. R. Hanson, "Diterpenoids.," *Nat. Prod. Rep.*, vol. 26, pp. 1156–1171, 2009.

[7] A. San Feliciano, M. Gordaliza, M. A. Salinero, and J. M. Miguel Del Corral, "Abietane acids: Sources, biological activities, and therapeutic uses," *Planta Med.*, vol. 59, no. 6, pp. 485–490, 1993.

[8] M. A. González, "Synthetic derivatives of aromatic abietane diterpenoids and their biological activities," *Eur. J. Med. Chem.*, vol. 87, pp. 834–842, 2014.

[9] M. A. González, "Aromatic abietane diterpenoids: their biological activity and synthesis," *Nat. Prod. Rep.*, vol. 32, no. 5, pp. 684–704, 2015.

[10] Y. Dong, S. L. Morris-Natschke, and K. Lee, "Biosynthesis, total syntheses, and antitumor activity of tanshinones and their analogs as potential therapeutic agents.," *Nat. Prod. Rep.*, vol. 28, no. 3, pp. 529–542, 2011.

[11] R. H. Thomson, *The Total Synthesis of Naturally Occurring Quinones.*, vol. 8. John Wiley & Sons, 1992.

[12] R. H. Thomson, *Naturally Occurring Quinones IV (Recent advances)*. Springer Netherlands, 1997.

[13] Q. Zhou, "Natural Diterpene and Triterpene Quinone Methides: Structures, Synthesis, and Biological Potentials," in *Quinone Methides*, S. E. Rokita, Ed. Hoboken, NJ, USA: John Wiley & Sons, Inc, 2009, pp. 269–295.

[14] O. E. Edwards, G. Feniak, and M. Los, “Diterpenoid Quinones of Inula royleana D. C.,” *Can. J. Chem.*, vol. 40, no. 8, pp. 1540–1546, 1962.

[15] I. C. Chopra, J. D. Kohli, and K. L. Handa, “Inula royleana DC; its chemistry and pharmacological action.,” *Indian J. Med. Res.*, vol. 33, no. 1, pp. 139–141, 1945.

[16] S. V. Bhat, P. S. Kalyanaraman, H. Kohl, N. J. de Souza, and H.-W. Fehlhaber, “Inuroyleanol and 7-ketoroyleanone, two novel diterpenoids of Inula royleana DC,” *Tetrahedron*, vol. 31, no. 8, pp. 1001–1004, 1975.

[17] X. Yunlong, M. Yunbao, Z. Lin, and S. Handong, “Abietane quinones from rabdosia lophanthoides,” *Phytochemistry*, vol. 27, no. 11, pp. 3681–3682, 1988.

[18] X. Yunlong, W. Dan, L. Xiaojie, and F. Jian, “Abietane quinones from rabdosia lophanthoides,” *Phytochemistry*, vol. 28, no. 1, pp. 189–191, 1989.

[19] L. T. Jonathan, C.-T. Che, J. M. Pezzuto, H. H. S. Fong, and N. R. Farnsworth, “7-O-Methylhorminone and Other Cytotoxic Diterpene Quinones from Lepechinia bullata,” *J. Nat. Prod.*, vol. 52, no. 3, pp. 571–575, 1989.

[20] S. M. Kupchan, A. Karim, and C. Marcks, “Taxodione and taxodone, two novel diterpenoid quinone methide tumor inhibitors from Taxodium distichum.,” *J. Am. Chem. Soc.*, vol. 90, no. 21, pp. 5923–5924, 1968.

[21] Y.-H. Kuo, J.-S. Shih, Y.-T. Lin, and Y.-T. Lin, “6β-Acetoxy-7α-Hydroxyroyleanone, A New Compound from Taiwania Cryptomerioides Hayata,” *J. Chinese Chem. Soc.*, vol. 26, no. 2, pp. 71–73, 1979.

[22] R. Mehrotra, R. A. Vishwakarma, and R. S. Thakur, “Abietane diterpenoids from Coleus zeylanicus,” *Phytochemistry*, vol. 28, no. 11, pp. 3135–3137, 1989.

[23] A. S. Romanova, G. F. Pribylova, A. V. Patudin, E. S. Leskova, D. A. Pakaln, and A. I. Ban’kovskii, “The quinones of some species of sage,” *Chem. Nat. Compd.*, vol. 8, no. 2, pp. 231–232, 1974.

[24] A. S. Romanova, G. F. Pribylova, P. I. Zakharov, V. I. Sheichenko, and A. I. Ban’kovskii, “A new quinone from Salvia nemorosa,” *Chem. Nat. Compd.*, vol. 7, no. 2, pp. 190–191, 1971.

[25] Z. Taira and W. H. Watson, “The structure of conacytone, C20H26O6, a diterpene quinone from Salvia ballotaeflorae,” *Acta Crystallogr.*, vol. B32, no. 7, pp. 2149–2152,

1976.

[26] M. A. Galicia, B. Esquivel, A.-A. Sánchez, J. Cárdenas, T. P. Ramamoorthy, and L. Rodríguez-Hahn, "Abietane diterpenoids from Salvia pubescens," *Phytochemistry*, vol. 27, no. 1, pp. 217–219, 1988.

[27] J. Cárdenas and L. Rodríguez-Hahn, "Abietane and icetexane diterpenoids from Salvia candicans," *Phytochemistry*, vol. 38, no. 1, pp. 199–204, 1995.

[28] K. S. Mukherjee, P. K. Ghosh, and R. K. Mukherjee, "Diterpenoid quinones of Salvia lanata," *Phytochemistry*, vol. 22, no. 5, pp. 1296–1297, 1983.

[29] A. Michavila, F. Fernández-Gadea, and B. Rodríguez, "Abietane diterpenoids from the root of Salvia lavandulaefolia," *Phytochemistry*, vol. 25, no. 1, pp. 266–268, 1985.

[30] A. G. González, Z. E. Aguiar, T. A. Grillo, and J. G. Luis, "Diterpenes and diterpene quinones from the roots of Salvia apiana," *Phytochemistry*, vol. 31, no. 5, pp. 1691–1695, 1992.

[31] M. Jimenez E., E. Portugal M., A. Lira-Rocha, M. Soriano-Garcia, and R. A. Toscano, "A New Royleanone-Type Diterpene from Salvia sessei," *J. Nat. Prod.*, vol. 51, no. 2, pp. 243–248, 1988.

[32] M. Hernández, B. Esquivel, J. Cárdenas, L. Rodríguez-Hahn, and T. P. Ramamoorthy, "Diterpenoid abietane quinones isolated from Salvia regla," *Phytochemistry*, vol. 26, no. 12, pp. 3297–3299, 1987.

[33] W. H. Lin, J. M. Fang, and Y. S. Cheng, "Diterpenoids and steroids from Taiwania cryptomerioides," *Phytochemistry*, vol. 48, no. 8, pp. 1391–1397, 1998.

[34] G. Nagy, G. Günther, I. Máthé, G. Blunden, M. H. Yang, and T. a Crabb, "12-Deoxy-6,7-dehydroroyleanone, 12-deoxy-6-hydroxy-6,7- dehydroroyleanone and 12-deoxy-7,7-dimethoxy-6-ketoroyleanone from Salvia nutans roots," *Phytochemistry*, vol. 51, no. 6, pp. 809–812, 1999.

[35] N. Tan *et al.*, "Abietane diterpenoids and triterpenoic acids from Salvia cilicica and their antileishmanial activities," *Phytochemistry*, vol. 61, no. 8, pp. 881–884, Dec. 2002.

[36] A. Ulubelen, N. Evren, E. Tuzlaci, and C. Johansson, "Diterpenoids from the Roots of Salvia hypargeia," *J. Nat. Prod.*, vol. 51, no. 6, pp. 1178–1183, 1988.

[37] U. Kolak, A. Kabouche, M. Öztürk, Z. Kabouche, G. Topçu, and A. Ulubelen, "Antioxidant diterpenoids from the roots of Salvia barrelieri," *Phytochem. Anal.*, vol. 20, no. 4, pp.

320–327, 2009.

[38] H.-K. K. Lee, S.-R. R. Oh, J.-W. J.-I. W. I. Kim, J.-W. J.-I. W. I. Kim, and C.-O. O. Lee, "Agastaquinone, a new cytotoxic diterpenoid quinone from Agastache rugosa.," *J. Nat. Prod.*, vol. 58, no. 11, pp. 1718–1721, 1995.

[39] A. G. González, L. S. Andrés, J. R. Herrera, J. G. Luis, and A. G. Ravelo, "Abietane diterpenes with antibiotic activity from the flowers of Salvia canariensis. Reaction of galdosol with diazomethane," *Can. J. Chem.*, vol. 67, no. 2, pp. 208–212, 1988.

[40] Wu Shun Hua, Zhang Hong Jie, Lin Zhong Wen, and Sun Han Dong, "Terpenoids from Isodon grandifolia var. atunitzensis," *Phytochemistry*, vol. 34, no. 4, pp. 1176–1178, 1993.

[41] K. G. Luis, T. A. Grillo, W. Quinones, and M. P. Kishi, "Columbaridione, a diterpenequinone from Salvia columbariae," *Phytochemistry*, vol. 36, no. 1, pp. 251–252, 1994.

[42] Z. Habibi, S. Gandomkar, M. Yousefi, and S. Ghasemi, "A new abietane diterpenoid from Salvia xanthocheila Boiss.," *Nat. Prod. Res.*, vol. 27, no. 3, pp. 266–269, 2013.

[43] Y. Ikeshiro, I. Mase, and Y. Tomita, "Abietane type diterpenoids from Salvia miltiorrhiza," *Phytochemistry*, vol. 28, no. 11, pp. 3139–3141, 1989.

[44] A. Ortega, J. Cárdenas, D. a. Gage, and E. Maldonado, "Abietane and clerodane diterpenes from Salvia regla," *Phytochemistry*, vol. 39, no. 4, pp. 931–933, 1995.

[45] G. Nagy, G. Günther, I. Máthé, G. Blunden, M. H. Yang, and T. a. Crabb, "Diterpenoids from Salvia glutinosa, S. austriaca, S. tomentosa and S. verticillata roots," *Phytochemistry*, vol. 52, no. 6, pp. 1105–1109, 1999.

[46] H. C. Lin, H. Y. Ding, and W. L. Chang, "Two new fatty diterpenoids from Salvia miltiorrhiza," *J. Nat. Prod.*, vol. 64, no. 5, pp. 648–650, 2001.

[47] M. Hensch, P. Rüedi, and C. H. Eugster, "Horminon, Taxochinon und weitere Royleanone aus 2 abessinischenPlectranthus-Spezies (Labiatae)," *Helv. Chim. Acta*, vol. 58, no. 7, pp. 1921–1934, 1975.

[48] P. Rüedi, "8α,9α-Epoxy-7-oxoroyleanon, ein Diterpen-Epoxychinon aus einer abessinischen Plectranthus-Art (Labiatae)," *Helv. Chim. Acta*, vol. 67, no. 4, pp. 1116–1120, 1984.

[49] T. Miyase, P. Rüedi, and C. H. Eugster, "Diterpenoide Drüsenfarbstoffe aus Labiaten: Coleone U, V, W und 14-O-Formyl-coleon -V sowie 2 Royleanone aus Plectranthus

myrianthus Briq.; cis- und trans-A/B-6, 7-Dioxoroyleanon," *Helv. Chim. Acta*, vol. 60, no. 8, pp. 2770–2779, 1977.

[50] F. Yoshizaki, P. Rüedi, and C. H. Eugster, "Diterpenoide Drüsenfarbstoffe aus Labiaten : 11 Coleone und Royleanone aus Coleus carnosus HASSK .," *Helv. Chim. Acta*, vol. 62, no. 8, pp. 2754–2762, 1979.

[51] M. Uchida, T. Miyase, F. Yoshizaki, J. H. Bieri, P. Rüedi, and C. H. Eugster, "14-Hydroxytaxodion als Hauptditerpen in Plectranthus grandidentatus GÜRKE; Isolierung von sieben neuen dimeren Diterpenen aus P. grandidentatus, P. myrianthus BRIQ. und Coleus carnosus HASSK.: Strukturen der Grandidone A, 7-Epi-A, B, 7-Epi-B, C, D und 7-E," *Helv. Chim. Acta*, vol. 64, no. 7, pp. 2227–2250, 1981.

[52] A. C. Alder, P. Rüdi, and H. Eugster, "Drüsenfarbstoffe aus Labiaten: Die polaren Diterpenoide aus Plectranthus argentatus S. T. BLAKE," *Helv. Chim. Acta*, vol. 67, no. 6, pp. 1523–1530, 1984.

[53] E. Giacomelli *et al.*, "Cancer chemopreventive diterpenes from Salvia corrugata," *Phytochemistry*, vol. 96, pp. 257–264, 2013.

[54] T. Matsumoto and S. Harada, "The Total Synthesis of (+)-Taxoquinone, (−)-7α-Acetoxyroyleanone, (−)-Dehydroroyleanone, (−)-Horminone, (−)-7-Oxoroyleanone, and (+)-Inuroyleanol," *Bull. Chem. Soc. Jpn.*, vol. 52, no. 5, pp. 1459–1463, 1979.

[55] A. Kabouche, Z. Kabouche, M. Öztürk, U. Kolak, and G. Topçu, "Antioxidant abietane diterpenoids from Salvia barrelieri," *Food Chem.*, vol. 102, no. 4, pp. 1281–1287, 2007.

[56] A. Ulubelen, G. Topçu, U. Sönmez, M. Iqbal Choudhary, and Atta-Ur-Rahman, "Abietane diterpenes from Salvia napifolia," *Phytochemistry*, vol. 40, no. 3, pp. 861–864, 1995.

[57] H. Kofujita, M. Ota, K. Takahashi, Y. Kawai, and Y. Hayashi, "A diterpene quinone from the bark of Cryptomeria japonica," *Phytochemistry*, vol. 61, no. 8, pp. 895–898, 2002.

[58] E. C. Da Cruz Araújo *et al.*, "Cytotoxic abietane diterpenes from Hyptis martiusii Benth.," *Zeitschrift fur Naturforsch. - Sect. C J. Biosci.*, vol. 61, no. 3–4, pp. 177–183, 2006.

[59] A. Ulubelen, G. Topcu, and C. B. Johansson, "Norditerpenoids and diterpenoids from Salvia multicaulis with antituberculous activity," *J. Nat. Prod.*, vol. 60, no. 12, pp. 1275–1280, 1997.

[60] Y. Takaishi *et al.*, "Triptoquinone A and B novel interleukin-1 inhibitors from Tripterygium

wilfordii var Regeli," *Tetrahedron Lett.*, vol. 33, no. 47, pp. 7177–7180, 1992.

[61] N. Uchiyama *et al.*, "Trypanocidal constituents of Dracocephalum komarovi," *Tetrahedron*, vol. 62, no. 18, pp. 4355–4359, 2006.

[62] L. Gu and X. Weng, "Antioxidant activity and components of Salvia plebeia R.Br. - A Chinese herb," *Food Chem.*, vol. 73, no. 3, pp. 299–305, 2001.

[63] A. a. Mahmoud, S. S. Al-Shihry, and B. W. Son, "Diterpenoid quinones from Rosemary (Rosmarinus officinalis L.)," *Phytochemistry*, vol. 66, no. 14, pp. 1685–1690, 2005.

[64] M. Bakir, D. a. C. Biggs, A. Lough, W. H. Mulder, W. Reynolds, and R. B. Porter, "7-Acetyl-12-methoxy-horminone from Jamaican Hyptis verticillata (Labiatae)," *Acta Crystallogr.*, vol. E62, no. 1, pp. 306–308, 2006.

[65] A.-H. Zhao *et al.*, "Micranthin C, a Novel 13(12→11)abeo-Abietanoid fromIsodon lophanthoids var.micranthus," *Helv. Chim. Acta*, vol. 86, no. 10, pp. 3470–3475, 2003.

[66] O. Batista, M. F. Simões, A. Duarte, M. L. Valdeira, M. C. de la Torre, and B. Rodríguez, "An antimicrobial abietane from the root of Plectranthus hereroensis.," *Phytochemistry*, vol. 38, no. 1, pp. 167–169, 1995.

[67] C. Gaspar-Marques *et al.*, "Abietanes from Plectranthus grandidentatus and P-hereroensis against methicillin- and vancomycin-resistant bacteria," *Phytomedicine*, vol. 13, no. 4, pp. 267–271, Mar. 2006.

[68] B. Rodríguez, F. Fernández-Gadea, and G. Savona, "A rearranged abietane diterpenoid from the root of Salvia aethiopis," *Phytochemistry*, vol. 23, no. 8, pp. 1805–1806, 1984.

[69] J. A. Hueso-Rodríguez, M. L. Jimeno, B. Rodríguez, G. Savonaa, and M. Bruno, "Abietane diterpenoids from the root of Salvia phlomoides," *Phytochemistry*, vol. 22, no. 9, pp. 266–268, 1983.

[70] B. Bakshi, N. B. Mulchandani, and J. Shankar, "Abietane diterpene quinones and a new diterpene epoxide from Salvia moorcraftiana," *J. Chem. Sci.*, vol. 97, no. 2, pp. 167–170, 1986.

[71] D. Slameňová *et al.*, "Cytotoxic and DNA-damaging effects of diterpenoid quinones from the roots of Salvia officinalis L. on colonic and hepatic human cells cultured in vitro," *Basic Clin. Pharmacol. Toxicol.*, vol. 94, no. 6, pp. 282–290, 2004.

[72] C. Areche, G. Schmeda-Hirschmann, C. Theoduloz, and J. a Rodríguez, "Gastroprotective

effect and cytotoxicity of abietane diterpenes from the Chilean Lamiaceae Sphacele chamaedryoides (Balbis) Briq.," *J. Pharm. Pharmacol.*, vol. 61, no. 12, pp. 1689–1697, 2009.

[73] A. P. Teixeira *et al.*, "Abietane diterpenoids from Plectranthus grandidentatus," *Phytochemistry*, vol. 44, no. 2, pp. 325–327, 1997.

[74] M. Fronza, E. Lamy, S. Günther, B. Heinzmann, S. Laufer, and I. Merfort, "Abietane diterpenes induce cytotoxic effects in human pancreatic cancer cell line MIA PaCa-2 through different modes of action," *Phytochemistry*, vol. 78, pp. 107–119, 2012.

[75] M. Fronza *et al.*, "In vitro cytotoxic activity of abietane diterpenes from Peltodon longipes as well as Salvia miltiorrhiza and Salvia sahendica," *Bioorganic Med. Chem.*, vol. 19, no. 16, pp. 4876–4881, 2011.

[76] F. Simões, A. Michavila, B. Rodríguez, C. Maria, García-Alvarez, and M. Hasan, "A quinone methide diterpenoid from the root of Salvia moorciuftiana," *Phytochemistry*, vol. 25, no. 3, pp. 755–756, 1986.

[77] N. Öztekin, S. Başkan, S. Evrim Kepekçi, F. B. Erim, and G. Topçu, "Isolation and analysis of bioactive diterpenoids in Salvia species (Salvia chionantha and Salvia kronenburgiii) by micellar electrokinetic capillary chromatography," *J. Pharm. Biomed. Anal.*, vol. 51, no. 2, pp. 439–442, 2010.

[78] S. Gandomkar, M. Yousefi, Z. Habibi, and M. A. As'habi, "A new triterpene from Salvia xanthocheila Boiss," *Nat. Prod. Res.*, vol. 26, no. 7, pp. 648–653, 2012.

[79] S. Saeidnia, M. Ghamarinia, A. R. Gohari, and A. Shakeri, "Terpenes from the root of Salvia hypoleuca benth," *DARU J. Pharm. Sci.*, vol. 20, no. 1, p. 66, 2012.

[80] A. Ulubelen, S. Öksüz, G. Topcu, A. C. Gören, and W. Voelter, "Antibacterial diterpenes from the roots of Salvia blepharochlaena," *J. Nat. Prod.*, vol. 64, no. 4, pp. 549–551, 2001.

[81] M. Martínez-vázquez *et al.*, "Antimicrobial Diterpenes From Salvia Reptans," vol. 36, no. 2, pp. 77–80, 1998.

[82] J. M. Schmid, P. Rüedi, and C. H. Eugster, "Diterpenoide Drüsenfarbstoffe aus Labiaten: 22 neue Coleone und Royleanone aus Plectranthus lanuginosus," *Helv. Chim. Acta*, vol. 65, no. 7, pp. 2136–2163, 1982.

[83] P. Rijo *et al.*, "Antimycobacterial metabolites from Plectranthus: Royleanone derivatives

against Mycobacterium tuberculosis strains," *Chem. Biodivers.*, vol. 7, no. 4, pp. 922–932, 2010.

[84] R. Kubínová, E. Švajdlenka, K. Schneiderová, Z. Hanáková, S. Dall'Acqua, and O. Farsa, "Polyphenols and diterpenoids from Plectranthus forsteri 'Marginatus,'" *Biochem. Syst. Ecol.*, vol. 49, no. 0, pp. 39–42, 2013.

[85] N. Kusumoto, T. Ashitani, T. Murayama, K. Ogiyama, and K. Takahashi, "Antifungal Abietane-Type Diterpenes from the Cones of Taxodium distichum Rich," *J. Chem. Ecol.*, vol. 36, no. 12, pp. 1381–1386, 2010.

[86] N. Kusumoto, N. Aburai, T. Ashitani, and K. Takahashi, "Pharmacological Prospects of Oxygenated Abietane-Type Diterpenoids from Taxodium distichum Cones," no. April, pp. 109–115, 2014.

[87] Z. C. Gazim *et al.*, "New natural Diterpene-Type abietane from tetradenia riparia essential oil with Cytotoxic and Antioxidant activities," *Molecules*, vol. 19, no. 1, pp. 514–524, 2014.

[88] C.-Z. Lin *et al.*, "Gerardianin A, a new abietane diterpenoid from Isodon lophanthoides var. gerardianus.," *J. Asian Nat. Prod. Res.*, vol. 10, no. 9–10, pp. 841–844, 2008.

[89] A. R. Jassbi, M. Mehrdad, F. Eghtesadi, S. N. Ebrahimi, and I. T. Baldwin, "Novel rearranged abietane diterpenoids from the roots of Salvia sahendica," *Chem. Biodivers.*, vol. 3, no. 8, pp. 916–922, 2006.

[90] S. Rungsimakan and M. G. Rowan, "Terpenoids, flavonoids and caffeic acid derivatives from Salvia viridis L. cvar. Blue Jeans," *Phytochemistry*, vol. 108, pp. 177–188, 2014.

[91] W.-H. Lin, J.-M. Fang, and Y.-S. Cheng, "Uncommon diterpenes with the skeleton of six-five-six fused-rings from Taiwania cryptomerioides," *Phytochemistry*, vol. 40, no. 3, pp. 871–873, 1995.

[92] O. Batista, A. Duarte, J. Nascimento, M. F. Simões, M. C. de la Torre, and B. Rodríguez, "Structure and antimicrobial activity of diterpenes from the roots of Plectranthus hereroensis.," *J. Nat. Prod.*, vol. 57, no. 6, pp. 858–861, 1994.

[93] F. Matloubi-Moghadam, P. Rüedi, and C. H. Eugster, "Drüsefarbstoffe aus Labiaten: Identifizierung von 17 Abietanoiden aus Plectranthus sanguineus BRITTEN," *Helv. Chim. Acta*, vol. 70, no. 4, pp. 975–983, 1987.

[94] V. K. Bajpai and S. C. Kang, "Antimycotic potential of a diterpenoid taxoquinone against Candida species isolated from Metasequoia glyptostroboides," *Bangladesh J. Pharmacol.*, vol. 9, no. 2, pp. 154–160, 2014.

[95] V. K. Bajpai, M. Na, and S. C. Kang, "The role of bioactive substances in controlling foodborne pathogens derived from Metasequoia glyptostroboides Miki ex Hu," *Food Chem. Toxicol.*, vol. 48, no. 7, pp. 1945–1949, 2010.

[96] V. K. Bajpai, Y.-H. Park, M. Na, and S. C. Kang, "α-Glucosidase and tyrosinase inhibitory effects of an abietane type diterpenoid taxoquinone from Metasequoia glyptostroboides," *BMC Complement. Altern. Med.*, vol. 15, no. 1, pp. 1–6, 2015.

[97] G. J. Huang *et al.*, "Anti-inflammatory activities of 6β-acetoxy-7α-hydroxyroyleanone from Taiwania cryptomerioides Hayata ex vivo and in vivo.," *J. Agric. Food Chem.*, vol. 59, no. 20, pp. 11211–11218, 2011.

[98] S. Y. Wang, J. H. Wu, L. F. Shyur, Y. H. Kuo, and S. T. Chang, "Antioxidant activity of abietane-type diterpenes from heartwood of Taiwania cryptomerioides Hayata," *Holzforschung*, vol. 56, no. 5, pp. 487–492, 2002.

[99] R. Kubínová *et al.*, "Antimicrobial and enzyme inhibitory activities of the constituents of Plectranthus madagascariensis (Pers.) Benth.," *J. Enzyme Inhib. Med. Chem.*, vol. 6366, pp. 1–4, 2014.

[100] C. Gaspar-Marques, M. F. Simoes, B. Rodriguez, M. F. Simões, and B. Rodríguez, "A trihomoabietane diterpenoid from Plectranthus grandidentatus and an unusual addition of acetone to the ortho-quinone system of cryptotanshinone," *J. Nat. Prod.*, vol. 68, no. 9, pp. 1408–1411, 2005.

[101] F. Cerqueira *et al.*, "Effect of abietane diterpenes from Plectranthus grandidentatus on T- and B-lymphocyte proliferation," *Bioorg. Med. Chem.*, vol. 12, no. 1, pp. 217–223, 2004.

[102] B. Esquivel, J. S. Calderon, E. Flores, C. Chavez, and M. Juarez, "Abietane and Icetexane Diterpenoids from Salvia Pubescens," *Nat. Prod. Lett.*, vol. 10, no. 2, pp. 87–93, 1997.

[103] B. S. Min, M. Hattori, H. K. Lee, and Y. H. Kim, "Inhibitory constituents against HIV-1 protease from Agastache rugosa.," *Arch. Pharm. Res.*, vol. 22, no. 1, pp. 75–77, 1999.

[104] K. Miura, H. Kikuzaki, and N. Nakatani, "Apianane terpenoids from Salvia officinalis," *Phytochemistry*, vol. 58, no. 8, pp. 1171–1175, 2001.

[105] K. Miura, H. Kikuzaki, and N. Nakatani, “Antioxidant activity of chemical components from sage (Salvia officinalis L.) and thyme (Thymus vulgaris L.) measured by the oil stability index method,” *J. Agric. Food Chem.*, vol. 50, no. 7, pp. 1845–1851, 2002.

[106] Z. Ma, M. Zhang, and Z. Song, “Characterization of tanshinones with quinone reductase induction activity from radix Salvia miltiorrhiza by liquid chromatography/tandem mass spectrometry,” *Rapid Commun. Mass Spectrom.*, vol. 23, no. 18, pp. 2857–2866, 2009.

[107] H.-B. Li and F. Chen, “Preparative isolation and purification of six diterpenoids from the Chinese medicinal plant Salvia miltiorrhiza by high-speed counter-current chromatography.,” *J. Chromatogr. A*, vol. 925, no. 1–2, pp. 109–114, 2001.

[108] J. M. Künzle, P. Rüedii, and C. H. Eugster, “Isolierung und Strukturaufklärung von 36 Diterpenoiden aus Trichomen von Plectranthus edulis (VATKE) T.T. AYE,” *Helv. Chim. Acta*, vol. 70, no. 7, pp. 1911–1929, 1987.

[109] A. C. Alder, P. Rüedi, R. Prewo, J. H. Bieri, and C. H. Eugster, “Neue Diterpenoide aus Blattdrüsen einer Plectranthus sp. aus Rwanda,” *Helv. Chim. Acta*, vol. 69, no. 6, pp. 1395–1417, 1986.

[110] C. G. Marques *et al.*, “Effect of abietane diterpenes from Plectranthus grandidentatus on the growth of human cancer cell lines,” *Planta Med.*, vol. 68, no. 9, pp. 839–840, Sep. 2002.

[111] J. Wellsow *et al.*, “Insect-antifeedant and antibacterial activity of diterpenoids from species of Plectranthus,” *Phytochemistry*, vol. 67, no. 16, pp. 1818–1825, 2006.

[112] H. Moritoki, T. Hisayama, K. Kida, W. Kondoh, S. Inoue, and Y. Takaishi, “Inhibition by triptoquinone-A of LPS- and IL-1β-primed induction of no synthase in rat thoracic aorta,” *Life Sci.*, vol. 59, no. 3, pp. 49–54, 1996.

[113] L.-Z. Lin, G. Blasko, and G. A. Cordell, “Diterpenes of Salvia prionitis,” *Phytochemistry*, vol. 28, no. 1, pp. 177–181, 1989.

[114] A. Michavila, M. C. De La Torre, and B. Rodríguez, “20-Nor-abietane and rearranged abietane diterpenoids from the root of Salvia argentea,” *Phytochemistry*, vol. 25, no. 8, pp. 1935–1937, 1986.

[115] Ł. Kuźma, E. Bruchajzer, and H. Wysokińska, “Diterpenoid production in hairy root culture of Salvia sclarea L.,” *Zeitschrift fur Naturforsch. - Sect. C J. Biosci.*, vol. 63, no. 7–8, pp.

621–624, 2008.

[116] Ł. Kuźma, M. Derda, E. Hadaś, and H. Wysokińska, "Abietane diterpenoids from Salvia sclarea transformed roots as growth inhibitors of pathogenic Acanthamoeba spp.," *Parasitol. Res.*, vol. 114, no. 1, pp. 323–327, 2015.

[117] Ł. Kuźma, M. Rózalski, E. Walencka, B. Rózalska, and H. Wysokińska, "Antimicrobial activity of diterpenoids from hairy roots of Salvia sclarea L.: Salvipisone as a potential anti-biofilm agent active against antibiotic resistant Staphylococci," *Phytomedicine*, vol. 14, no. 1, pp. 31–35, 2007.

[118] A. Rustaiyan, M. Samadizadeh, Z. Habibi, and J. Jakupovic, "Two diterpenes with rearranged abietane skeletons from Zhumeria majdae," *Phytochemistry*, vol. 39, no. 1, pp. 163–165, May 1995.

[119] A. Ulubelen *et al.*, "Terpenoids from Salvia sclarea," *Phytochemistry*, vol. 36, no. 4, pp. 971–974, 1994.

[120] W. H. Lin, J. M. Fang, and Y. S. Cheng, "Diterpenesand related cycloadducts from Taiwania cryptomerioides," *Phytochemistry*, vol. 42, no. 6, pp. 1657–1663, 1996.

[121] C.-I. Chang, S.-C. Chien, S.-M. Lee, and Y.-H. Kuo, "Three novel 5(6-->7)abeoabietane-type diterpenes from the bark of Taiwania cryptomerioides.," *Chem. Pharm. Bull. (Tokyo).*, vol. 51, no. 12, pp. 1420–1422, 2003.

[122] K. Kawazoe *et al.*, "Rearranged abietane-type diterpenes from Salvia dichroantha," *Phytochemistry*, vol. 50, no. 3, pp. 493–497, 1998.

[123] N. Uchiyama *et al.*, "New icetexane and 20-norabietane diterpenes with trypanocidal activity from Dracocephalum komarovi," *J. Nat. Prod.*, vol. 66, no. 1, pp. 128–131, 2003.

[124] L. Rodríguez-Hahn *et al.*, "New highly oxidized diterpene quinones from Salvia fruticulosa (labiatae)," *Tetrahedron Lett.*, vol. 27, no. 45, pp. 5459–5462, 1986.

[125] L. Rodríguez-Hahn *et al.*, "Abietane type diterpenoids from Salvia fruticulosa. A revision of the structure of fruticulin B," *Phytochemistry*, vol. 28, no. 2, pp. 567–570, 1989.

[126] A. Ohsaki, S. Kawamata, M. Ozawa, A. Kishida, X. Gong, and C. Kuroda, "Salviskinone A, a diterpene with a new skeleton from Salvia przewalskii," *Tetrahedron Lett.*, vol. 52, no. 12, pp. 1375–1377, 2011.

[127] N. N. Sabri *et al.*, "Two new rearranged abietane diterpene quinones from Salvia

aegyptiaca L," *J. Org. Chem.*, vol. 54, no. 17, pp. 4097–4099, 1989.

[128] Y.-H. Liu *et al.*, "Two new rearranged abietane diterpenoids from tropical Isodon coetsa.," *J. Asian Nat. Prod. Res.*, vol. 8, no. 8, pp. 671–675, 2006.

[129] P. Rüedi and C. H. Eugster, "Coleon D, ein Diterpen aus Coleus aquaticus Guercke mit trans-A/B-6,7-Dioxostruktur," *Helv. Chim. Acta*, vol. 55, no. 5, pp. 1736–1745, 1972.

[130] M. Moir, P. Rüedi, and C. H. Eugster, "Diterpenoids from coleus somaliensis (S. Moore): Coleons G, and J," *Helv. Chim. Acta*, vol. 56, no. 7, pp. 2539–2548, 1973.

[131] M. Moir, P. Rüedi, and C. H. Eugster, "Diterpenoid Hydroquinones from Coleus somaliensis (S. Moore): Coleons H, I, and K," *Helv. Chim. Acta*, vol. 56, no. 7, pp. 2534–2539, 1973.

[132] P. Rüedi and C. H. Eugster, "Coleone C, D, I, I' aus einer madegassischen Plectranthus sp. nov. Interkonversion von cis- und trans-A/B-6,7-Diketoditerpenen," *Helv. Chim. Acta*, vol. 58, no. 7, pp. 1899–1912, 1975.

[133] P. Rüedi and C. H. Eugster, "Diterpenoide Drüsenfarbstoffe: Coleon L, ein neues Diosphenol aus Coleus somaliensis S. MOORE; Revision der Strukturen von Coleon H, I, I' und K," *Helv. Chim. Acta*, vol. 60, no. 4, pp. 1233–1238, 1977.

[134] S. Arihara, P. Rüedi, and C. H. Eugster, "Neue spiro-Cyclopropyl-cyclohexendion-Diterpene: Coleone M, N, P, Q, R sowie Barbatusin aus Plectranthus caninus ROTH und Coleon O aus Coleus somaliensis S. MOORE," *Helv. Chim. Acta*, vol. 58, no. 2, pp. 343–356, 1975.

[135] K. Grob, P. Rüedi, and C. H. Eugster, "Drüsenfarbstoffe aus Labiaten: Strukturen von 16 Diterpenen (Coleone und Royleanone) aus Coleus coerulescens GÜRKE," *Helv. Chim. Acta*, vol. 61, no. 2, pp. 871–884, 1978.

[136] T. Miyase, F. Yoshizaki, N. Kabengele, P. Rüedi, and C. H. Eugster, "Strukturen von 13 Diterpenen (Coleonen) aus Blattdrüsen von Solenostemon sylvaticus und Coleus garckeanus (Labiatae)," *Helv. Chim. Acta*, vol. 62, no. 7, pp. 2374–2383, 1979.

[137] T. Miyase, P. Rüedi, and C. H. Eugster, "Struktur von sechs Coleonen (Diterpenen) aus Solenostemon monostachys (P. BEAUV.) BRIQ. (Labiatae)," *Helv. Chim. Acta*, vol. 63, no. 1, pp. 95–101, 1980.

[138] P. Rüedi, J. M. Schmid, R. Prewo, J. H. Bieri, and C. H. Eugster, "Spirocoleone: Synthese

und Charakterisierung von vier diastereomeren Spiro (methylcyclopropan)-Substrukturen; Revision der Konfiguration an C(12) und C(15) von Coleon P und Derivaten sowie von Coleon-Z-Derivaten; Röntgenstrukturanalysen von Lanugon J und," *Helv. Chim. Acta*, vol. 66, no. 2, pp. 429–449, 1983.

[139] F. Matloubi-Moghadam, P. Rüedi, and C. H. Eugster, "Neue Coleone und Royleanone aus Coleus somaliensis S. MOORE," *Helv. Chim. Acta*, vol. 67, no. 1, pp. 201–208, 1984.

[140] A. C. Alder, P. Rüedi, and C. H. Eugster, "Plectranthone A, B, C und D. Diterpenoide Phenanthren-1,4-dione aus Blattdrüsen einer Plectranthuus sp. (Labiatae)," *Helv. Chim. Acta*, vol. 67, no. 4, pp. 1003–1011, 1984.

[141] P. Rüedi, "Neue Diterpene aus Blattdrüsen von Plectranthus barbatus (Labiatae). Die absolute Konfiguration der 2-Hydroxypropyl-Seitenkette in Coleon E," *Helv. Chim. Acta*, vol. 69, no. 5, pp. 972–984, 1986.

[142] N. Uchiyama *et al.*, "Antichagasic Activity of Komaroviquinone Is Due to Generation of Reactive Oxygen Species Catalyzed by," *Society*, vol. 49, no. 12, pp. 5123–5126, 2005.

[143] T. Matsumoto, Y. Ohsuga, S. Harada, and K. Fukui, "Synthesis of Taxodione, Royleanone, Cryptojaponol, and Methyl 11-Hydroxy-12-methoxy-7-oxoabieta-8,11)13-trien-18-oate," *Bull. Chem. Soc. Jpn.*, vol. 50, no. 1, pp. 266–272, 1977.

[144] L. S. Liebeskind, R. Chidambaram, S. Nimkar, and D. Liotta, "A synthesis of the abietane diterpenoid quinone (±)-royleanone via maleoylcobalt technology.," *Tetrahedron Lett.*, vol. 31, no. 26, pp. 3723–3726, Jan. 1990.

[145] R. L. Danheiser, D. S. Casebier, and F. Firooznia, "Aromatic annulation strategy for the synthesis of angularly-fused diterpenoid quinones. Total synthesis of (+)-neocryptotanshinone, (-)-cryptotanshinone, tanshinone IIA, and (??)-royleanone," *J. Org. Chem.*, vol. 60, no. 26, pp. 8341–8350, 1995.

[146] M. C. Carreño, J. L. García Ruano, and M. a Toledo, "Enantioselective synthesis of (+)-royleanone from sulfinyl quinones.," *Chem. - A Eur. J.*, vol. 6, no. 2, pp. 288–291, 2000.

[147] Z. Yang *et al.*, "Synthesis of variously oxidized abietane diterpenes and their antibacterial activities against MRSA and VRE," *Bioorganic Med. Chem.*, vol. 9, no. 2, pp. 347–356, 2001.

[148] J. King, P. Quayle, and J. F. Malone, "A new synthesis of 12-O-methyl royleanone," *Tetrahedron Lett.*, vol. 31, no. 36, pp. 5221–5224, 1990.

[149] M. Hensch, C. H. Eugster, and H.-P. Weber, “Säurekatalysierte Umlagerung von 7-Hydroxy-royleanon in ein 20(10->9) abeo-Abietan-Derivat und zwei Phenalenone,” *Helv. Chim. Acta*, vol. 58, no. 7, pp. 1934–1939, Nov. 1977.

[150] P. Rüedi and C. H. Eugster, “14-Hydroxytaxodion: Partialsynthese und Reaktionen,” *Helv. Chim. Acta*, vol. 64, no. 7, pp. 2219–2226, 1981.

[151] P. Rijo, A. Duarte, A. P. Francisco, T. Semedo-Lemsaddek, and M. F. Simóes, “In vitro antimicrobial activity of royleanone derivatives against gram-positive bacterial pathogens,” *Phyther. Res.*, vol. 28, no. 1, pp. 76–81, 2014.

[152] J. G. Marrero, L. S. Andrés, and J. G. Luis, “Quinone derivatives by chemical transformations of 16-hydroxycarnosol from Salvia species.,” *Chem. Pharm. Bull. (Tokyo).*, vol. 53, no. 12, pp. 1524–1529, 2005.

[153] F. M. Moghaddam and M. M. Farimani, “A simple and efficient total synthesis of (±)-danshexinkun A, a bioactive diterpenoid from Salvia miltiorrhiza,” *Tetrahedron Lett.*, vol. 51, no. 3, pp. 540–542, 2010.

[154] H. Meier, P. Rüedi, and C. H. Eugster, “Synthese und Charakterisierung der 8 isomeren, im Ring B mono- bzw. dihydroxylierten Royleanone,” *Helv. Chim. Acta*, vol. 64, no. 3, pp. 630–642, 1981.

[155] Y. I. Matsushita, Y. Iwakiri, S. Yoshida, K. Sugamoto, and T. Matsui, “Synthesis of 12-deoxyroyleanone, cryptoquinone, 11,14-dihydroxy-8,11,13- abietatrien-7-one, and related derivatives from dehydroabietic acid,” *Tetrahedron Lett.*, vol. 46, no. 21, pp. 3629–3632, 2005.

[156] M. J. Sexmero Cuadrado, M. C. De la Torre, L. Z. Lin, G. A. Cordell, B. Rodriguez, and A. Perales, “Cyclization reactions of the o-naphthoquinone diterpene aethiopinone. A revision of the structure of prionitin.,” *J. Org. Chem.*, vol. 57, no. 17, pp. 4722–4728, Aug. 1992.

[157] R. Tapia *et al.*, “General access to taiwaniaquinoids based on a hypothetical abietane C7-C8 cleavage biogenetic pathway,” *J. Org. Chem.*, vol. 77, no. 1, pp. 573–584, 2012.

[158] E. Alvarez-Manzaneda, R. Chahboun, E. Alvarez, R. Tapia, and R. Alvarez-Manzaneda, “Enantioselective total synthesis of cytotoxic taiwaniaquinones A and F.,” *Chem. Commun. (Camb).*, vol. 46, no. 48, pp. 9244–9246, 2010.

[159] J. Deng *et al.*, "Divergent total synthesis of taiwaniaquinones A and F and taiwaniaquinols B and D," *Org. Lett.*, vol. 15, no. 8, pp. 2022–2025, 2013.

[160] M. Banerjee, R. Mukhopadhyay, B. Achari, and A. K. Banerjee, "General route to 4a-methylhydrofluorene diterpenoids: Total syntheses of (±)-taiwaniaquinones D and H, (±)-taiwaniaquinol B, (±)-dichroanal B, and (±)-dichroanone," *J. Org. Chem.*, vol. 71, no. 7, pp. 2787–2796, 2006.

[161] C. Thommen, C. K. Jana, M. Neuburger, and K. Gademann, "Syntheses of taiwaniaquinone F and taiwaniaquinol A via an unusual remote C-H functionalization," *Org. Lett.*, vol. 15, no. 6, pp. 1390–1393, 2013.

[162] E. Alvarez-Manzaneda *et al.*, "A thermal 6pi electrocyclization strategy towards taiwaniaquinoids. First enantiospecific synthesis of (-)-taiwaniaquinone G.," *Chem. Commun. (Camb).*, no. 5, pp. 592–594, 2009.

[163] J. Wang *et al.*, "Synthesis of 5-epi-taiwaniaquinone G," *J. Org. Chem.*, vol. 79, no. 13, pp. 6354–6359, Jul. 2014.

[164] E. Alvarez-Manzaneda *et al.*, "A very efficient route toward the 4a-methyltetrahydrofluorene skeleton: short synthesis of (±)-dichroanone and (±)-taiwaniaquinone H," *J. Org. Chem.*, vol. 74, no. 9, pp. 3384–3388, 2009.

[165] M. Node *et al.*, "Efficient asymmetric synthesis of abeo-abietane-type diterpenoids by using the intramolecular Heck reaction," *J. Org. Chem.*, vol. 75, no. 1, pp. 190–196, 2010.

[166] C. K. Jana, R. Scopelliti, and K. Gademann, "A synthetic entry into the taiwaniaquinoids based on a biogenetic hypothesis: Total synthesis of (-)-taiwaniaquinone H," *Chem. - A Eur. J.*, vol. 16, no. 26, pp. 7692–7695, 2010.

[167] S. E. Shockley, J. C. Holder, and B. M. Stoltz, "A Catalytic, Enantioselective Formal Synthesis of (+)-Dichroanone and (+)-Taiwaniaquinone H," *Org. Lett.*, vol. 16, no. 24, pp. 6362–6365, 2014.

[168] M. Banerjee, R. Mukhopadhyay, B. Achari, and A. K. Banerjee, "First Total Synthesis of the 4a-Methyltetrahydrofluorene Diterpenoids (±)-Dichroanal B and (±)-Dichroanone," *Org. Lett.*, vol. 5, no. 21, pp. 3931–3933, 2003.

[169] S. Tang *et al.*, "Application of a domino Friedel-Crafts acylation/alkylation reaction to the formal syntheses of (+/-)-taiwaniaquinol B and (+/-)-dichroanone," *Org. Lett.*, vol. 10, no. 9, pp. 1855–1858, 2008.

[170] R. M. McFadden and B. M. Stoltz, “The catalytic enantioselective, protecting group-free total synthesis of (+)-dichroanone,” *J. Am. Chem. Soc.*, vol. 128, no. 24, pp. 7738–7739, Jun. 2006.

[171] E. Alvarez-Manzaneda *et al.*, “An enantiospecific route towards taiwaniaquinoids. First synthesis of (-)-taiwaniaquinone H and (-)-dichroanone.,” *Org. Biomol. Chem.*, vol. 7, no. 24, pp. 5146–5155, 2009.

[172] S. Sengupta, M. G. B. Drew, R. Mukhopadhyay, B. Achari, and A. K. Banerjee, “Stereoselective syntheses of (±)-komaroviquinone and (±)-faveline methyl ether through intramolecular Heck reaction,” *J. Org. Chem.*, vol. 70, no. 19, pp. 7694–7700, 2005.

[173] A. Padwa, M. J. Chughtai, J. Boonsombat, and P. Rashatasakhon, “A Rh(II)-catalyzed cycloaddition approach toward the synthesis of komaroviquinone,” *Tetrahedron*, vol. 64, no. 21, pp. 4758–4767, May 2008.

[174] A. Padwa, J. Boonsombat, P. Rashatasakhon, and J. Willis, “Efficient Construction of the Oxatricyclo[6.3.1.00,0]dodecane Core of Komaroviquinone Using a Cyclization/Cycloaddition Cascade of a Rhodium Carbenoid Intermediate,” *Org. Lett.*, vol. 7, no. 17, pp. 3725–3727, 2005.

[175] Y. Suto, K. Kaneko, N. Yamagiwa, and G. Iwasaki, “A short and efficient asymmetric synthesis of komaroviquinone,” *Tetrahedron Lett.*, vol. 51, no. 48, pp. 6329–6330, 2010.

[176] D. Kaliakoudas, C. H. Eugster, and P. Rüedi, “Synthese von Plectranthonen, diterpenoiden Phenanthren-1,4-chinonen,” *Helv. Chim. Acta*, vol. 73, pp. 48–62, Jan. 1990.

[177] Z. Zhang, F. Flachsmann, F. M. Moghaddam, and P. Rüedi, “Ultrasound-Promoted synthesis of substituted phenanthrene-1,4-quinones; the structure of plectranthon D,” *Tetrahedron Lett.*, vol. 35, no. 14, pp. 2153–2156, Apr. 1994.

[178] A.-M. Faucher and R. H. Burnell, “The conversion of 7-acetoxyroyleanone to 14-methoxytaxodione,” *Can. J. Chem.*, vol. 67, no. 1, pp. 1–4, 1989.

[179] G. Topçu and A. C. Gören, “Biological activity of diterpenoids isolated from Anatolian Lamiaceae plants.,” *Rec. Nat. Prod.*, vol. 1, pp. 1–16, 2007.

[180] Y. B. Wu *et al.*, “Constituents from salvia species and their biological activities,” *Chem. Rev.*, vol. 112, no. 11, pp. 5967–6026, 2012.

[181] H. Sun, S. Huang, and Q. Han, "Diterpenoids from Isodon species and their biological activities.," *Nat. Prod. Rep.*, vol. 23, no. 5, pp. 673–698, 2006.

[182] F. Piozzi, M. Bruno, S. Rosselli, and A. Maggio, "The diterpenoids from the genus Hyptis (Lamiaceae)," *Heterocycles*, vol. 78, no. 6, pp. 1413–1426, 2009.

[183] S. Zielińska and A. Matkowski, "Phytochemistry and bioactivity of aromatic and medicinal plants from the genus Agastache (Lamiaceae)," *Phytochem. Rev.*, vol. 13, no. 2, pp. 391–416, 2014.

[184] S. Waldia, B. C. Joshi, U. Pathak, and M. C. Joshi, "The genus plectranthus in India and its chemistry," *Chem. Biodivers.*, vol. 8, no. 2, pp. 244–252, 2011.

[185] M. Abdel-Mogib, H. A. Albar, and S. M. Batterjee, "Chemistry of the genus Plectranthus," *Molecules*, vol. 7, no. 2, pp. 271–301, 2002.

[186] M. Niwa *et al.*, "Suppression of inducible nitric oxide synthase mRNA expression by tryptoquinone A.," *Biochem. Biophys. Res. Commun.*, vol. 224, no. 2, pp. 579–585, 1996.

[187] J. Ji *et al.*, "Discovery of novel aromatase inhibitors using a homogeneous time-resolved fluorescence assay," *Acta Pharmacol. Sin.*, vol. 35, no. 8, pp. 1082–1092, 2014.

[188] B. Zapata, M. Rojas, L. Betancur-Galvis, A. C. Mesa-Arango, D. Perez-Guaita, and M. a Gonzalez, "Cytotoxic, immunomodulatory, antimycotic, and antiviral activities of semisynthetic 14-hydroxyabietane derivatives and triptoquinone C-4 epimers," *Medchemcomm*, vol. 4, no. 9, pp. 1239–1246, 2013.

[189] I. Ramírez-Macías *et al.*, "Taiwaniaquinoid and abietane quinone derivatives with trypanocidal activity against T. cruzi and Leishmania spp.," *Parasitol. Int.*, vol. 61, no. 3, pp. 405–413, 2012.

[190] T. D. Gootz, "The global problem of antibiotic resistance.," *Crit. Rev. Immunol.*, vol. 30, no. 1, pp. 79–93, 2010.

[191] F. von Nussbaum, M. Brands, B. Hinzen, S. Weigand, and D. Häbich, "Antibacterial Natural Products in Medicinal Chemistry—Exodus or Revival?," *Angew. Chemie Int. Ed.*, vol. 45, no. 31, pp. 5072–5129, Aug. 2006.

[192] C. W. Lukhoba, M. S. J. Simmonds, and A. J. Paton, "Plectranthus: A review of ethnobotanical uses," *J. Ethnopharmacol.*, vol. 103, no. 1, pp. 1–24, 2006.

[193] A. C. Abreu, A. J. McBain, and M. Simões, "Plants as sources of new antimicrobials and

resistance-modifying agents," *Nat. Prod. Rep.*, vol. 29, no. 9, p. 1007, Sep. 2012.

[194] D. Savoia, "Plant-derived antimicrobial compounds: alternatives to antibiotics," *Future Microbiol.*, vol. 7, no. 8, pp. 979–990, Aug. 2012.

[195] D. Ladeiras, C. M. Monteiro, F. Pereira, C. P. Reis, C. A. M. Afonso, and P. Rijo, "Reactivity of Diterpenoid Quinones: Royleanones.," *Curr. Pharm. Des.*, vol. 22, no. 12, pp. 1682–1714, Mar. 2016.

[196] M. Hensch, P. Ruedi, and C. H. Eugster, "Horminon, Taxochinon und weitere Royleanone aus 2 abesstuischen Plectruntkus-Spezies (Labiatae)," *Helv. Chim. Acta*, vol. 58, no. 7, pp. 1921–1934, 1975.

[197] P. Rijo *et al.*, "Antimycobacterial metabolites from *Plectranthus*: royleanone derivatives against *Mycobacterium tuberculosis* strains.," *Chem. Biodivers.*, vol. 7, no. 4, pp. 922–932, 2010.

[198] P. Pereira, M. G. Bernardo-Gil, M. J. Cebola, E. Mauricio, and A. Romano, "Supercritical fluid extracts with antioxidant and antimicrobial activities from myrtle (Myrtus communis L.) leaves. Response surface optimization," *J. Supercrit. Fluids*, vol. 83, pp. 57–64, 2013.

[199] E. Ghasemi, F. Raofie, and N. M. Najafi, "Application of response surface methodology and central composite design for the optimisation of supercritical fluid extraction of essential oils from Myrtus communis L. leaves," *Food Chem.*, vol. 126, no. 3, pp. 1449–1453, Jun. 2011.

[200] M. G. Bernardo-Gil, R. Roque, L. B. Roseiro, L. C. Duarte, F. Gírio, and P. Esteves, "Supercritical extraction of carob kibbles (Ceratonia siliqua L.)," *J. Supercrit. Fluids*, vol. 59, pp. 36–42, 2011.

[201] Haynes W. M., *CRC Handbook of Chemistry and Physics, 97th Edition*. 2017.

[202] T. Fornari, G. Vicente, E. Vázquez, M. R. García-Risco, and G. Reglero, "Isolation of essential oil from different plants and herbs by supercritical fluid extraction," *J. Chromatogr. A*, vol. 1250, pp. 34–48, Aug. 2012.

[203] S. Machmudah, Y. Kawahito, M. Sasaki, and M. Goto, "Process optimization and extraction rate analysis of carotenoids extraction from rosehip fruit using supercritical CO2," *J. Supercrit. Fluids*, vol. 44, no. 3, pp. 308–314, 2008.

[204] M. Herrero, A. Cifuentes, and E. Ibañez, "Sub- and supercritical fluid extraction of

functional ingredients from different natural sources: Plants, food-by-products, algae and microalgae: A review," *Food Chem.*, vol. 98, no. 1, pp. 136–148, 2006.

[205] M. Esquível and M. G. Bernardo-Gil, "El uso de fluidos supercríticos en la industria de aceites alimentarios," *Grasas y Aceites*, vol. 44, no. 1, pp. 1–5, 1993.

[206] E. Reverchon, "Supercritical fluid extraction and fractionation of essential oils and related products," *J. Supercrit. Fluids*, vol. 10, no. 1, pp. 1–37, Apr. 1997.

[207] P. Rijo, M. Batista, M. Matos, H. Rocha, S. Jesus, and M. F. Simões, "Screening of antioxidant and antimicrobial activities on Plectranthus spp . extracts Pesquisa das actividades antioxidante e antimicrobiana em extractos de plantas do," *Biomed. Biopharm. Res.*, vol. 9, no. 2, pp. 225–235, 2012.

[208] P. Rijo, P. L. Falé, M. L. Serralheiro, M. F. Simões, A. Gomes, and C. Reis, "Optimization of medicinal plant extraction methods and their encapsulation through extrusion technology," *Measurement*, vol. 58, pp. 249–255, 2014.

[209] P. Rijo, D. Matias, A. S. Fernandes, M. F. Simões, M. Nicolai, and C. P. Reis, "Antimicrobial plant extracts encapsulated into polymeric beads for potential application on the skin," *Polymers (Basel).*, vol. 6, no. 2, pp. 479–490, 2014.

[210] C. S. D. Lopes, F. Agapito, C. E. S. Bernardes, and M. E. M. da Piedade, "Thermochemistry of 4-HOC6H4COR (R=H, CH3, C2H5, n-C3H7, n-C4H9, n-C5H11, and n-C6H13) compounds," *J. Chem. Thermodyn.*, vol. 104, pp. 281–287, 2017.

[211] Bruker Analytical Systems, "Apex 2." Madison, 2010.

[212] Bruker AXS Inc., "Saint: Area-Detector Integration Software (version 7.23)." Madison, 2004.

[213] G. Sheldrick, "SADABS – Siemens Area Detector ABSorption correction program," *Siemens/Bruker AXS inc.*, pp. 51–33, 1995.

[214] G. M. Sheldrick, "A short history of SHELX," *Acta Crystallogr. Sect. A Found. Crystallogr.*, vol. 64, no. 1, pp. 112–122, Jan. 2008.

[215] G. M. Sheldrick, "SHELX-97, program for the solution and refinement of crystal structures," *Univ. Göttingen, Ger.*, 1997.

[216] L. J. Farrugia, "WinGX suite for small-molecule single-crystal crystallography," *J. Appl. Crystallogr.*, vol. 32, no. 4, pp. 837–838, Aug. 1999.

[217] C. F. Macrae *et al.*, "Mercury CSD 2.0 – new features for the visualization and investigation of crystal structures," *J. Appl. Crystallogr.*, vol. 41, no. 2, pp. 466–470, Apr. 2008.

[218] A. L. Spek, "Structure validation in chemical crystallography," *Acta Cryst*, vol. 65, pp. 148–155, 2009.

[219] H.-K. Fun, S. Chantrapromma, A. W. Salae, I. A. Razak, and C. Karalai, "Redetermined structure, intermolecular interactions and absolute configuration of royleanone," *Acta Crystallogr. Sect. E Struct. Reports Online*, vol. 67, no. 5, pp. o1032–o1033, May 2011.

[220] I. A. Razak, A. W. Salae, S. Chantrapromma, C. Karalai, and H.-K. Fun, "Redetermination and absolute configuration of 7α-hy-droxy-royleanone," *Acta Crystallogr. Sect. E Struct. Reports Online*, vol. 66, no. Pt 7, pp. o1566–o1567, Jul. 2010.

[221] D. Cremer and J. A. Pople, "General definition of ring puckering coordinates," *J. Am. Chem. Soc.*, vol. 97, no. 6, pp. 1354–1358, Mar. 1975.

[222] J. Bernstein, R. E. Davis, L. Shimoni, and N.-L. Chang, "Patterns in Hydrogen Bonding: Functionality and Graph Set Analysis in Crystals," *Angew. Chemie Int. Ed. English*, vol. 34, no. 15, pp. 1555–1573, Aug. 1995.

[223] M. C. Etter, J. C. MacDonald, J. Bernstein, and IUCr, "Graph-set analysis of hydrogen-bond patterns in organic crystals," *Acta Crystallogr. Sect. B Struct. Sci.*, vol. 46, no. 2, pp. 256–262, Apr. 1990.

[224] F. Yoshizaki, P. Rüedi, and C. H. Eugster, "Diterpenoide Drüsenfarbstoffe aus Labiaten: 11 Coleone und Royleanone aus *Coleus carnosus* H ASSK," *Helv. Chim. Acta*, vol. 62, no. 8, pp. 2754–2762, Dec. 1979.

[225] F. Matloubi-Moghadam, P. Rüedi, and C. H. Eugster, "Drüsefarbstoffe aus Labiaten: Identifizierung von 17 Abietanoiden aus Plectranthus sanguineus B RITTEN," *Helv. Chim. Acta*, vol. 70, no. 4, pp. 975–983, Jul. 1987.

[226] L. Palacios *et al.*, "Staphylococcal Phenotypes Induced by Naturally Occurring and Synthetic Membrane-Interactive Polyphenolic beta-Lactam Resistance Modifiers," *PLoS One*, vol. 9, no. 4, pp. e93830–e93830, 2014.

[227] M. M. Elhassan, H. A. Ozbak, H. A. Hemeg, M. A. Elmekki, and L. M. Ahmed, "Absence of the mecA Gene in Methicillin Resistant Staphylococcus aureus Isolated from Different

Clinical Specimens in Shendi City, Sudan.," *Biomed Res. Int.*, vol. 2015, p. 895860, 2015.

[228] M. Y. Lin and M. K. Hayden, "Methicillin-resistant Staphylococcus aureus and vancomycin-resistant enterococcus: Recognition and prevention in intensive care units," *Crit. Care Med.*, vol. 38, no. 8 Suppl, pp. S335–S344, Aug. 2010.

[229] S. J. Greay and K. A. Hammer, "Recent developments in the bioactivity of mono- and diterpenes: anticancer and antimicrobial activity," *Phytochem. Rev.*, vol. 14, no. 1, pp. 1–6, Feb. 2015.

[230] P. Rijo, "Phytochemical Study And Biological Activities Of Diterpenes And Derivatives From Plectranthus Species," Universidade De Lisboa Faculdade De Farmácia, 2010.

[231] D. Matias *et al.*, "Cytotoxicity screening of Plectranthus spp. extracts and individual components in MDA-MB-231 cells," *Toxicol. Lett.*, vol. 238, no. 2, p. S240, Oct. 2015.

[232] O. Batista *et al.*, "A rearranged abietane diterpenoid from Plectranthus hereroensis," *Phytochem.* , vol. 41, pp. 571–573, 1996.

[233] J. T. Marquês, A. S. Viana, and R. F. M. de Almeida, "A Biomimetic Platform to Study the Interactions of Bioelectroactive Molecules with Lipid Nanodomains," *Langmuir*, vol. 30, no. 42, pp. 12627–12637, Oct. 2014.

[234] J. Guillén, R. F. M. de Almeida, M. Prieto, and J. Villalaín, "Structural and Dynamic Characterization of the Interaction of the Putative Fusion Peptide of the S2 SARS-CoV Virus Protein with Lipid Membranes," *J. Phys. Chem. B*, vol. 112, no. 23, pp. 6997–7007, Jun. 2008.

[235] C. W. McClare, "An accurate and convenient organic phosphorus assay.," *Anal. Biochem.*, vol. 39, no. 2, pp. 527–30, Feb. 1971.

[236] A. C. Carreira, R. F. M. de Almeida, and L. C. Silva, "Development of lysosome-mimicking vesicles to study the effect of abnormal accumulation of sphingosine on membrane properties," *Sci. Rep.*, vol. 7, no. 1, p. 3949, Dec. 2017.

[237] K. Mukhopadhyay *et al.*, "In vitro susceptibility of Staphylococcus aureus to thrombin-induced platelet microbicidal protein-1 (tPMP-1) is influenced by cell membrane phospholipid composition and asymmetry," *Microbiology*, vol. 153, no. Pt 4, pp. 1187–1197, 2007.

[238] I. R. Grilo, A. M. Ludovice, A. Tomasz, H. de Lencastre, and R. G. Sobral, "The

glucosaminidase domain of Atl - the major Staphylococcus aureus autolysin - has DNA-binding activity," *Microbiologyopen*, vol. 3, no. 2, pp. 247–256, 2014.

[239] B. L. . De Jonge, Y. Chang, D. Gage, and A. Tomasz, "Peptidoglycan composition of a highly methicillin-resistant Staphylococcus aureus strain. The role of penicillin binding protein 2A," *J. Biol. Chem.*, vol. 267, no. 16, pp. 11248–54, 1992.

[240] R. G. Sobral, A. M. Ludovice, H. de Lencastre, and A. Tomasz, "Role of murF in Cell Wall Biosynthesis: Isolation and Characterization of a murF Conditional Mutant of Staphylococcus aureus," *J. Bacteriol.*, vol. 188, no. 7, pp. 2543–2553, Apr. 2006.

[241] T. A. Figueiredo *et al.*, "Identification of Genetic Determinants and Enzymes Involved with the Amidation of Glutamic Acid Residues in the Peptidoglycan of Staphylococcus aureus," *PLoS Pathog.*, vol. 8, no. 1, p. e1002508, Jan. 2012.

[242] F. He, Y. Yang, G. Yang, and L. Yu, "Studies on antibacterial activity and antibacterial mechanism of a novel polysaccharide from Streptomyces virginia H03," *Food Control*, vol. 21, no. 9, pp. 1257–1262, Sep. 2010.

[243] H. Mohammad *et al.*, "Antibacterial Characterization of Novel Synthetic Thiazole Compounds against Methicillin-Resistant Staphylococcus pseudintermedius.," *PLoS One*, vol. 10, no. 6, p. e0130385, 2015.

[244] C. M. Kusuma and J. F. Kokai-Kun, "Comparison of four methods for determining lysostaphin susceptibility of various strains of Staphylococcus aureus.," *Antimicrob. Agents Chemother.*, vol. 49, no. 8, pp. 3256–63, Aug. 2005.

[245] A. S. Bayer *et al.*, "Low-level resistance of Staphylococcus aureus to thrombin-induced platelet microbicidal protein 1 in vitro associated with qacA gene carriage is independent of multidrug efflux pump activity.," *Antimicrob. Agents Chemother.*, vol. 50, no. 7, pp. 2448–54, Jul. 2006.

[246] S.-J. Yang, N. N. Mishra, A. Rubio, and A. S. Bayer, "Causal role of single nucleotide polymorphisms within the mprF gene of Staphylococcus aureus in daptomycin resistance.," *Antimicrob. Agents Chemother.*, vol. 57, no. 11, pp. 5658–64, Nov. 2013.

[247] S. Halder *et al.*, "Alteration of Zeta potential and membrane permeability in bacteria: a study with cationic agents," *Springerplus*, vol. 4, no. 1, p. 672, Dec. 2015.

[248] A. E. P. Bastos, H. S. Marinho, A. M. Cordeiro, A. M. de Soure, and R. F. M. de Almeida,

"Biophysical properties of ergosterol-enriched lipid rafts in yeast and tools for their study: characterization of ergosterol/phosphatidylcholine membranes with three fluorescent membrane probes," *Chem. Phys. Lipids*, vol. 165, no. 5, pp. 577–588, Jul. 2012.

[249] E. E. Ambroggio, F. Separovic, J. H. Bowie, G. D. Fidelio, and L. A. Bagatolli, "Direct Visualization of Membrane Leakage Induced by the Antibiotic Peptides: Maculatin, Citropin, and Aurein," *Biophys. J.*, vol. 89, no. 3, pp. 1874–1881, Sep. 2005.

[250] C. Jacqueline *et al.*, "In vitro and in vivo synergistic activities of linezolid combined with subinhibitory concentrations of imipenem against methicillin-resistant Staphylococcus aureus.," *Antimicrob. Agents Chemother.*, vol. 49, no. 1, pp. 45–51, Jan. 2005.

[251] M. Zuzarte, a M. Dinis, C. Cavaleiro, J. Canhoto, and L. Salgueiro, "Trichomes Morphology and Essential Oils Characterization of Field-Growing and In Vitro Propagated Plants of Lavandula pedunculata.," *Microsc. Microanal.*, vol. 14 Suppl 3, pp. 148–149, 2008.

[252] J. B. Salas, T. R. Téllez, F. M. V Pardo, M. J. P. A. Alonso, and M. Á. C. C. Capdevilla, "Study of the essential oil of three species of thyme in their limit of distribution in Spain," *Acta Bot. Gall.*, vol. 158, no. 2, pp. 251–262, 2011.

[253] F. Matos *et al.*, "Antioxidant Capacity of the Essential Oils From Lavandula luisieri, L. stoechas subsp. lusitanica, L. stoechas subsp. lusitanica x L. luisieri and L. viridis Grown in Algarve (Portugal)," *J. Essent. Oil Res.*, vol. 21, no. 4, pp. 327–336, Jul. 2009.

[254] M. Zuzarte *et al.*, "Lavandula luisieri essential oil as a source of antifungal drugs," *Food Chem.*, vol. 135, no. 3, pp. 1505–1510, 2012.

[255] M. Zuzarte, M. J. Gonçalves, C. Cavaleiro, A. M. Dinis, J. M. Canhoto, and L. R. Salgueiro, "Chemical Composition and Antifungal Activity of the Essential Oils of Lavandula pedunculata (Miller) Cav.," *Chem. Biodivers.*, vol. 6, no. 8, pp. 1283–1292, Aug. 2009.

[256] T. G., C. A.I., V. T., D. A., O. N., and M. A.M., "Lavandula stoechas subsp. luisieri and L. pedunculata: comparative antibacterial activity," *J. Phytother. Pharmacol.*, vol. 1, no. 4, pp. 11–15, 2012.

[257] A. Ferreira, C. Proença, M. L. M. Serralheiro, and M. E. M. Araújo, "The in vitro screening for acetylcholinesterase inhibition and antioxidant activity of medicinal plants from Portugal," *J. Ethnopharmacol.*, vol. 108, no. 1, pp. 31–37, Nov. 2006.

[258] J. A. Bouwstra, P. L. Honeywell-Nguyen, G. S. Gooris, and M. Ponec, "Structure of the skin

barrier and its modulation by vesicular formulations," *Prog. Lipid Res.*, vol. 42, no. 1, pp. 1–36, Jan. 2003.

[259] A. Mihranyan, N. Ferraz, and M. Strømme, "Current status and future prospects of nanotechnology in cosmetics," *Prog. Mater. Sci.*, vol. 57, no. 5, pp. 875–910, Jun. 2012.

[260] Z. Zhang, P.-C. Tsai, T. Ramezanli, and B. B. Michniak-Kohn, "Polymeric nanoparticles-based topical delivery systems for the treatment of dermatological diseases," *Wiley Interdiscip. Rev. Nanomedicine Nanobiotechnology*, vol. 5, no. 3, pp. 205–218, May 2013.

[261] S. S. Guterres, M. P. Alves, and A. R. Pohlmann, "Polymeric Nanoparticles, Nanospheres and Nanocapsules, for Cutaneous Applications," *Drug Target Insights*, vol. 2, pp. 147–157, Jul. 2007.

[262] G. J. Nohynek, E. Antignac, T. Re, and H. Toutain, "Safety assessment of personal care products/cosmetics and their ingredients," *Toxicol. Appl. Pharmacol.*, vol. 243, no. 2, pp. 239–259, Mar. 2010.

[263] T. W. Prow *et al.*, "Nanoparticles and microparticles for skin drug delivery," *Adv. Drug Deliv. Rev.*, vol. 63, no. 6, pp. 470–491, May 2011.

[264] D. Papakostas, F. Rancan, W. Sterry, U. Blume-Peytavi, and A. Vogt, "Nanoparticles in dermatology," *Arch. Dermatol. Res.*, vol. 303, no. 8, p. 533, 2011.

[265] J. Panyam and V. Labhasetwar, "Biodegradable nanoparticles for drug and gene delivery to cells and tissue," *Adv. Drug Deliv. Rev.*, vol. 55, no. 3, pp. 329–347, 2003.

[266] C. P. Reis *et al.*, "Development and Evaluation of a Novel Topical Treatment for Acne with Azelaic Acid-Loaded Nanoparticles," *Microsc. Microanal.*, vol. 19, no. 5, pp. 1141–1150, 2013.

[267] A. Kumari, S. K. Yadav, and S. C. Yadav, "Biodegradable polymeric nanoparticles based drug delivery systems," *Colloids and Surfaces B-Biointerfaces*, vol. 75, no. 1, pp. 1–18, 2010.

[268] V. L. Singleton and J. A. Rossi, "Colorimetry of Total Phenolics with Phosphomolybdic-Phosphotungstic Acid Reagents," *Am. J. Enol. Vitic.*, vol. 16, no. 3, p. 144 LP-158, Jan. 1965.

[269] L. M. Cheung, P. C. K. Cheung, and V. E. C. Ooi, "Antioxidant activity and total phenolics of edible mushroom extracts," *Food Chem.*, vol. 81, no. 2, pp. 249–255, May 2003.

[270] J. Zhishen, T. Mengcheng, and W. Jianming, "The determination of flavonoid contents in mulberry and their scavenging effects on superoxide radicals," *Food Chem.*, vol. 64, no. 4, pp. 555–559, Mar. 1999.

[271] C. Liégeois, G. Lermusieau, and S. Collin, "Measuring Antioxidant Efficiency of Wort, Malt, and Hops against the 2,2'-Azobis(2-amidinopropane) Dihydrochloride-Induced Oxidation of an Aqueous Dispersion of Linoleic Acid," *J. Agric. Food Chem.*, vol. 48, no. 4, pp. 1129–1134, Apr. 2000.

[272] C. Sarikurkcu, B. Tepe, D. Daferera, M. Polissiou, and M. Harmandar, "Studies on the antioxidant activity of the essential oil and methanol extract of Marrubium globosum subsp. globosum (lamiaceae) by three different chemical assays," *Bioresour. Technol.*, vol. 99, no. 10, pp. 4239–4246, Jul. 2008.

[273] A. S. Fernandes *et al.*, "Protective role of ortho -substituted Mn(III) N -alkylpyridylporphyrins against the oxidative injury induced by tert -butylhydroperoxide," *Free Radic. Res.*, vol. 44, no. 4, pp. 430–440, Jan. 2010.

[274] K. AM and E. CHRISTOPHERS, "Preparation of isolated sheets of human stratum corneum," *Arch. Dermatol.*, vol. 88, no. 6, pp. 702–705, Dec. 1963.

[275] A. K. Kohli and H. O. Alpar, "Potential use of nanoparticles for transcutaneous vaccine delivery: effect of particle size and charge," *Int. J. Pharm.*, vol. 275, no. 1–2, pp. 13–17, May 2004.

[276] M. M. A. Abdel-Mottaleb, B. Moulari, A. Beduneau, Y. Pellequer, and A. Lamprecht, "Surface-Charge-Dependent Nanoparticles Accumulation in Inflamed Skin," *J. Pharm. Sci.*, vol. 101, no. 11, pp. 4231–4239, Nov. 2012.

[277] S. Parveen, R. Misra, and S. K. Sahoo, "Nanoparticles: A boon to drug delivery, therapeutics, diagnostics and imaging," *Nanomedicine Nanotechnology, Biol. Med.*, vol. 8, no. 2, pp. 147–166, Feb. 2012.

[278] S. Laube, "Skin infections and ageing," *Ageing Res. Rev.*, vol. 3, no. 1, pp. 69–89, 2004.

[279] M. X. Chen, K. S. Alexander, and G. Baki, "Formulation and Evaluation of Antibacterial Creams and Gels Containing Metal Ions for Topical Application," *J. Pharm.*, vol. 2016, pp. 1–10, 2016.

[280] J. M. Munita and C. A. Arias, "Mechanisms of Antibiotic Resistance," *Microbiol. Spectr.*, vol. 4, no. 2, p. 10.1128/microbiolspec.VMBF-0016-2015, Apr. 2016.

[281] J. Davies and D. Davies, “Origins and Evolution of Antibiotic Resistance,” *Microbiol. Mol. Biol. Rev.*, vol. 74, no. 3, pp. 417–433, Sep. 2010.

[282] A. Brauner, O. Fridman, O. Gefen, and N. Q. Balaban, “Distinguishing between resistance, tolerance and persistence to antibiotic treatment,” *Nat Rev Micro*, vol. 14, no. 5, pp. 320–330, May 2016.

[283] S. Ranghar, P. Sirohi, P. Verma, and V. Agarwal, “Nanoparticle-based drug delivery systems: promising approaches against infections ,” *Brazilian Archives of Biology and Technology* , vol. 57. scielo , pp. 209–222, 2014.

[284] M. S. Dryden, “Novel antibiotic treatment for skin and soft tissue infection,” *Curr. Opin. Infect. Dis.*, vol. 27, no. 2, pp. 116–124, 2014.

[285] M. Falcone *et al.*, “Acute bacterial skin and skin structure infections in internal medicine wards: old and new drugs,” *Intern. Emerg. Med.*, vol. 11, no. 5, pp. 637–648, 2016.

[286] J.-M. Rolain, C. Abat, M.-T. Jimeno, P.-E. Fournier, and D. Raoult, “Do we need new antibiotics?,” *Clin. Microbiol. Infect.*, vol. 22, no. 5, pp. 408–415, May 2016.

[287] A. L. Parkes and I. A. Yule, “Hybrid antibiotics – clinical progress and novel designs,” *Expert Opin. Drug Discov.*, vol. 11, no. 7, pp. 665–680, Jul. 2016.

[288] S. Marin, G. M. Vlasceanu, R. E. Tiplea, I. R. Bucur, M. Lemnaru, and M. M. M. and A. M. Grumezescu, “Applications and Toxicity of Silver Nanoparticles: A Recent Review,” *Current Topics in Medicinal Chemistry*, vol. 15, no. 16. pp. 1596–1604, 2015.

[289] P. Logeswari, S. Silambarasan, and J. Abraham, “Synthesis of silver nanoparticles using plants extract and analysis of their antimicrobial property,” *J. Saudi Chem. Soc.*, vol. 19, no. 3, pp. 311–317, May 2015.

[290] H. H. Lara, E. N. Garza-Treviño, L. Ixtepan-Turrent, and D. K. Singh, “Silver nanoparticles are broad-spectrum bactericidal and virucidal compounds.,” *J. Nanobiotechnology*, vol. 9, no. 1, pp. 1–8, 2011.

[291] Z. S. Pillai and P. V. Kamat, “What Factors Control the Size and Shape of Silver Nanoparticles in the Citrate Ion Reduction Method?,” *J. Phys. Chem. B*, vol. 108, no. 3, pp. 945–951, 2004.

[292] L. Mulfinger, S. D. Solomon, M. Bahadory, A. V Jeyarajasingam, S. A. Rutkowsky, and C. Boritz, “Synthesis and Study of Silver Nanoparticles,” *J. Chem. Educ.*, vol. 84, no. 2, p. 322,

Feb. 2007.

[293] B. Buszewski, K. Rafiſska, P. Pomastowski, J. Walczak, and A. Rogowska, "Novel aspects of silver nanoparticles functionalization," *Colloids Surfaces A Physicochem. Eng. Asp.*, vol. 506, pp. 170–178, Oct. 2016.

[294] M. Balouiri, M. Sadiki, and S. K. Ibnsouda, "Methods for in vitro evaluating antimicrobial activity: A review," *J. Pharm. Anal.*, vol. 6, no. 2, pp. 71–79, Apr. 2016.

[295] A. Roberto, "A high-throughput screening method for general cytotoxicity part I Chemical toxicity," *Rev. Lusófona Ciências e Tecnol. da Saúde; n. 2*, Oct. 2005.

[296] C. O. Silva *et al.*, "Polymeric nanoparticles modified with fatty acids encapsulating betamethasone for anti-inflammatory treatment," *Int. J. Pharm.*, vol. 493, no. 1–2, pp. 271–284, Sep. 2015.

[297] S. Niazi, *Handbook of Pharmaceutical Manufacturing Formulations: Liquid Products*. 2009.

[298] F. Bakkali, S. Averbeck, D. Averbeck, A. Zhiri, and M. Idaomar, "Cytotoxicity and gene induction by some essential oils in the yeast Saccharomyces cerevisiae," *Mutat. Res. Toxicol. Environ. Mutagen.*, vol. 585, no. 1–2, pp. 1–13, Aug. 2005.

[299] F. A. Simion, E. S. Abrutyn, and Z. D. Draelos, "Ability of moisturizers to reduce dry skin and irritation and to prevent their return," *Int. J. Cosmet. Sci.*, vol. 28, no. 3, pp. 232–232, Jun. 2006.

[300] C. Halin *et al.*, "Inhibition of Chronic and Acute Skin Inflammation by Treatment with a Vascular Endothelial Growth Factor Receptor Tyrosine Kinase Inhibitor," *Am. J. Pathol.*, vol. 173, no. 1, pp. 265–277, Jul. 2008.

[301] V. Amendola, O. M. Bakr, and F. Stellacci, "A Study of the Surface Plasmon Resonance of Silver Nanoparticles by the Discrete Dipole Approximation Method: Effect of Shape, Size, Structure, and Assembly," *Plasmonics*, vol. 5, no. 1, pp. 85–97, 2010.

[302] A. Pyatenko, M. Yamaguchi, and M. Suzuki, "Synthesis of Spherical Silver Nanoparticles with Controllable Sizes in Aqueous Solutions," *J. Phys. Chem. C*, vol. 111, no. 22, pp. 7910–7917, Jun. 2007.

[303] S. Iravani, H. Korbekandi, S. V Mirmohammadi, and B. Zolfaghari, "Synthesis of silver nanoparticles: chemical, physical and biological methods," *Res. Pharm. Sci.*, vol. 9, no. 6,

pp. 385–406, Aug. 2014.

[304] D. D. Evanoff and G. Chumanov, “Size-controlled synthesis of nanoparticles. 1. ‘Silver-only’ aqueous suspensions via hydrogen reduction,” *J. Phys. Chem. B*, vol. 108, no. 37, pp. 13948–13956, 2004.

[305] A. N. Brown, K. Smith, T. A. Samuels, J. Lu, S. O. Obare, and M. E. Scott, “Nanoparticles Functionalized with Ampicillin Destroy Multiple-Antibiotic-Resistant Isolates of Pseudomonas aeruginosa and Enterobacter aerogenes and Methicillin-Resistant Staphylococcus aureus,” *Appl. Environ. Microbiol.*, vol. 78, no. 8, pp. 2768–2774, Apr. 2012.

[306] H. H. Lara, D. G. Romero-Urbina, C. Pierce, J. L. Lopez-Ribot, M. J. Arellano-Jiménez, and M. Jose-Yacaman, “Effect of silver nanoparticles on Candida albicans biofilms: an ultrastructural study,” *J. Nanobiotechnology*, vol. 13, p. 91, Dec. 2015.

[307] T. C. Dakal, A. Kumar, R. S. Majumdar, and V. Yadav, “Mechanistic Basis of Antimicrobial Actions of Silver Nanoparticles,” *Front. Microbiol.*, vol. 7, p. 1831, Nov. 2016.

[308] L. Ge, Q. Li, M. Wang, J. Ouyang, X. Li, and M. M. Q. Xing, “Nanosilver particles in medical applications: synthesis, performance, and toxicity,” *Int. J. Nanomedicine*, vol. 9, pp. 2399–2407, May 2014.

[309] I. Calinescu, G. Mustatea, A. I. Gavrila, A. Dobre, and C. Pop, “Silver Nanoparticles: Synthesis, Characterization and Antibacterial Activity,” *Rev. Chim.*, vol. 65, no. 1, pp. 15–19, Jan. 2014.

[310] L. Xinping, L. Shengli, Z. Miaotao, Z. Wenlong, and L. Chuanghong, “Evaluations of Antibacterial Activity and Cytotoxicity on Ag Nanoparticles,” *Rare Met. Mater. Eng.*, vol. 40, no. 2, pp. 209–214, 2011.

[311] M. P. Patil and G.-D. Kim, “Eco-friendly approach for nanoparticles synthesis and mechanism behind antibacterial activity of silver and anticancer activity of gold nanoparticles,” *Appl. Microbiol. Biotechnol.*, vol. 101, no. 1, pp. 79–92, 2017.

[312] M. E. Samberg, S. J. Oldenburg, and N. A. Monteiro-Riviere, “Evaluation of Silver Nanoparticle Toxicity in Skin in Vivo and Keratinocytes in Vitro,” *Environ. Health Perspect.*, vol. 118, no. 3, pp. 407–413, Mar. 2010.

[313] B. Le Ouay and F. Stellacci, “Antibacterial activity of silver nanoparticles: A surface science

insight," *Nano Today*, vol. 10, no. 3, pp. 339–354, 2015.

[314] J. S. Kim *et al.*, "Antimicrobial effects of silver nanoparticles," *Nanomedicine Nanotechnology, Biol. Med.*, vol. 3, no. 1, pp. 95–101, 2007.

[315] J. K. Dunnick, S. L. Eustis, J. E. Huff, and J. K. Haseman, "Two-year toxicity and carcinogenicity studies of ampicillin trihydrate and penicillin VK in rodents," *Fundam. Appl. Toxicol.*, vol. 12, no. 2, pp. 252–257, 1989.

[316] P. Clarys, K. Alewaeters, R. Lambrecht, and A. O. Barel, "Skin color measurements: comparison between three instruments: the Chromameter®, the DermaSpectrometer® and the Mexameter®," *Ski. Res. Technol.*, vol. 6, no. 4, pp. 230–238, 2000.

[317] M.-W. W. Huang, P.-Y. Y. Lo, K.-S. S. Cheng, M.-W. W. Huang, and P.-Y. Y. Lo, "Objective Assessment of Sunburn and Minimal Erythema Doses: Comparison of Noninvasive In Vivo Measuring Techniques after UVB Irradiation," *EURASIP J. Adv. Signal Process.*, vol. 2010, no. 1, p. 483562, 2010.

[318] P. Morganti *et al.*, "Topical clindamycin 1% vs. linoleic acid-rich phosphatidylcholine and nicotinamide 4% in the treatment of acne: a multicentre-randomized trial," *Int. J. Cosmet. Sci.*, vol. 33, no. 5, pp. 467–476, 2011.

[319] A. R. Matias, M. Ferreira, P. Costa, and P. Neto, "Skin colour, skin redness and melanin biometric measurements: comparison study between Antera® 3D, Mexameter® and Colorimeter®," *Ski. Res. Technol.*, vol. 21, no. 3, pp. 346–362, 2015.

[320] S. Gajbhiye and S. Sakharwade, "Silver Nanoparticles in Cosmetics," *J. Cosmet. Dermatological Sci. Appl.*, vol. 6, no. 1, pp. 48–53, 2016.